Proceedings of the

*13th International Symposium on*

*Vibrations of Continuous Systems*

*Pomeroy, Kananaskis Mountain Lodge,*

*Alberta, Canada,*

*July 30- August 4, 2023*

# Preface

The International Symposium on Vibrations of Continuous Systems (ISVCS) is a forum for leading researchers from across the globe to meet with their colleagues and to present both old and new ideas in the field. Each participant has been encouraged either to present results of recent research or to reflect on some aspect of the vibration of continuous systems, which is particularly interesting, unexpected or unusual. This type of presentation is meant to encourage participants to draw on understanding obtained through many years of research in the field.
ISVCS focuses on the vibrations of the vibrations of the fundamental structural elements: strings, rods, beams, membranes, plates, shells, bodies of revolution and other solid bodies of simple geometry. Structures composed of assemblies of structural elements are also of interest, especially if such structures display interesting or unusual response.

The ISVCS started 26 years ago, at Stanley Hotel, Estes Park, Colorado, USA August 11-15, 1997. It comes every two years. Due to covid pandemic time the present 13th Symposium takes place 4 years later the previous one held in August 2019 in Corvara in Badia, Italy. We are back to North America in the wonderful parks ak Alberta. Typical days at the Symposium will consist of morning technical presentations, afternoon hikes or excursions in the local area and, in the evening, further technical discussions and social gatherings. The various outings and social gatherings provide important opportunities for relaxed and informal discussion of technical and not-so-technical topics surrounded by the natural beauty of the Alberta.

This volume of Proceedings contains 26 short summaries of the technical presentations to be made at the Symposium, as well as short biographical sketches of the participants. Unfortunately a few Scientists have experienced difficulties to get Visa and the number of presentation would be less than 26.

The present edition is the second one without the presence of Art Leissa, founder and Honorary Chairman of ISVCS. We all miss Art. We have new comers and a few young Scientists that could make ISVCS going further.

Last but not least we remember with pain that Wolfgang Seeman, a frequent attendee of past Symposia, left us unexpectedly on February 8$^{th}$ 2022 at the age of 61. An obituary by Prof Peter Hagedorn is made in these proceedings.

*General Chairman* Erasmo Carrera
*Editorial Chairman* Piotr Cupial
*Local Arrangements Chairman* Mark S. Ewing, Shudong Yu
*Publicity Chairman* Shinya Honda
*Honorary Chairman* Arthur William Leissa

## Past Symposia

The 1st International Symposium:
The Stanley Hotel, Estes Park, Colorado, USA
August 11-15, 1997
The 2nd International Symposium:
The Sunstar Hotel, Grindelwald, Switzerland
July 11-16, 1999
The 3rd International Symposium:
Jackson Lake Lodge, Grand Teton National Park, Wyoming, USA
July 23-27, 2001
The 4th International Symposium
Keswick, Lake District, England
July 23-27, 2003
The 5th International Symposium:
Berchtesgaden at Lake Königssee, Germany
July 25-29, 2005
The 6th International Symposium:
PlumpJack Squaw Valley Inn, Olympic Valley, California, USA
July 23-27, 2007
The 7th International Symposium:
Zakopane, Poland
July 19-25, 2009
The 8th International Symposium:
Whistler, British Columbia, Canada
July 18-22, 2011
The 9th International Symposium:
Courmayeur, Italy
July 22-26, 2013
The 10th International Symposium:
Stanley Hotel, Estes Park, Colorado, USA,
July 26-31, 2015
The 11th International Symposium:
the Royal Victoria Hotel, Llanberis, Snowdonia, Wales, UK,
July 16-21, 2017

The 12th International Symposium:
the Sporthotel Panorama, Str. Sciuz, 1, 39033 Corvara In Badia BZ – Italy,
July 28 - August 2, 2019

Details of the Proceedings of the past Symposia can be found at
http://www.isvcs.org

# Table of Contents

## **Presentation Summaries** (Presenting author is shown underlined)

**Biosketches of partecipants page**

# Obituary

## Professor Wolfgang Seeman 1961-2022

Professor Wolfgang Seemann passed away suddenly on February 8, 2022 at age 61. Wolfgang was a specialist on vibrations of continuous systems and for many years an extremely active participant of many ISVCS symposia. Not only did he always present solutions to interesting problems in his very personal, vivid and clear style, but he was also involved in the organization of many of the ISVCS symposia both in Europe and in the US and Canada. Wolfgang was an extremely successful scientist and gifted teacher, able to present even complicated situations in a succinct way. His students loved him for it. Wolfgang was at the same time always available to students and colleagues, who would regularly meet him in the search for advice. He served as advisor to many PhD students at Kaiserslautern, Darmstadt and Karlsruhe.

At the same time Wolfgang was also very involved in the administration of mechanical engineering at different levels.

He was above all a dedicated friend to many of us. We all will thoroughly miss him.

Joerg Wauer and Peter Hagedorn

# Free Vibration of an Axially Loaded Beam Using Frequency-Dependent Mass, Elastic and Geometric Stiffness Matrices

**J.R. Banerjee***
*School of Science and Technology, City, University of London
Northampton Square, London EC1V 0HB
Email: j.r.banerjee@city.ac.uk

## Summary

The frequency-dependent mass, elastic and geometric stiffness matrices of an axially loaded Bernoulli-Euler beam are developed through extensive application of symbolic computation, and their relationship with the dynamic stiffness matrix is established so that an exact free vibration analysis can be carried out by using the dynamic stiffness method (DSM) through the application of the Wittrick-Williams algorithm. The results are obtained for different boundary conditions of the beam carrying both tensile and compressive loads. The duality between the free vibration and buckling problems is captured in that when the compressive load in the beam approaches the buckling load, its fundamental natural frequency tends to zero, hence buckling can be interpreted as free vibration at zero frequency. The investigation has opened the possibility of including damping in free vibration analysis of beams and frameworks by using DSM.

The original idea of the frequency dependency of mass and stiffness properties of structural elements for free vibration analysis was put forward by Przemieniecki [1] who formulated the frequency dependent mass and stiffness matrices of a beam and provided series expansions of the matrices by retaining two frequency dependent terms. Przemieniecki's work was further developed by subsequent researchers [2-5] who also relied on power series expansion of the mass and stiffness matrices and truncated the series at some point. By contrast, explicit algebraic expressions for the elements of the frequency-dependent mass and stiffness matrices of a Bernoulli-Euler beam using symbolic computation were published recently [6] which circumvented the limitation of earlier research by including all terms of the infinite series implicitly. However, the presence of an axial load in a beam, which can have significant effects on the free vibration characteristics, was not considered in an exact sense in all of the previous publications. The current paper is set out to fill this gap in the literature by applying symbolic computation [7], rigorously. The resulting frequency-dependent mass, elastic and geometric stiffness matrices of the beam are related to its dynamic stiffness matrix which is finally utilised by applying the Wittrick-Williams algorithm [8] to compute the natural frequencies of an axially loaded beam under different boundary conditions.

The first step in developing the frequency-dependent mass, elastic, and geometric stiffness matrices of an axially loaded beam is to derive the frequency-dependent shape functions of the beam which relate the displacement within the beam to its nodal displacements when the beam is undergoing free natural vibration. Figure 1 shows the coordinate system and notations for an axially loaded Bernoulli-Euler beam with bending rigidity $EI$, mass per unit length $\rho A$ where $\rho$ is the density of material and $A$ is the area of cross-section and $L$ is the length of the beam. Note that node 1 of the beam is located at the origin $O$ and node 2 is at the other end at a distance $L$ from the origin, as shown in Figure 1. The compressive axial load $P$ shown in the figure, is assumed to be positive, acting through the centroid of the cross-section, but $P$ can be negative so that tension is included in the theory.

The kinetic energy ($T$) and potential energy ($V$) of the beam in the usual notation can be expressed as

$$T = \frac{1}{2}\int_0^L \rho A \dot{w}^2 dx; \quad V = \frac{1}{2}\int_0^L EI\,(w'')^2 dx - \frac{1}{2}\int_0^L P(w')^2 dx \tag{1}$$

where $w(x, t)$ is the bending or transverse deflection in the $Z$-direction and a prime and an over-dot represent differentiation with respect to the length coordinate $x$ and time $t$, respectively.

The governing differential equation of motion of the axially loaded beam in free natural vibration can now be obtained from the expressions of kinetic and potential energies given by Equation (1), to give

$$EIw'''' + Pw'' + \rho A\ddot{w} = 0 \tag{2}$$

Assuming harmonic oscillation so that $w(x,t) = We^{i\omega t}$ where $W$ is the amplitude of bending of flexural vibration, $\omega$ is the circular or angular frequency and $i = \sqrt{-1}$, the above partial differential equation can be converted into the following ordinary differential equation.

$$(D^4 + p^2D^2 - b^2)W = 0 \tag{3}$$

where

$$p^2 = \frac{PL^2}{EI}; \qquad b^2 = \frac{\rho A\omega^2 L^4}{EI}; \quad D = \frac{d}{d\xi}; \quad \xi = \frac{x}{L} \tag{4}$$

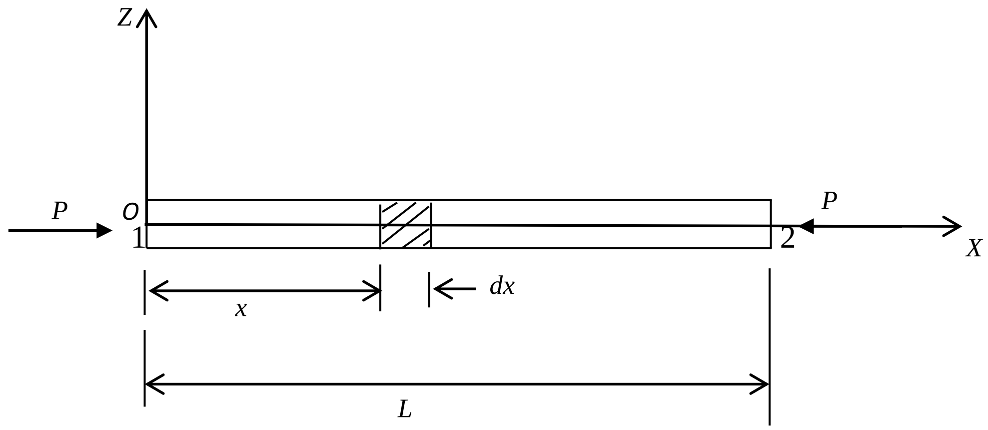


**Figure 1.** Coordinate system and notation for an axially loaded Bernoulli-Euler beam.

The solution of the governing differential equation (3) for the amplitudes of bending displacement $W(\xi)$ and bending rotation $\theta(\xi) = \frac{1}{L}W'(\xi)$ can be obtained as

$$W(\xi) = A_1 \cosh \alpha\xi + A_2 \sinh \alpha\xi + A_3 \cos \beta\xi + A_4 \sin \beta\xi \tag{5}$$

$$\theta(\xi) = \frac{1}{L}(A_1\alpha \sinh \alpha\xi + A_2\alpha \cosh \alpha\xi - A_3\beta \cos \beta\xi + A_4\beta \sin \beta\xi) \tag{6}$$

where

$$\alpha^2 = \frac{1}{2}\left(-p^2 + \sqrt{p^4 + 4b^2}\right); \quad \beta^2 = \frac{1}{2}\left(p^2 + \sqrt{p^2 + 4b^2}\right) \tag{7}$$

By eliminating the constants $A_1$-$A_4$ from Equations (5) and (6) with the help of nodal boundary conditions at $\xi$ =0 and $\xi$ = 1, respectively, the shape function **N** relating the displacements **δ** within the beam element (i.e. $W(\xi)$) to its nodal displacements $\boldsymbol{\delta}_N$ (i.e. the displacements and rotations ($W_1$, $\theta_1$) at node 1 and ($W_2$, $\theta_2$) at node 2) is given by the following relationships:

$$\boldsymbol{\delta} = \mathbf{N}\boldsymbol{\delta}_{\mathrm{N}} \text{ or } \{W(\xi)\} = [N_1 \quad N_2 \quad N_3 \quad N_4]\begin{Bmatrix} W_1 \\ \theta_1 \\ W_2 \\ \theta_2 \end{Bmatrix} \tag{8}$$

The expressions for the shape functions $N_1$, $N_2$, $N_3$ and $N_4$ were derived by extensive application of symbolic computation [7]. These are given by

$$N_1 = -\mu_1\beta \cosh \alpha\xi + \mu_3\beta \sinh \alpha\xi + \mu_2\, \alpha \cos \beta\xi - \mu_3\, \alpha \sin \beta\xi \tag{9}$$

$$N_2 = L(-\mu_4 \cosh \alpha\xi + \mu_2 \sinh \alpha\xi + \mu_4 \cos \beta\xi - \mu_1 \sin \beta\xi) \tag{10}$$

$$N_3 = -\mu_7\alpha\beta \cosh \alpha\xi - \mu_5\, \beta \sinh \alpha\xi + \mu_7\alpha\beta \cos \beta\xi + \mu_5\alpha \sin \beta\xi \tag{11}$$

$$N_4 = L(\mu_6 \cosh \alpha\xi - \mu_7\beta \sinh \alpha\xi - \mu_6 \cos \beta\xi + \mu_7\, \alpha \sin \beta\xi) \tag{12}$$

where

$$\mu_1 = (\alpha \cosh \alpha \cos \beta + \beta \sinh \alpha \sin \beta - \alpha)/\Delta \tag{13}$$

$$\mu_2 = (\alpha \sinh \alpha \sin \beta - \beta \cosh \alpha \cos \beta + \beta)/\Delta \tag{14}$$

$$\mu_3 = (\alpha \sinh \alpha \cos \beta + \beta \cosh \alpha \sin \beta)/\Delta \tag{15}$$

$$\mu_4 = (\alpha \cosh \alpha \sin \beta - \beta \sinh \alpha \cos \beta)/\Delta \tag{16}$$

$$\mu_5 = (\alpha \sinh \alpha + \beta \sin \beta)/\Delta \tag{17}$$

$$\mu_6 = (\alpha \sin \beta - \beta \sinh \alpha)/\Delta \tag{18}$$

$$\mu_7 = (\cos \beta - \cosh \alpha)/\Delta \tag{19}$$

with

$$\Delta = (\alpha^2 - \beta^2) \sinh \alpha \sin \beta + 2\alpha\beta(1 - \cosh \alpha \cos \beta) \tag{20}$$

The frequency-dependent mass (**m**), elastic ($\mathbf{k}_e$) and geometric ($\mathbf{k}_g$) stiffness matrices can now be formulated as follows.

$$\mathbf{m} = \rho AL \int_0^1 \begin{bmatrix} N_1 \\ N_2 \\ N_3 \\ N_4 \end{bmatrix} [N_1 \quad N_2 \quad N_3 \quad N_4] d\xi \tag{21}$$

$$\mathbf{k}_{\mathrm{e}} = \frac{EI}{L^3}\int_0^1 \begin{bmatrix} N_1'' \\ N_2'' \\ N_3'' \\ N_4'' \end{bmatrix} [N_1'' \quad N_2'' \quad N_3'' \quad N_4''] \, d\xi \tag{22}$$

$$\mathbf{k}_{\mathrm{g}} = -\frac{P}{L}\int_0^1 \begin{bmatrix} N_1' \\ N_2' \\ N_3' \\ N_4' \end{bmatrix} [N_1' \quad N_2' \quad N_3' \quad N_4'] d\xi \tag{23}$$

where a prime now denotes differentiation with respect to $\xi$.

The dynamic stiffness matrix $\mathbf{k}_{\mathrm{D}}$ of the axially loaded Bernoulli-Euler beam can be expressed as

$$\mathbf{k}_{\mathrm{D}} = \mathbf{k}_{\mathrm{e}} + \mathbf{k}_{\mathrm{g}} - \omega^2 \mathbf{m} \tag{24}$$

The Wittrick-Williams algorithm [8] is now applied to the dynamic stiffness matrix $\mathbf{k}_{\mathrm{D}}$ given above by Equation (24) to investigate the free vibration behaviour of an axially loaded Bernoulli-Euler beam. The natural frequencies with clamped-free (CF), pinned-pinned (PP), and clamped-clamped (CC) boundary conditions were computed for a range of tensile and compressive loads which were non-dimensionalised with respect to the corresponding critical buckling loads $P_{cr}$ by using the parameter $\lambda = P/P_{cr}$ noting that $P_{cr}$ for the CF, PP and CC cases are $\pi^2 EI/4L^2$, $\pi^2 EI/L^2$ , $4\pi^2 EI/L^2$, respectively. If $\omega_1^P$ and $\omega_1^0$ are the fundamental (angular) natural frequency in rad/s in the presence and absence of the axial load $P$, respectively, the ratio $R = \omega_1^P/\omega_1^0$ is computed and shown in Table 1 for a wide range of $\lambda$ values and boundary conditions. Note that $\omega_1^0$ for the CF, PP and CC cases are $3.516\sqrt{EI/\rho AL^4}$, $\pi^2\sqrt{EI/\rho AL^4}$ and $22.373\sqrt{EI/\rho AL^4}$, respectively. As expected, the natural frequency increases with tensile loads whereas it diminishes with compressive loads and eventually it becomes zero when critical buckling load is reached. The theory can be applied to frameworks with the prospects of including damping in free vibration analysis using DSM.

**Table 1.** Fundamental natural frequency of an axially loaded beam for different boundary conditions.

| Boundary conditions | Non-dimensional fundamental natural frequency ratio $R = \omega_1^P/\omega_1^0$ | | | | | | | | |
|---|---|---|---|---|---|---|---|---|---|
| | $\lambda = P/P_{cr}$ | | | | | | | | |
| | -1.0 | -0.75 | -0.5 | -0.25 | 0.0 | 0.25 | 0.5 | 0.75 | 1.0 |
| CF | 1.369 | 1.290 | 1.204 | 1.108 | 1.000 | 0.8741 | 0.7209 | 0.5152 | 0.0000 |
| PP | 1.414 | 1.323 | 1.225 | 1.118 | 1.000 | 0.8660 | 0.7071 | 0.5000 | 0.0000 |
| CC | 1.397 | 1.310 | 1.217 | 1.114 | 1.000 | 0.8694 | 0.7130 | 0.5066 | 0.0000 |

**References**


[1] Przemieniecki, J.S. : Theory of Matrix Structural Analysais. Dover Publications Inc, New York, 1985.

[2] Paz, M., and Dung, L.: Power Series Expansion of the General Stiffness Matrix for Beam Elements. International Journal for Numerical Methods in Engineering, Vol. 9(2), pp. 449-459, 1975.

[3] Downs, B.: Vibration Analysis of Continuous Systems by Dynamic Discretization. ASME Journal of Mechanical Design, Vol. 102, pp. 391-398, 1980. https://doi.org/10.1115/1.3254757

[4] Fergusson, N.J. and Pilkey, W.D.: Frequency-Dependent Element Mass Matrices. Journal of Applied Mechanics, Vol. 59 (1), pp. 136-139, 1992. https://doi.org/10.1115/1.2899418

[5] Dumont, N.A., and de Oliveira, R.: From Frequency-Dependent Mass and Stiffness Matrices to the Dynamic Response of Elastic Systems. International Journal of Solids and Structures, Vol. 38(10-13), pp. 1813-1830, 2001.

[6] Banerjee, J.R.:Frequency Dependent Mass and Stiffness Matrices of Bar and Beam Elements and Their Equivalency with the Dynamic Stiffness Matrix, Computers & Structures, Vol. 254, p.106616. 2021. doi: 10.1016/j.compstruc.2021.106616.

[7] Hearn, A.C.: REDUCE User's Manual, Version 3.8, Santa Monica, CA, USA, 2004.

[8] Wittrick, W.H., and Williams, F.W. : A General Algorithm for Computing Natural Frequencies of Elastic Structures, Quarterly Journal of Mechanics and Applied Mathematics, Vol. 24 (3), pp. 263–284, 1971. http://dx.doi.org/10.1093/qjmam/24.3.263

# An advanced discontinuous Timoshenko beam model for the analysis of free and forced vibrations of multi-cracked systems

**Francesco Cannizzaro, Ilaria Fiore, Salvatore Caddemi, Ivo Caliò**

Department of Civil and Architectural Engineering
University of Catania
Via S. Sofia 64, 95123 Catania, Italy
[francesco.cannizzaro,ilaria.fiore, salvatore.caddemi, ivo.calio]@unict.it

## Summary

The influence of shear deformation in the dynamics of beam-like problems can be studied by means of the classical Timoshenko formulation. The latter model can be enriched by means of the presence of discontinuities to account for the presence of multiple cracks. In fact, the effect of $n$ along axis cracks based on localised flexibility models implies the presence of discontinuities of the axial displacement $\Delta u_{x,i}(t)$, of the transversal displacement $\Delta u_{z,i}(t)$ and the rotation $\Delta\varphi_i(t)$ at damaged cross-sections $0 \le \xi_i \le 1, i = 1, n$, being $\xi$ the abscissa normalised with respect to the beam length $L$. The study of free vibrations of such a discontinuous Timoshenko model is classically approached by means of imposition of continuity and discontinuity conditions at the cracked cross sections. The latter procedure requires the introduction of additional integration constants with regard to those related to the standard boundary conditions making the problem computationally disadvantageous. Alternatively, a widely accepted procedure aiming at treating the problem in an effective, although approximate, manner relies on a finite element discretisation of the undamaged and damaged segments of the beam. A convenient way to treat multiple cracked shear deformable beams by accounting for the localised shear deformability due to the presence of cracks consists in the application of the so-called transfer matrix method [1]. The method is based on the knowledge of the fundamental solution of each beam segment comprised between cracks and leads to the formulation of the free vibration response of the multi-cracked Timoshenko beam in terms of the integration constants of the first beam segment. All the above solution procedures share the common view of a discontinuous beam as an assemblage of continuous sub-beams each with its own specific governing equation and relevant integration constants. Even when size of the problem does not increase with the number of cracks the free vibration modes are expressed in a recurrence manner not suitable for explicit calculations.
Among the latter contributions, limited to the presence of the localised bending flexibility only, the work proposed by Khiem and Hung [2] stands out for the formulation of an explicit closed form solution of the free vibration modes of the multi-cracked Timoshenko beam. However, the closed form expression therein proposed is always founded on the sub-division of the discontinuous beam into undamaged beam segments.
In order to dismantle the governing equation fragmentation of the multi-cracked Timoshenko beam, in this work an original distributional model, to account for axial, flexural and shear concentrated flexibilities due to multiple cracks, is presented. New governing equations of the Timoshenko beam, enriched by suitable distributional terms, over a single integration domain are formulated.

Precisely, the axial strain $\varepsilon(\xi,t)$, the shear strain $\gamma(\xi,t)$ and the curvature function $\chi(\xi,t)$ are characterised by $n$ occurrences of Dirac's deltas $\delta(\xi-\xi_i)$, representing the distributional derivative of the unit step Heaviside generalised function $U(\xi-\xi_i)$, as follows:

$$\begin{aligned}
\varepsilon(\xi,t) &= \bar{\varepsilon}(\xi,t)+\frac{1}{L}\sum_{i=1}^{n}\Delta u_{x,i}(t)\delta(\xi-\xi_i)\\
\gamma(\xi,t) &= \bar{\gamma}(\xi,t)+\frac{1}{L}\sum_{i=1}^{n}\Delta u_{z,i}(t)\delta(\xi-\xi_i)\\
\chi(\xi,t) &= \bar{\chi}(\xi,t)+\frac{1}{L}\sum_{i=1}^{n}\Delta \varphi_{i}(t)\delta(\xi-\xi_i)
\end{aligned} \tag{1}$$

where the discontinuities are given in terms of the axial $\lambda_{x,i}$, shear $\lambda_{z,i}$ and bending $\lambda_{\varphi,i}$ crack flexibilities as follows:

$$\Delta u_{x,i}=\lambda_{x,i}\,u_x^I(\xi_i^-,t) \quad , \quad \Delta u_{z,i}=\lambda_{z,i}\left[u_z^I(\xi_i^-,t)+L\varphi(\xi_i^-,t)\right] \quad , \quad \Delta\varphi_i=\lambda_{\varphi,i}\,\varphi^I(\xi_i^-,t) \tag{2}$$

The governing differential equations of the above distributional model formulated over a unique integration domain can be expressed as follows in terms of time independent spatial vibration modes $u_x(\xi), u_z(\xi), \varphi(\xi)$ by means of the introduction of additional distributional terms:

$$\begin{aligned}
&u_x^{II}(\xi)+\mu^4\rho^2u_x(\xi)=\sum_{i=1}^{n}\lambda_{x,i}u_x^I(\xi_i^-)\delta^I(\xi-\xi_i)\\
&u_z^{IV}(\xi)+K_1u_z^{II}(\xi)+K_2u_z(\xi)=\sum_{i=1}^{n}\left[\Delta u_{z,i}\delta^{III}(\xi-\xi_i)-\Delta\varphi_iL\delta^{II}(\xi-\xi_i)+\mu^4\rho^2\Delta u_{z,i}\delta^I(\xi-\xi_i)\right]\\
&\varphi^{IV}(\xi)+K_1\varphi^{II}(\xi)+K_2\varphi(\xi)=\sum_{i=1}^{n}\left[\Delta\varphi_i\delta^{III}(\xi-\xi_i)+\mu^4\eta^2\Delta\varphi_i\delta^I(\xi-\xi_i)-\frac{1}{L}\mu^4\Delta u_{z,i}\delta(\xi-\xi_i)\right]
\end{aligned} \tag{3}$$

where $K_1=\mu^4(\rho^2+\eta^2)$, $K_2=\mu^4(\mu^4\eta^2\rho^2-1)$, the frequency parameter $\mu^4=\omega^2mL^4/EI$ and the parameters $\rho^2=I/AL^2$ and $\eta^2=EI/(\kappa GAL^2)$ have been introduced and $\omega$ is the natural frequency. Equations (3) can be integrated in closed form leading to the following explicit expressions:

$$u_x(\xi)=\sum_{k=1}^{2}G_k f_{x,k}(\xi), \qquad u_z(\xi)=\sum_{j=1}^{4}R_j f_{z,j}(\xi), \qquad \varphi(\xi)=\sum_{j=1}^{4}R_j f_{\varphi,j}(\xi) \tag{4}$$

where $f_{x,k}(\xi),\ f_{z,j}(\xi),\ f_{\varphi,j}(\xi)$ are frequency dependent generalised functions accounting for the superposition of spatial waves influenced by the presence of cracks and $G_k,\ k=1,2,\ R_j,\ j=1,...,4,$ boundary condition dependent integration constants.

Classical imposition of ad hoc boundary conditions at both ends of the multi-cracked beam, by making use of the explicit solution reported in Eq. (4) leads to the characteristic equation providing the natural frequencies $\omega$. The free vibration modes for each natural frequency are given by evaluating the integration constants and replacing in Eq. (4).

As an example, the frequency decay with respect to the undamaged beam versus an increasing number of cracks propagating in the middle of a clamped-clamped beam is plotted in Fig.1. It has to be remarked that the minimal change in the second natural frequency is strictly dependent on the crack distribution in the vicinity of a position of a zero curvature causing a small influence of the bending flexibility (no influence at all in the case of a single crack in the middle zero curvature cross-section). Nevertheless, the frequency change is still influenced by the presence of the localised shear crack flexibility.

Based on the closed form solution in Eq. (4) the explicit frequency dependent relationship between the end displacements and the related end forces for the multi-cracked beam can be inferred. A proper formulation of a new damaged spectral Timoshenko beam element is formulated together with its dynamic stiffness matrix. The assemblage of spectral elements is appropriate for the analysis of damaged frames. The latter can be used either for the forced vibration analysis in the frequency domain as well as the evaluation of the natural frequencies by making use of the Wittrick and Williams algorithm.

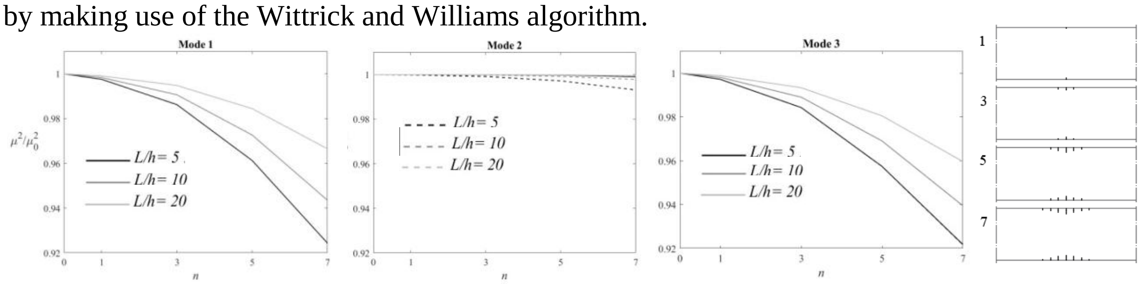


**Figure 1.** Clamped-clamped beam**:** first, second and third frequency ratio versus number of cracks for different slenderness ratio and schematization of the location and depth of the cracks.

An example of evaluation of the first six natural frequencies with the proposed approach is reported in Tab.1 for a frame in the presence of two cracks already analysed in [3] by subdivision of each cracked beam into three elements. The proposed approach and that presented in [3] show coincident results. The relevant mode shapes are depicted in Fig.2.

**Table 1.** Comparison of natural angular (Hz) for the double cracked frame analysed in [3].

| Frequency | $f_1$ | $f_2$ | $f_3$ | $f_4$ | $f_5$ | $f_6$ |
|---|---|---|---|---|---|---|
| Proposed model [Hz] | 14,823 | 58,413 | 94,965 | 103,146 | 206,652 | 254,073 |
| Sun [3] [Hz] | 14,82 | 58,41 | 94,97 | 103,15 | 206,65 | 254,07 |

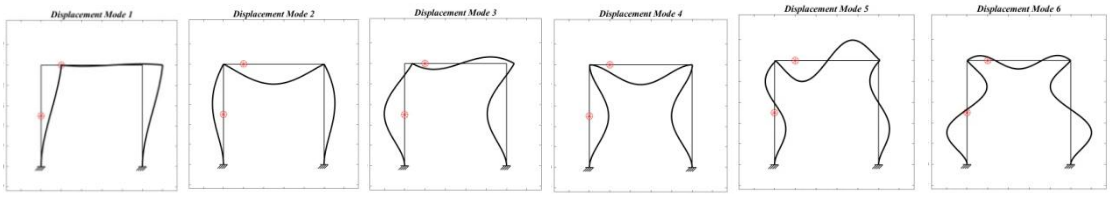


**Figure 2.** First six displacement mode shapes for the portal frame with two cracks analysed in [3].

The governing equations of the damaged Timoshenko beam formulated in Eq. (2) can be enriched by additional Dirac's delta terms to model the action of point loads at a generic abscissa of the beam axis. The solution of the generalised governing equations in the presence of point loads provides the explicit expressions of the so-called Green's functions. Suitable convolution of the Green's functions allows the evaluation of the response to any load of the multi-cracked Timoshenko beam.

## References


[1] Aydin, K.; "Vibratory characteristics of axially-loaded Timoshenko beams with arbitrary number of cracks," Journal of Vibration and Acoustics, Vol. 129, pp. 341-354, 2007.

[2] Khiem, T.; Hung, D. T.; "A closed-form solution for free vibration of multiple cracked Timoshenko beam and application," Vietnam Journal of Mechanics, Vol. 39, No. 4, pp. 315-328, 2017.

[3] Sun, X.; "The application of the Wittrick-Williams algorithm for free vibration analysis of cracked skeletal structures," Thin-Walled Structures, Vol. 159, pp. 1-13, 2021.

# Electromechanically Tunable Topological Interface States for Plate Bending Waves

**Yingjie Chen[*], Bin Wu[*#], Michel Destrade[#], Weiqiu Chen[*]**

[*] Department of Engineering Mechanics
Zhejiang University
No. 38, Zheda Road, 310027
Hangzhou, China
chenwq@zju.edu.cn

# School of Mathematical and Statistical Sciences
University of Galway
University Road, Galway, Ireland
bin.wu@nuigalway.ie

**Summary**

Topological mechanics is a new research front of mechanics, which deals with the interesting topology-related phenomena that cannot be observed macroscopically in traditional materials and structures [1]. These phenomena have already been predicted by quantum mechanics theory for microscopic systems, but only recently were they realized in macroscopic ones. The key is to take advantage of the microstructure in a macroscopically homogenized material, which is now widely called metamaterial or metastructured material [2].

A properly designed elastic metamaterial can exhibit an unusual wave propagation behavior (e.g. a topologically protected, defect-immune edge or interface wave state), which is usually associated with the topology of the unit cells [3-6]. Breaking the time-reversible symmetry or spatial symmetry is the main strategy to achieve the nontrival topological phase transition, leading to the unusual topological edge or interface wave states.

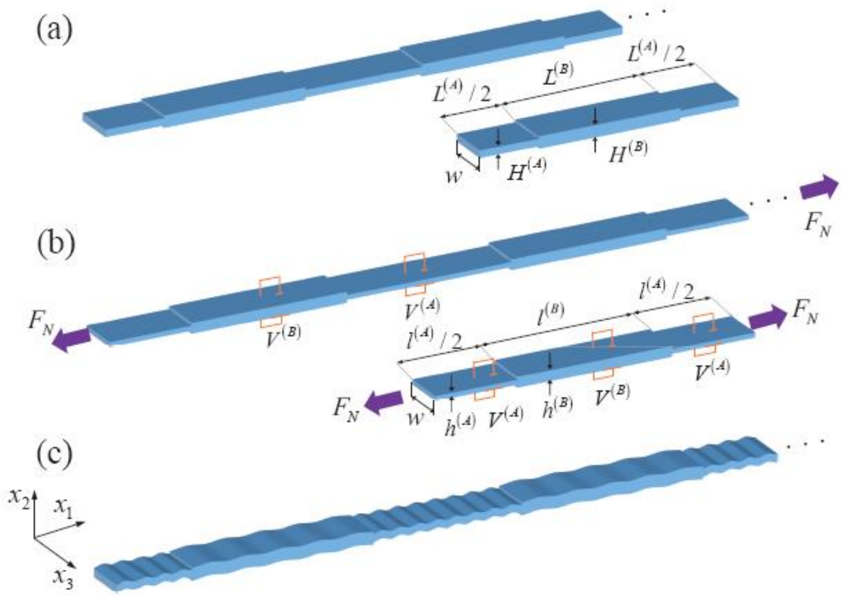


**Figure 1.** A soft dielectric plate (infinite along $x_3$ and periodic in $x_1$) with step-wise cross-sections: (a) undeformed configuration; (b) deformed configuration when subjected to an axial force $F_N$, as well as electric voltages $V^{(A)}$ and $V^{(B)}$ in the thickness direction; (c) incremental bending waves in the deformed plate in (b).

The frequency range for topological edge or interface states in a fixed design of mechanical metamaterial is usually very narrow. Here, we report a design of an electromechanically tunable topological interface state in a soft dielectric elastomer plate structure, see Fig. 1. The frequency range of the bending waves along $x_1$ (the axial direction) in the plate (with an infinite size in the $x_3$ direction) can be adjusted by applying the axial force and the transverse electric voltages as indicated in the figure.

Under the external mechanical and electric stimuli, the plate, which is periodic along $x_1$, deforms significantly. We have to employ the nonlinear electroelastic theory (in the absence of damping) to predict the deformed configuration [7]. To predict the elastic waves superimosed on the static deformation, one needs to adopt the linear incremental theory, which can be derived by perturbation from the general nonlinear theory. A key point is to calculate the instantaneous electroelastic moduli tensors according to the following formulas:

$$\begin{aligned} &\mathcal{A}_{0piqj} = J^{-1}F_{p\alpha}F_{q\beta}\mathcal{A}_{\alpha i\beta j} = \mathcal{A}_{0qjpi}, \quad \mathcal{M}_{0piq} = F_{p\alpha}F_{\beta q}^{-1}\mathcal{M}_{\alpha i\beta} = \mathcal{M}_{0ipq}, \\ &\mathcal{R}_{0ij} = JF_{\alpha i}^{-1}F_{\beta j}^{-1}\mathcal{R}_{\alpha\beta} = \mathcal{R}_{0ji} \end{aligned} \tag{1}$$

where $F_{p\alpha}$ is the deformation gradient tensor corresponding to the deformed configuration, $J$ is the volume ratio (= 1 for incompressible materials), and

$$\begin{aligned} &\mathcal{A}_{\alpha i\beta j} = \partial^2\Omega / (\partial F_{i\alpha}\partial F_{j\beta}), \quad \mathcal{M}_{\alpha i\beta} = \partial^2\Omega / (\partial F_{i\alpha}\partial \mathcal{D}_{\beta}), \\ &\mathcal{R}_{\alpha\beta} = \partial^2\Omega / (\partial \mathcal{D}_{\alpha}\partial \mathcal{D}_{\beta}). \end{aligned} \tag{2}$$

where $\Omega$ is the energy density function, and $\mathcal{D}_{\alpha}$ is the Lagrangian electric displacement vector. As can be seen from Eqs. (1) and (2), applying the pre-deformation $F_{p\alpha}$ as well as the biasing electric displacement $\mathcal{D}_{\alpha}$ changes the instantaneous electroelastic properties of the deformed plate, which further endows it with the capability of tuning the elastic wave propagation behavior.

We employ the spectral element method which is numerically stable to predict the bending wave propagation characteristics in the deformed plate, based on the classical elastic plate assumptions. In the following numerical simulations, we set the geometric parameters of the undeformed unit cell as: $L^{(A)} = L(1+\delta)/2$ and $H^{(A)}$ =1 cm for the length and thickness of sub-plate $A$; for sub-plate $B$, the length is $L^{(B)} = L(1-\delta)/2$ with the thickness being $H^{(B)}$ = 3 cm, where $L$ = 15 cm is the total length of the unit cell and $\delta$ is a structural parameter ranging from –1 to 1. For the commercial product Fluorosilicone 730, the initial density, shear modulus and relative permittivity of the soft dielectric plate are $\rho$ = 1400 kg/m$^3$, $\mu$ = 167.67 kPa and $\varepsilon_r$ = 7.11, respectively. We define the dimensionless axial force as $\bar{F}_N = F_N / \mu w H^{(B)}$. The frequency $f$ is measured in Hz.

As shown in Figs. 2(a)–(c), with a decrease in $\delta$ the second bandgap (BG) for $V^{(A)} = V^{(B)} = 0$ closes at the center of the Brillouin zone, where a linear crossover, termed the Dirac cone, occurs and marks a topological transition point. We see that the occurrence of BG degeneracy at $\delta$ = –0.659 corresponds to the case where sub-plates $A$ and $B$ are not equally divided in the unit cell. The second BG may reopen when decreasing $\delta$ further. Hence, varying the geometrical parameter $\delta$ can result in the second BG being open, closed and open again. This band inversion process is related to the exchange of topological phase. The Zak phase of isolated passbands is marked in magenta in Fig. 2. According to Figs. 2(a) and (c), we see that for configurations S1 ($\delta$=–0.3) and S2 ($\delta$=–0.8), the Zak phase of the first band is 0; S1 and S2 have an overlap part in the second BG frequency range; and when the soft dielectric plate turns from S1 to S2, the Zak phase of the second passband undergos a transition from $\pi$ to 0. This indicates that the topological phase transition is nontrival, and we can make a mixed plate structure to support the topological interface state. More details can be found in our recent work [8].

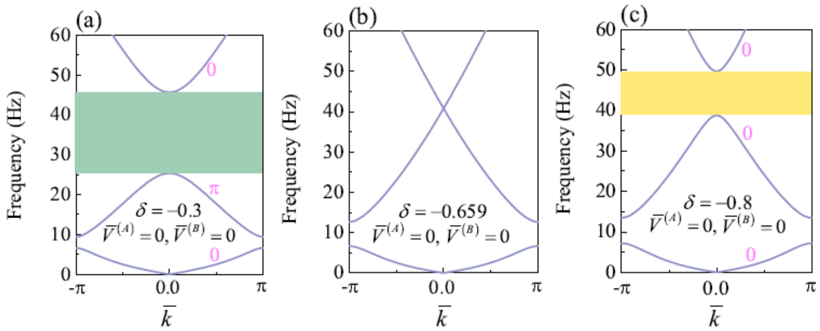


**Figure 2.** Band structures of bending waves in the dielectric plate of Gent hyperelastic model without axial force ($F_N$ = 0) for different electric voltages and initial geometrical parameter $\delta$: (a)–(c) topological transition process in the absence of electric voltage for three different values of $\delta$, respectively. $k$ with an overbar is the dimensionless Bloch wave number .

## References


[1] Huber, S.D.: Topological mechanics. Nature Physics, Vol. 12, pp. 621-623, 2016.

[2] Wang, Y.F.; Wang, Y.Z.; Wu, B.; Chen, W.Q.; Wang, Y.S.: Tunable and active phononic crystals and metamaterials. Applied Mechanics Reviews, Vol. 72, no. 040801, 2020.

[3] Wang, P.; Lu, L.; Bertoldi, K.: Topological phononic crystals with one-way elastic edge waves. Physical Review Letters, Vol. 115, no. 104302, 2015.

[4] Zhou, W.J.; Chen, W.Q.; Destrade, M.; Lim, C.W.: Actively controllable topological phase transition in phononic beam systems. International Journal of Mechanical Sciences, Vol. 180, no. 105668, 2020.

[5] Zhou, W.J.; Wu, B.; Chen, Z.Y.; Chen, W.Q.; Lim, C.W.; Reddy, J.N. : Actively controllable topological phase transition in homogeneous piezoelectric rod system. Journal of the Mechanics and Physics of Solids, Vol. 137, no. 103824, 2020.

[6] Chen, Y.J.; Wu, B.; Li, J.; Rudykh, S.; Chen, W.Q.: Low-frequency tunable topological interface states in soft phononic crystal cylinders. International Journal of Mechanical Sciences, Vol. 191, no. 106098, 2021.

[7] Dorfmann, L.; Ogden, R.W.: Nonlinear Theory of Electroelastic and Magnetoelastic Interactions. Springer, 2014.

[8] Chen, Y.J.; Wu, B.; Destrade, M.; Chen, W.Q.: Voltage-controlled topological interface states for bending waves in soft dielectric phononic crystal plates. International Journal of Solids and Structures, Vol. 259, no. 112013, 2022.

# Dynamic Thermal Stress in a Solid Target of a High-Energy Physics Experiment

**Piotr Cupiał**

Faculty of Mechanical Engineering and Robotics
AGH University of Science and Technology
Al. Mickiewicza 30, Kraków, Poland
pcupial@agh.edu.pl

## Summary

*Background*

In particle physics experiments high-power proton beams interact with solid or liquid targets to produce elementary particles. The beam power is extremely high and in some presently designed experiments can be as high as 5 MW [1]. A proton beam interacts with the target material in a sequence of short pulses repeated at a given frequency. In the future experiment described in [1], a 5 MW beam will be split into four sub-beams, each with a power of 1.25 MW; each pulse will be about 1 μs long, repeated at a frequency of 14 Hz. Only part of the beam power is deposited in the target, which can be estimated using Monte Carlo simulations of the interaction of protons with the target material. Beams with nanosecond pulse lengths are also considered for some future experiments.

Different solid target geometries have been used in the past, including rods, circular discs or cylinders, as well as targets of more complex composition. In the experiment described in [1], the aim of which will be to study CP symmetry violation for neutrinos, it is proposed to use the so-called pebble-bed (or granular) target, which consists of a large number of small spheres with 3 mm diameter, randomly packed inside a cylindrical container 3 cm in diameter and 78 cm long. The study of the stress levels in solids under short thermal pulses is of great importance. Some commercial finite element codes are available that allow for such calculations, e.g., LS-Dyna. However, due to a short pulse length, much care needs to be exercised in the choice of the mesh size and the time step in order to obtain reliable results. Since a very fine mesh and very short time steps need to be used, the computational time can be long, especially for three-dimensional geometries. This makes the study of the influence of various parameters (including the pulse length, the sphere diameter or the material used) burdensome. Therefore, analytical models are of much usefulness. Stress calculations have been done using a wave approach (d'Alembert's solution) in [2], the mode superposition method in [3] for rods, discs and cylinders, and for a sphere in [4], by expanding dynamic stress in terms of vibration modes. In this summary some results of thermal shock in a sphere caused by a single proton beam pulse are discussed. More detailed discussion can be found in [4].

*Formulation of the problem*

Under a spherical symmetry condition the radial displacement is obtained as the solution of:

$$\frac{\partial^2 u(r,t)}{\partial r^2} + \frac{2}{r}\frac{\partial u(r,t)}{\partial r} - \frac{2u(r,t)}{r^2} = \frac{1+\nu}{1-\nu}\alpha\frac{\partial T(r,t)}{\partial r} + \frac{1}{c_1^2}\frac{\partial^2 u(r,t)}{\partial t^2} \qquad (1)$$

with boundary conditions:

$$u(0,t) = 0, \qquad (1-\nu)\frac{\partial u(R,t)}{\partial r} + 2\nu\frac{u(R,t)}{R} = (1+\nu)\alpha T(R,t) \tag{2}$$

Here: ν is Poisson's ratio, α – linear thermal expansion coefficient, $c_1$ is the speed of propagation of the longitudinal wave, $R$ stands for the sphere radius and $T$ is the temperature above that of the neutral undeformed state. It is taken that the outer surface of the sphere is free from surface tractions.

It is further assumed that the proton beam deposits energy uniformly inside the volume of a sphere, which is a realistic approximation for sphere sizes small compared to the beam transverse size. The solution to problem (1), (2) can be obtained as the sum of a quasi-static and a dynamic term:

$$u(r,t) = \alpha T(t) r + u_2(r,t) \tag{3}$$

One can verify that for a sphere which is not restrained on its surface the quasi-static term does not contribute to stress. The dynamic part of solution (3) satisfies:

$$\frac{\partial^2 u_2(r,t)}{\partial r^2} + \frac{2}{r}\frac{\partial u_2(r,t)}{\partial r} - \frac{2u_2(r,t)}{r^2} = \frac{1}{c_1^2}\alpha r \ddot{T}(t) + \frac{1}{c_1^2}\frac{\partial^2 u_2(r,t)}{\partial t^2} \tag{4}$$

The second of boundary conditions (2) is homogenous when expressed in terms of the dynamic displacement $u_2(r,t)$, therefore the solution of Eq. (4) can be sought as a series of the vibration modes of a sphere [4]. The stress is then calculated using the displacement thus obtained. Since temperature increases linearly during the pulse, the second time derivative of temperature in Eq. (4) is given as follows:

$$\ddot{T}(t) = \frac{T_0}{\tau}[\delta(t) - \delta(t-\tau)] \tag{5}$$

where $T_0$ is the temperature increase caused by a complete pulse, calculated from the known energy deposited by the pulse in one kilogram of the material of the sphere, τ is the pulse duration and $\delta$ is Dirac's delta.

*Some numerical results and discussion*

The response depends on the pulse duration relative to the time it takes for a stress wave to travel the distance equal to the sphere radius. Figure 1 shows the radial component of stress vs. time for a sphere of diameter 1 mm made of titanium, for a long and short pulse, respectively. The following material constants have been used in obtaining the plots: mass density $\rho=4.5\cdot10^3$ kg/m$^3$, Young's modulus $E=1.06\cdot10^{11}$ N/m$^2$, $\nu=0.34$, $\alpha=8.4\cdot10^{-6}$ 1/K. Both plots have been obtained under the conditions of a linear temperature rise of 100 K during the pulse length. A small amount of modal damping has been used, with the same modal damping ratio of each mode equal to 0.002. The number of terms in the series solution required to ensure convergence of the computed stress depends on the pulse length. For very short pulses 5000 terms have been used without encountering numerical instability problems.

Figure 1a shows the response to a pulse 1.2 μs long. This time is 7.2 times longer that the time the stress wave takes to travel the distance equal to the sphere radius. Oscillations with the lowest

frequency are clearly visible in Fig. 1a. Higher order modes have also a significant contribution to the dynamic stress. The stress level is quite acceptable. Fig. 1b is for a pulse length 50 times shorter than that shown in Figure 1a. Stress spikes appear at the sphere core, the first of which corresponds to the time required for the wave to travel the distance of the sphere radius. Subsequent spikes occur at 3, 5 … times this time. This is because the wave has to travel the distance of the radius twice to return to the sphere centre again. The magnitude of stress near the sphere core is prohibitively high, for the same temperature increase as for a long pulse. It can be seen that apart from the temperature rise, the major parameter that determines the stress level is the non-dimensional pulse length (pulse length relative to the time of wave propagation over a characteristic distance). Therefore, dynamic stress can be reduced by using spheres with a smaller radius. However, for the shorter of the two pulses considered in Figure 1 spheres with unrealistically small radii would have to be used to ensure acceptable stress levels.
The spikes appear as a result of a constructive superposition of the contribution from many vibration modes. It is expected that stress focusing will be sensitive to the assumption of the perfect symmetry of energy deposition inside the sphere. The effect of non-symmetric energy deposition is under investigation.

a) b)

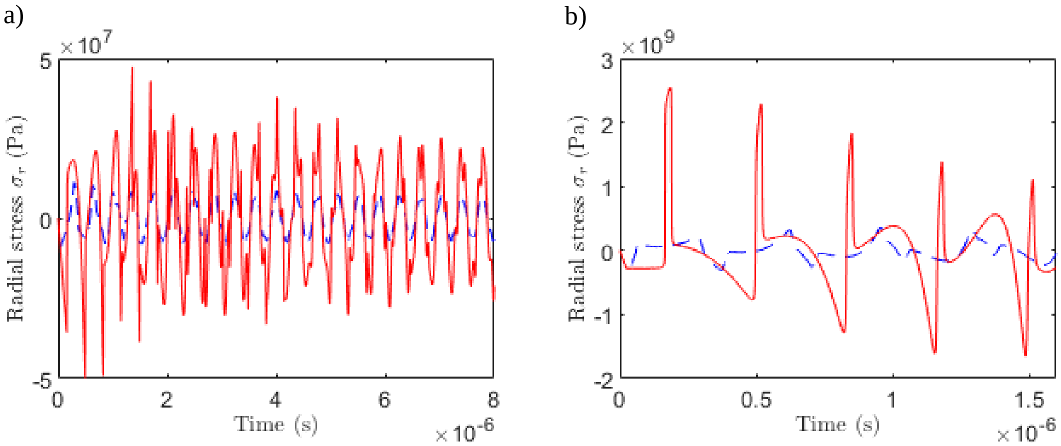


Figure 1: Radial stress for a titanium sphere of radius 1mm, for a pulse length 1.2 μs a) and 0.024 μs b). Solid line shows the stress history at the sphere core, the dashed line corresponds to r=0.75 mm.

## References

[1] Alekou A, *et al.*: The European Spallation Source neutrino superbeam conceptual design report. European Physical Journal Special Topics, Vol. 231, No. 21, pp. 3779–3955, 2022

[2] Bergmann H.: Dynamic response of external targets under thermal shock. CERN LAB.II/BT/Int./73-3, 1973.

[3] Sievers P.: Elastic stress waves in matter due to rapid heating by an intense high-energy particle beam. CERN LAB.II/BI/74-2, 1974.

[4] Cupiał P.: Thermal shock in a sphere due to a proton beam pulse, Journal of Thermal Stresses, Vol. 46, pp. 387–398, 2023.

# Nonlinear Vibration and Control of Pipes Conveying High-speed Fluid

**Hu Ding***

* School of Mechanics and Engineering Science,
Shanghai University,
Shanghai 200444, China
dinghu3@shu.edu.cn

## Abstract

As an essential engineering structure, high-speed fluid conveying pipes are widely used in various engineering fields such as aerospace engineering, petroleum engineering and nuclear industry. With the excitation of internal fluid and external environment, pipes in operation will inevitably undergo excessive vibration, which may cause structural damage. Therefore, the dynamic modeling and analysis of pipes conveying high-speed fluid are very necessary. In this work, the following questions are addressed: How to establish a dynamic model of the pipe and its constraints? How to analyze pipe vibration response with nonlinear boundary conditions? What are the differences in the effect of high-speed flow on pipe vibration? What is the influence of the configuration of curved pipe on its vibration? And how to control the vibration? A dynamic model of a curved pipe is established by means of the generalized Hamiltonian principle and absolute node coordinate method, respectively. Considering the width and thickness of the clip, a pipe dynamic model with elastic clip constraints was established. Nonlinear modal methods are developed to deal with pipe vibration responses with nonlinear boundaries. The pipe vibration characteristics at subcritical and supercritical flow velocities are studied and compared. In particular, the effect of the degree of curvature is investigated. Finally, several methods to control pipe vibration are proposed. Therefore, this work is a brief summary of dynamic modeling, analysis and vibration control of pipes conveying high-speed fluid.

## 1. Introduction

Pipes conveying fluids, like muscles of human body, control the attitude and maneuver of a mechanical system [1]. Under the influence of aero-engine excitation and hydraulic fluid fluctuation, pipes may have bending resonances and may fracture in flight. The fracture of pipes will cause the loss of hydraulic pressure, affect the movement of the control surface and endanger the safety of aircraft. Therefore, the research of the vibration of pipes conveying fluids is deemed essential. However, the study of pipe dynamics is still insufficient in many aspects. For example, the dynamic modeling of curved pipes, the influence of high-speed flow on pipe vibration, the dynamic modeling of pipe constraint, the dynamic analysis method of pipe under non-ideal boundary conditions, the vibration control of a pipe, etc.

## 2. Equations of Motion

Figure 1 is a schematic diagram of a pipe conveying fluid with fixed-fixed ends and restrained by a middle clip. $L_c$ represents the width of the clip. $L_1$ and $L_2$ are, respectively, the lengths of the pipe on the left and right sides of the clip. The total length of the integral pipe is $L$. In this work, a rigid body with a certain width is used to model the clip and the constrained pipe, which is connected to the base by vertical and torsional springs at two ends. $K$ is the vertical stiffness of the retaining clip in the $Y$-axis direction. $K_\theta$ describes the torsional stiffness of the clip in the $XOY$ plane. Two coordinate systems, namely $X_1O_1Y_1$ and $X_2O_2Y_2$ are chosen for the pipe on the left and right sides of the clip, respectively. $V_1(X_1, T)$ and $V_2(X_2, T)$ are the transverse vibration displacements of the left pipe and the right pipe in terms of the axial coordinates $X_1$ and $X_2$ and the time $T$, respectively.

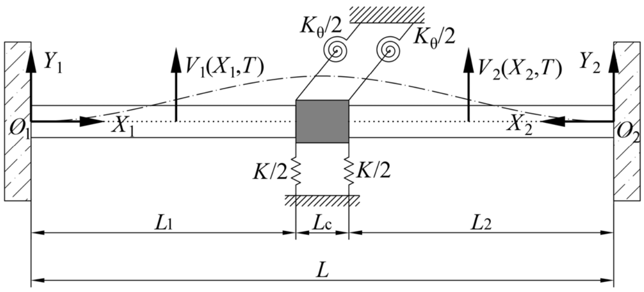


**Figure 1.** A pipe conveying fluid restrained by a clip in the middle.

The natural vibration of the pipe conveying fluid is considered. According to the Euler-Bernoulli beam theory assumption, two differential equations governing the vibrations of the left section and the right section pipe can be derived as follows [1,2]:

$$\begin{aligned}&\left(\rho_\mathrm{p} A_\mathrm{p} + \rho_\mathrm{f} A_\mathrm{f}\right) Y_1,_{TT} + 2\rho_\mathrm{f} A_\mathrm{f} \Gamma Y_1,_{X_1T} + \rho_\mathrm{f} A_\mathrm{f} \Gamma^2 Y_1,_{X_1X_1} \\ &+ EI_\mathrm{b} Y_1,_{X_1X_1X_1X_1} - \frac{EA_\mathrm{p}}{2L}\left(Y,_{X_1X_1} + Y_1,_{X_1X_1}\right)\int_0^L \left(Y_1,_{X_1}^2 + 2Y_1,_{X_1} Y,_{X_1}\right)\mathrm{d}X_1 = 0\end{aligned} \tag{1}$$

$$\begin{aligned}&\left(\rho_\mathrm{p} A_\mathrm{p} + \rho_\mathrm{f} A_\mathrm{f}\right) Y_1,_{TT} + 2\rho_\mathrm{f} A_\mathrm{f} \Gamma Y_2,_{X_2T} + \rho_\mathrm{f} A_\mathrm{f} \Gamma^2 Y_2,_{X_2X_2} \\ &+ EI_\mathrm{b} Y_2,_{X_2X_2X_2X_2} - \frac{EA_\mathrm{p}}{2L}\left(Y,_{X_2X_2} + Y_2,_{X_2X_2}\right)\int_0^L \left(Y_2,_{X_2}^2 + 2Y_2,_{X_2} Y,_{X_2}\right)\mathrm{d}X_2 = 0\end{aligned} \tag{2}$$

The boundary conditions are [3]:

$$\begin{aligned}&EIV_1,_{XXX}\left(L_1,T\right) + EIV_2,_{XXX}\left(L_2,T\right) - \frac{K}{2}V_1\left(L_1,T\right) - \frac{K}{2}V_2\left(L_2,T\right) \\ &- m\left(V_1,_{TT}\left(L_1,T\right) + \frac{L_\mathrm{c}}{2}V_1,_{XTT}\left(L_1,T\right)\right) = 0\end{aligned} \tag{3}$$

$$\begin{aligned}&EIV_1,_{XX}\left(L_1,T\right) + \frac{K_\theta}{2}V_1,_X\left(L_1,T\right) + \frac{L_\mathrm{c}}{2}EIV_1,_{XXX}\left(L_1,T\right) + \frac{L_\mathrm{c}}{2}\frac{K}{2}V_2\left(L_2,T\right) + JV_1,_{XTT}\left(L_1,T\right) \\ &- EIV_2,_{XX}\left(L_2,T\right) - \frac{K_\theta}{2}V_2,_X\left(L_2,T\right) - \frac{L_\mathrm{c}}{2}EIV_2,_{XXX}\left(L_2,T\right) - \frac{L_\mathrm{c}}{2}\frac{K}{2}V_1\left(L_1,T\right) = 0\end{aligned} \tag{4}$$

where $E$ is the Young's modulus of the pipe, and $I$ represents the area moment of inertia. $\rho_\mathrm{p}$ and $A_\mathrm{p}$ are the density and the cross-sectional area of the uniform pipe, respectively. $\rho_\mathrm{f}$ and $A_\mathrm{f}$ stand for the density and the cross-sectional area of the fluid, respectively, where $m$ is the total mass of the clip and the constrained pipe within the clip width. $J$ denotes the rotational inertia of the clip and the constrained pipe within the clip width. $Y(X) = A_0 \sin(\pi X/L)$ is the initial curvature.

## 3. Vibration of the pipe

As shown in Figs. 2(a)-2(b), when the initial curvature is increased, the natural frequency of the pipe with simply supported ends decreases with the increase in the flow velocity $\Gamma$ in the subcritical regime. On the contrary, in the supercritical regime, the natural frequency increases with the increase in the velocity [1].

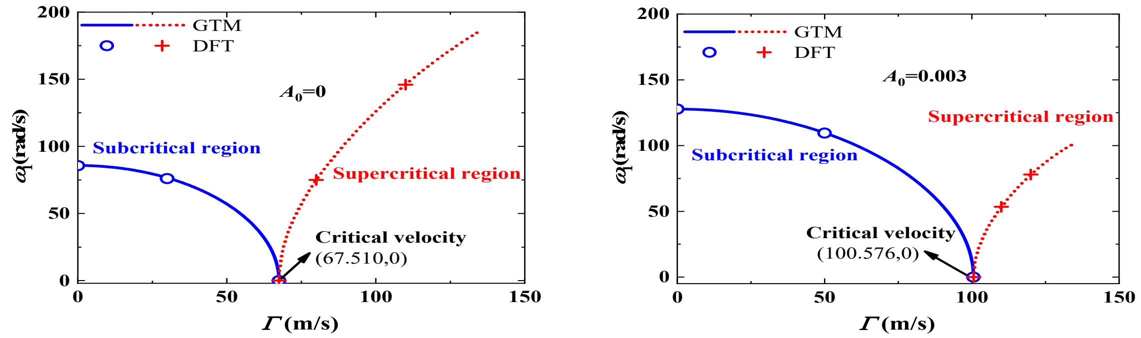


(a) $A_0 = 0$ (b) $A_0 = 0.003$m

**Figure 2.** Natural frequencies for different initial curvature values $A_0$

Figure 3 illustrates the effect of the clip torsional stiffness on the natural frequencies and vibration modes of the integral pipe and the half pipe. The small figures depict the vibration modes of the half pipe and the integral pipe. It can be found that the vibration frequency of the pipe is particularly sensitive to the weak clip stiffness. With the increase of the clip torsional stiffness, the vibration frequencies of the integral pipe and the half pipe tend to be close [3].

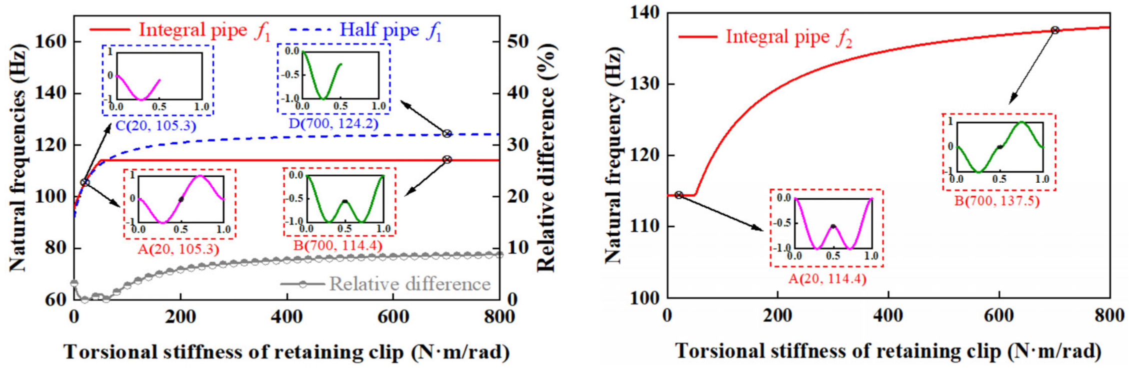


(a) the first order (b) the second order

**Figure 3.** Effect of the clip torsional stiffness on the natural frequencies and vibration modes

## Acknowledgments

The authors gratefully acknowledge the support of the National Natural Science Foundation of China (No. 12025204).

## References

[1] Ye, S.Q., Ding, H., Wei, S., Ji, J.C. and Chen, L.Q.: Non-trivial equilibriums and natural frequencies of a slightly curved pipe conveying supercritical fluid. Ocean Eng. 227, 108899 (2021)

[2] Deng, T.C., Ding, H., Chen, L.Q. Critical velocity and supercritical natural frequencies of fluid-conveying pipes with retaining clips. Int J Mech Sci. 222, 107254 (2022)

[3] Dou, B., Ding, H., Mao, X.Y., Feng, H.R. and Chen, L.Q.: Modeling and parametric studies of retaining clips on pipes. Mech Syst Signal Pr. 186, 109912 (2023)

# Analytical Solutions for Vibrations of Shallow Shells with All Possible In-Plane and Out-of-Plane Combinations of Boundary Conditions

**Moshe Eisenberger** [*], **Aharon Deutsch** [#]

[*] Faculty of Civil and Env. Engng.
Technion – Israel Inst. of Technology
Technion City, Haifa, Israel
cvrmosh@technion.ac.il

[#] Cobus and
Faculty of Civil and Env. Engng.
Technion – Israel Inst. of Technology
Technion City, Haifa, Israel
tvruis@gmail.com

**Summary**

New analytical solutions for vibrations of shallow shells with two principal constant curvatures are presented in this work. The new solutions address all different cases of in-plane and out-of-plane boundary conditions, and provide insight into the dynamics of such shells. The formulation is here applied to cylindrical, spherical, elliptical paraboloidal, and hyperbolic paraboloidal shallow shells, as illustrated in Figure 1. Previous works in this field have only addressed one possible set of in-plane restraints for such shells[1-4], simply supported out-of-plane restraints and shear diaphragm in-plane restraints.

| *Spherical* | *Cylindrical* | *Hyperbolic* | *Paraboloidal* |
|---|---|---|---|
| *Rx = Ry = 100* | *Rx = 100; Ry = 10000* | *Rx = 100; Ry = -150* | *Rx =100; Ry = 200* |

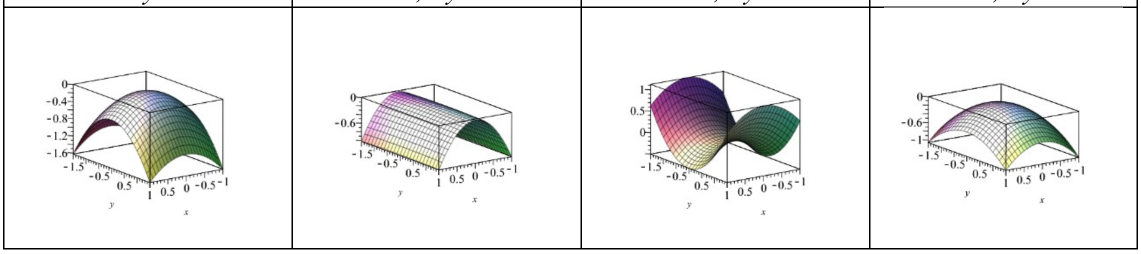

Figure 1: Sample shallow shells with two principle constant curvatures

The linearized equations of motion for the harmonic linear vibrations of shallow shells are three coupled differential equations with three unknowns, u(x,y), v(x,y), and w(x,y), and are given as [1,2]

$$\frac{\partial^2 u}{\partial x^2}+\frac{(1-\nu)}{2}\frac{\partial^2 u}{\partial y^2}+\frac{(1+\nu)}{2}\frac{\partial^2 v}{\partial x\partial y}-\left(\frac{1}{R_x}+\frac{\nu}{R_y}\right)\frac{\partial w}{\partial x}=-\frac{\rho(1-\nu^2)}{E}\frac{\partial^2 u}{\partial t^2} \tag{1}$$

$$\frac{(1+\nu)}{2}\frac{\partial^2 u}{\partial x\partial y}+\frac{\partial^2 v}{\partial y^2}+\frac{(1-\nu)}{2}\frac{\partial^2 v}{\partial x^2}-\left(\frac{\nu}{R_x}+\frac{1}{R_y}\right)\frac{\partial w}{\partial y}=-\frac{\rho(1-\nu^2)}{E}\frac{\partial^2 v}{\partial t^2} \tag{2}$$

$$\left(\frac{1}{R_x}+\frac{\nu}{R_y}\right)\frac{\partial u}{\partial x}+\left(\frac{\nu}{R_x}+\frac{1}{R_y}\right)\frac{\partial v}{\partial y}-\left(\frac{1}{{R_x}^2}+\frac{2\nu}{R_xR_y}+\frac{1}{{R_y}^2}\right)w-\frac{h^2}{12}\nabla^4 w=-\frac{\rho(1-\nu^2)}{E}\frac{\partial^2 w}{\partial t^2} \tag{3}$$

where the origin of the coordinate system is placed at the apex in each case. The possible in-plane and out-of-plane boundary conditions on the four edges are summerized in Table 1:

Table 1: Shell Boundary Conditions

| Out-of-Plane Restraints | | In-Plane Restraints | |
|---|---|---|---|
| C- Clamped | No Deflection, No Rotation | C - Clamped | No Displacements of the Edge |
| S – Simply Supported | No Delfection, No Moment | N – Normal | No Translation Normal to the Edge |
| G - Guided | No Rotaion, No Shear | P – Parallel | No Translation Parallel to the Edge |
| F - Free | No Moment, No Shear | F - Free | No Tractions on the Edge |

The proposed solution for the three displacements is

$$U(x,y) = U_1(x,y) + U_2(x,y) = \sum_{m=1,2,3}^{\infty} S_m(x)\, u_1(y) + \sum_{n=1,2,3}^{\infty} C_n(y)\, u_2(x) \qquad (4)$$
$$V(x,y) = V_1(x,y) + V_2(x,y) = \sum_{m=1,2,3}^{\infty} C_m(x)\, v_1(y) + \sum_{n=1,2,3}^{\infty} S_n(y)\, v_2(x) \qquad (5)$$
$$W(x,y) = W_1(x,y) + W_2(x,y) = \sum_{m=1,2,3}^{\infty} C_m(x)\, w_1(y) + \sum_{n=1,2,3}^{\infty} C_n(y)\, w_2(x) \qquad (6)$$

with $C_m(x) = \cos(\Phi_m(x))$, $S_m(x) = \sin(\Phi_m(x))$, $C_n(y) = \cos(\Phi_n(y))$, $S_n(y) = \sin(\Phi_n(y))$, and $\Phi_m(x) = m\pi\left(\frac{x}{a} - \frac{1}{2}\right)$, $\Phi_n(y) = n\pi\left(\frac{y}{b} - \frac{1}{2}\right)$.
Substitution of the components of the functions, i.e. $U_1$ , $V_1$ , $W_1$ and then $U_2$ , $V_2$ , $W_2$ , into the set of equations of motion will result in six ordinary differential equations [5,6]. The solution of the resulting coupled ordinary differential equations is in the form of hyperbolic functions and 4 constants for each value of *m* and *n*, a total of 8 constants. Applying the set of boundary conditions for the four edges of the shell results in 4 equations for every edge multiplied by the number of terms in the series in Eqs. (4-6). The number of terms is taken equal, *m=n,* as there is no advance knowledge of the resulting modes. All together the number of linear equations that are obtained for the completion of the solution is *16*m*. As on each edge only two values are given by the restaints, the final set is obtained by choosing 8*m equations. The natural frequencies are found when the determinant of the coefficient matrix is zero.

This solution satisfies exactly the coupled diffential equations of motion and approximately the boundary conditions. Increasing the number of terms *m* will increase the accuracy up to the desired value, i.e. until the frequency parameter is unchanged for the number of digits desired.

As an example of the results a comparisson is here made with the Rayleigh-Ritz solution for spherical shell from reference [7] with SSSS-CCCC boundary conditions, and from [4] for the SSSS-PPPP case in Table 2 below. The frequency parameter is defined as $\lambda = \omega a^2\sqrt{\rho h/D}$ . The effect of the in-plane restraints on the frequencies, that was not examined in the past is added for 5 more combinations of boundary conditions.

Table 2: Frequency parameters for SSSS boundary conditions (a/b=1,a/h=20, $\nu$=0.3)

| In-Plane | Mode 1 | Mode 2 | Mode 3 | Mode 4 | Mode 5 | Mode 6 |
|---|---|---|---|---|---|---|
| PPPP | 23.7179 | 51.0271 | 51.0271 | 80.0104 | 99.5331 | 99.5331 |
| PPPP-[4] | 23.70 | 51.04 | 51.04 | 80.02 | - | - |
| NNNN | 27.8516 | 50.9644 | 50.9644 | 79.9519 | 99.5090 | 99.5090 |
| FFFF | 27.8760 | 53.4914 | 53.4914 | 80.0761 | 99.5847 | 99.5847 |
| CCCC | 27.9924 | 51.5169 | 51.5169 | 80.3844 | 99.6434 | 99.6434 |
| CCCC-[7] | 27.99 | 51.52 | 51.52 | 80.40 | 99.64 | 99.79 |
| NNPN | 23.5371 | 50.9439 | 50.9869 | 79.9703 | 98.7996 | 99.5161 |
| FNPC | 24.0553 | 50.0927 | 50.9485 | 79.7715 | 99.4735 | 99.5396 |

From these results one can see that for the symmetric in-plane cases there are repeated values for the second and third, and fifth and sixth parameters. Changing one restraint leads to a split in these, and it is seen in the modes (not shown here). It can be seen that such changes can lead to more then 15% change in the parameter for the first frequency.

For the shallow shells, the present results indicate that specific changes in boundary conditions investigated here have a significant influence on the frequencies and on the modes of vibration.

**References**


[1] Eisenberger, M., Godoy, L.A.: Navier type exact analytical solutions for vibrations of thin-walled shallow shells with rectangular planform, Thin-Walled Structures, Vol. 160, 107356, 2021.

[2] Leissa, A.W. and Kadi, A.S.: Curvature effects on shallow shell vibrations, Jour. of Sound and Vibration, Vol. 16, pp. 173-187, 1971.

[3] Mochida, Y., Ilanko, S., Duke, M., Narita, Y.: Free vibration analysis of doubly curved shallow shells using the Superposition-Galerkin method, Jour. of Sound and Vibration, Vol. 331, pp. 1413-1425, 2012.

[4] Qatu, M.S., Asadi, E.: Vibration of doubly curved shallow shells with arbitrary boundaries, Applied Acoustics, Vol. 73, pp. 21–27, 2012.

[5] Deutsch, A., Eisenberger, M.: Benchmark analytic in-plane vibration frequencies of orthotropic rectangular plates, Jour. of Sound and Vibration, Vol. 541, 117248, 2022.

[6] Eisenberger, M., Deutsch, A.: Solution of thin rectangular plate vibrations for all combinations of boundary conditions, Jour. of Sound and Vibration, Vol. 452, pp. 1-12, 2019.

[7] Ilanko, S., Monterrubio, L.E., Mochida, Y.: The Rayleigh-Ritz Method for Structural Analysis, ISTE and Wiley, 2014.

# Plate Vibration as the Basis for Models of Acoustic Guitar Function

**Mark S. Ewing**
Associate Professor and Director of the Flight Research Laboratory
Department of Aerospace Engineering, University of Kansas, Lawrence, Kansas, USA, mewing@ku.edu

The sounds produced by stringed instruments played in the "acoustic" mode can be largely described in terms of the plate-like modes of vibration of the instrument top surface. At lower frequencies, the resonances of a guitar are actually the result of the coupled motion of the top plate of the guitar (the "sound board") and an "air mass" moving in-and-out of a "port". One simplified model of this coupled motion is based on the model in Figure 1. The guitar top plate is modelled as a piston of equivalent area $A$ and mass $m_p$ connected to a spring of equivalent stiffness $k_p$. The guitar body is modeled as a Helmholtz resonator with an "air mass" piston in its port of area $S$ and mass $m_a$. A pair of differential equations developed by Christensen [2], describe the coupling of the piston-like deflections of the sound board and the air mass:

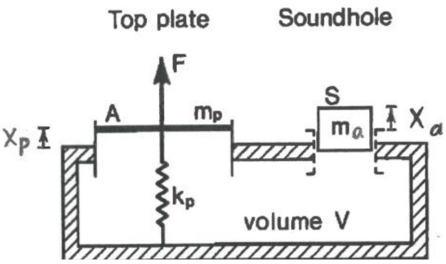


**Figure 1.** Simplified model for guitar function at low frequencies. [Figure copied from Reference 2]

$$m_p\ddot{x}_p = F - x_p\left(k_p + \mu A^2\right) - R_p\dot{x}_p - \mu SAx_a \qquad (1a)$$
$$m_a\ddot{x}_a = -\mu S^2 x_a - R_a\dot{x}_a - \mu SAx_p \qquad (1b)$$

$F$ is the force applied by the bridge of the instrument (due to plucking of the strings), the $R$'s are resistances to piston motion and $\mu$ is a coupling term. Davis [1] used these equations to compute the acoustic radiation of a number of sound boards coupled with a vented box. In Figure 2, these predictions are compared with that of a sound board alone.

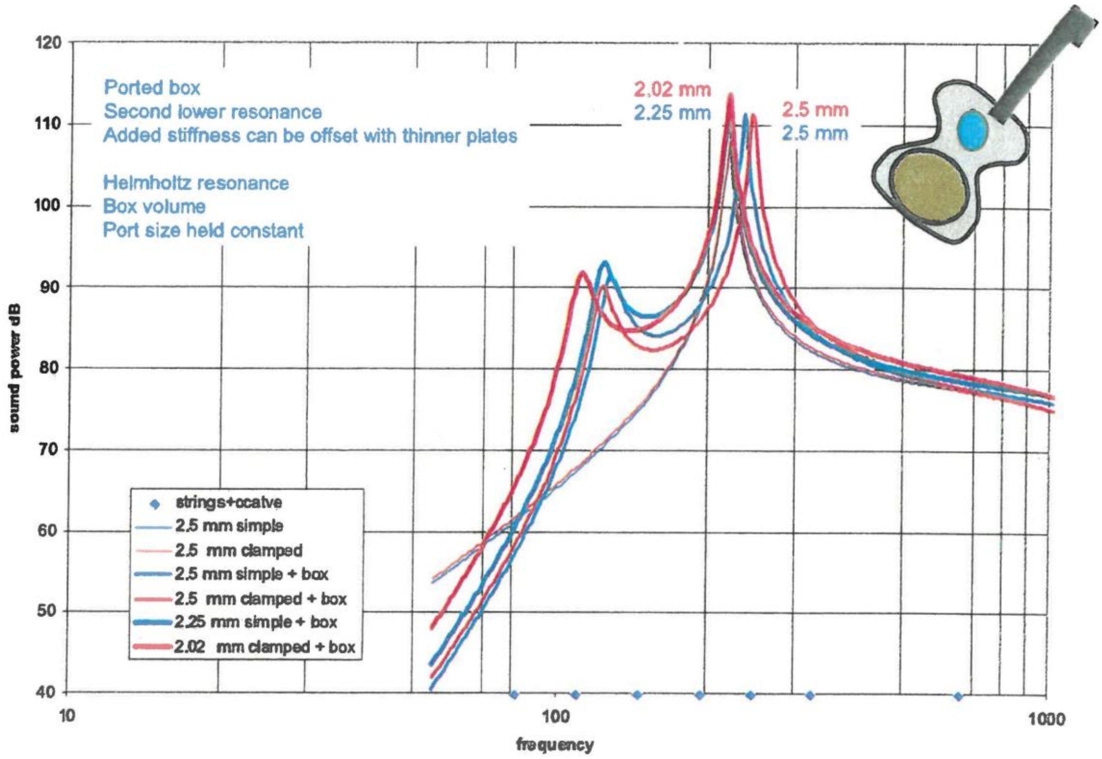


**Figure 2.** Predicted sound power radiated from a uniform-thickness circular plate sound board with a fundamental frequency of 220 Hz (the curve with a single peak) *and* from sound boards coupled with a vented box with a fundamental frequency half that of the sound board. [Figure copied from Reference 1]

Note that the sound power level (SPL) is very closely related to the (velocity) frequency response function more commonly used to express vibratory response in the engineering vibration community. Also note that the boundary condition assumed for the sound board disk (simply-supported or clamped) has only a slight effect on acoustic radiation.

Due to the substantial damping in the coupled system, the acoustic response of the guitar over the interval between these two frequencies is enhanced. Further, above the (coupled) natural frequency of the sound board, the response declines with frequency rather slowly, thereby allowing the radiation of sound at higher frequencies. In fact, a properly-designed guitar has good sound producing qualities over a large frequency range. According to Davis [1], to ensure the wide frequency response of a "good" guitar, the fundamental frequency of the sound board, $f_{wood}$, should be designed (by selection of the guitar dimensions and thicknesses) to be at the geometric mean of: the frequency of the lowest open string, $f_{low\text{-}open}$; and, one octave above the highest open string frequency, that is, at $2f_{high\text{-}open}$. Further, the fundamental frequency of the air mode, $f_{air}$, is best placed at one half of the wood mode, $f_{wood}$. That is:

$$f_{wood} = \sqrt{f_{low-open} * 2 f_{high-open}} \qquad\qquad f_{air} = \frac{f_{wood}}{2} \qquad (2)$$

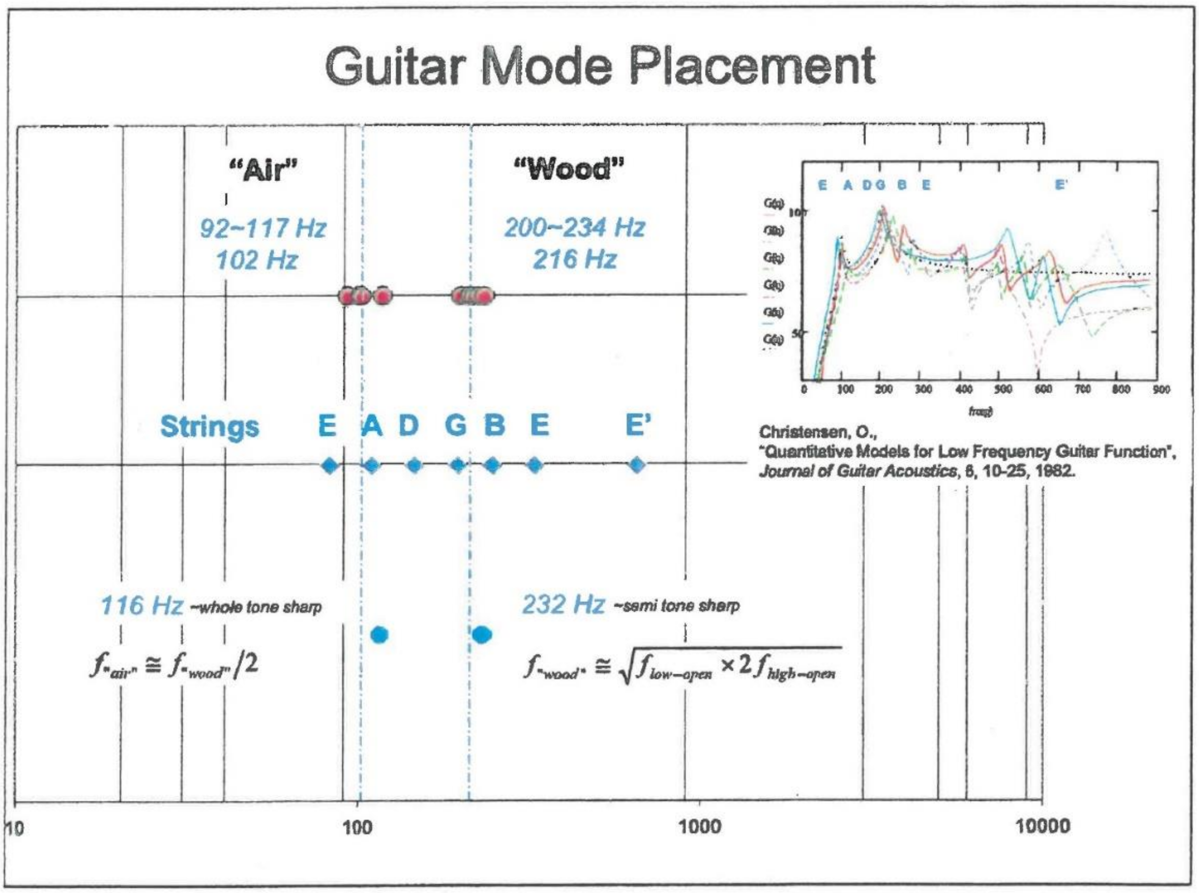


**Figure 3.** Placement of the two lowest guitar natural frequencies (Hz) from measurement and prediction: upper dark, circular markers are $f_{air}$ and $f_{wood}$ for a number of good classical guitars; lower circular markers are $f_{air}$ and $f_{wood}$ calculated from Equations 2; diamond markers are the six open string frequencies. The inset shows the measured SPL versus frequency for classical guitars, originally published by Christensen [2]. [Figure copied from Reference 1]

As shown in Figure 3, the two lowest natural frequency predictions compare well with those measured for five classical guitars. In the inset in Figure 3, the SPL *vs* frequency plots clearly show resonances at frequencies above the “air” and “wood” modes. The response of the guitar at these frequencies, then, extends the favorable radiation of sound to frequencies higher than the lowest two modes.

To explain some of the higher resonances, a description of the higher modes of plate vibration of the top of the instrument is useful. Figure 4 has sketches of the four lowest modes of vibration of a typical guitar. The first mode is responsible for the “wood mode” in the coupled vibration model described earlier.

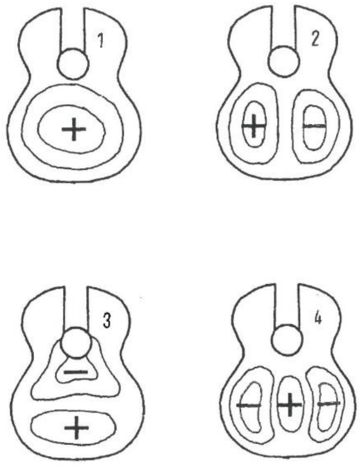


**Figure 4.** Contours of deflection for the first four modes of vibration (labelled 1 to 4) for a typical guitar. [Figure copied from Reference 3]

Now consider the second mode of vibration for a typical guitar, at top-right in Figure 4. This is a mode which is antisymmetric across the line of symmetry; that is, it is aligned with the fingerboard. However, this mode does not radiate well because the oscillatory air velocities above the top plate on either side of the fingerboard ***cancel each other out*** after only a very short distance from the guitar.

However, the next two modes, due to the oblong shape of the guitar body, have regions which radiate well. For mode 3, the upper and lower regions are of differnt sizes and magnitudes of velocity, so there is a net radiation. For mode 4, the two regions on either side of the fingerboard (-), which have motion out of phase with the central region (+), dominate the sound radiation at its natural frequency. As such, the 3rd and 4th modes of the guitar top plate extend the frequency range of the guitar beyond that of the two lower modes described earlier, thereby enhancing the sound of the instrument.

## References

1. Davis, Evan B., “Designing soundboards with flexural disk models”, Proceedings of Meetings of the Acoustical Society of America, May 23 2011. [Proc. Mtgs. Acoust. 12, 035003 (2011)]
2. Christensen, Ove and Vistisen, Bo B., “Simple model for low-frequency guitar function”, Journal of the Acoustical Society of America, vol 68, no 3, September 1, 1980. [J Acoust Soc Am 68(3), 758-766 (1980)]
3. Christensen, Ove, “An Oscillator Model for Analysis of Guitar Sound Pressure Response”, Acta Acustica, vol 54, pages 289-295, 1984.

# Variable-kinematic finite elements for dynamic analyses of rotating structures

**Matteo Filippi***, **Rodolfo Azzara***, **Erasmo Carrera***

* Departement of Mechanical and Aerospace Engineering
Politecnico di Torino
Corso Duca degli Abruzzi 24, 10129, Turin, Italy
matteo.filippi, rodolfo.azzara, erasmo.carrera@polito.it

## Summary

In the *11th International Symposium on Vibrations of Continuous Systems*, we presented the extension of variable-kinematic finite beam elements developed with the Carrera Unified Formulation (CUF) to study the dynamics of rotating structures. In particular, we adopted the so-called node-dependent kinematic (NDK) approach to analyze multi-section rotors. This strategy enabled assemblies consisting of rigid (shaft) and highly deformable (thin disks) components to be modeled by merely modifying the order and the type of structural theory locally. As a result, the NDK finite element (FE) solutions provided accurate results with a considerable reduction of the computational burden if compared with high-fidelity models.

Over the last six years, further advances have been made in the rotordynamics field with the CUF-based finite elements, such as extending the analyses to the geometrically nonlinear regime [1] and deriving formulations for two- and multidimensional models [2, 3, 4]. In particular, the CUF multidimensional models, which consist of solid (3D) and beam (1D) elements, exploit the feature of a specific 1D kinematic formulation that encompasses only displacements as degrees of freedom. This property is shared with conventional solid FEs; therefore, the 1D/3D connection is performed by merely summing inertial and elastic contributions at the interface nodes. Moreover, the unified formalism allows one to derive 3D and 1D FEs. Indeed, the three-dimensional displacement field $\mathbf{u}(x,y,z,t) = (u_x\, u_y\, u_z)$ can be approximated as:

$$
\begin{aligned}
3D-FE &\longrightarrow \mathbf{u}(x,y,z,t) = \mathbf{u}_i(t)\cdot N_i(x,y,z)\cdot 1 && && i = 1\dots N_n^{3D} \\
1D-FE &\longrightarrow \mathbf{u}(x,y,z,t) = \mathbf{u}_{i\tau}(t)\cdot N_i(y)\cdot F_\tau(x,z) && \tau = 1\dots M; && i = 1\dots N_n^{1D}
\end{aligned} \quad (1)
$$

where $N_i$ are the lagrangian 1D and 3D FE shape functions, $F_\tau$ are the functions used to approximate the solution over the beam cross-section ($x-z$ plane), while $\mathbf{u}_{i\tau}(t)$ and $\mathbf{u}_i(t)$ are the vectors of unknown coefficients. The index $i$ refers to the finite element approximation, and it ranges from 1 to the maximum number of element nodes, which is $N_n^{3D}$ for the solid and $N_n^{1D}$ for the beam. The subscript $\tau$ is related to the expansion used for defining the cross-sectional kinematics, and its maximum value, $M$, is an input parameter of the analysis. As mentioned above, the connection between 1D and 3D finite elements is particularly simple when the so-called Lagrange-type expansions (LE) are used. The LE kinematics is obtained by combining Lagrange polynomials defined within sub-regions (or elements) delimited by an arbitrary number of points (or nodes). Figure 1 schematically illustrates the idea behind the methodology. Among various problems, multidimensional models are highly advantageous to analyzing structures with complicated geometries, such as swept-tip helicopter blades. The 3D-FE formulation used in Refs. [3, 4], however, limited the proposed CUF multidimensional model to small displacements and rotations. Such a hypothesis is acceptable for most operational conditions of a rotating blade, but it might be too restrictive when the rotational speed is not high

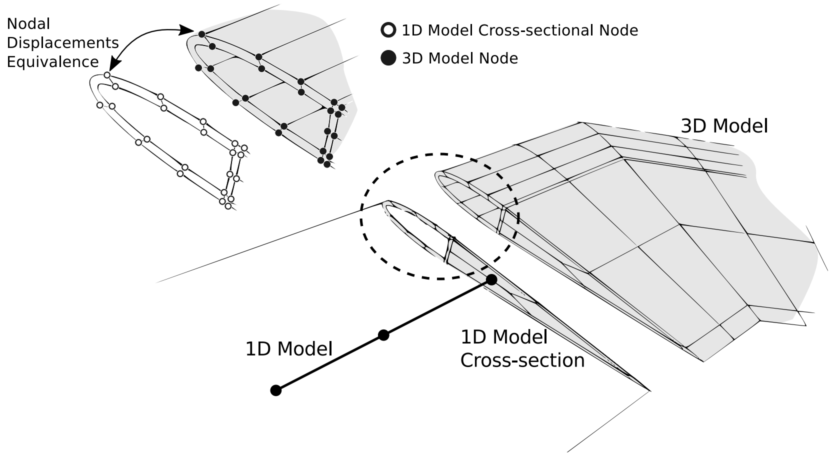


Figure 1: The multidimensional model. Figure taken from Ref. [3]

enough to balance the aerodynamic loads and the blade's weight. The current work overcomes this limitation by including the nonlinear terms of the strain tensor, $\boldsymbol{\varepsilon}$, in the derivation of solid elements:

$$\boldsymbol{\varepsilon} = (\mathbf{b_l} + \mathbf{b_{nl}})\,\mathbf{u} = (\mathbf{b_l} + \mathbf{b_{nl}})\,N_i(x,y,z)\mathbf{u}_i = (\mathbf{B_l^i} + \mathbf{B_{nl}^i})\mathbf{u}_i \tag{2}$$

where $\mathbf{B_l^i}$ and $\mathbf{B_{nl}^i}$ are the algebraic matrices of derivatives operators applied to the 3D shape functions, here not reported. The FE matrices of the 1D/3D models can be obtained with ease through a conventional assembly procedure. Consequently, it is possible to compute the natural frequencies and mode shapes associated with small-amplitude vibrations ($\hat{\mathbf{u}}$) of a rotating structure by assuming a harmonic solution in Equation (3):

$$\mathbf{M}\ddot{\hat{\mathbf{u}}} + \mathbf{G}\dot{\hat{\mathbf{u}}} + (\mathbf{K}_T\,(\mathbf{u}_e) + \mathbf{K}_\Omega)\hat{\mathbf{u}} = 0 \tag{3}$$

where $\mathbf{M}$, $\mathbf{G}$, and $\mathbf{K}_\Omega$ are the mass, Coriolis and spin softening matrices. The operator $\mathbf{K}_T$ is the tangent stiffness matrix computed at an equilibrium solution ($\mathbf{u}_\mathrm{e}$) that is, in turn, determined by solving with a Newton-Raphson scheme the nonlinear problem of Equation (4):

$$\mathbf{K}_S(\mathbf{u})\,\mathbf{u}_e = \mathbf{F}_{ext} + \mathbf{F}_\Omega \tag{4}$$

The matrix $\mathbf{K}_S(\mathbf{u})$ is the secant matrix, and $\mathbf{F}_{ext}$ and $\mathbf{F}_\Omega$ represent the vectors of external and centrifugal forces, respectively. For demonstration purposes, the nonlinear multidimensional model, consisting of nine 4-node beam elements and four 27-node hexahedral solid elements, has been adopted to calculate the static response of the blade shown in Figure 2 subjected to a transverse load (along the z-direction) and applied at its tip. The geometrical and material properties have been taken from Ref. [3]. Figure 3 shows the transverse deflection calculated at the loaded point using the linear and nonlinear multidimensional formulations. As expected, for this problem, the geometrical nonlinearities become relevant when the deformation is equal to or larger than 20% of the structure's length.

## References

[1] Filippi, M.; Pagani, A.; Carrera, E.: Accurate Nonlinear Dynamics and Mode Aberration of Rotating Blades. Journal of Applied Mechanics, Vol. 85, pp. 111004 (1-7), 2018.

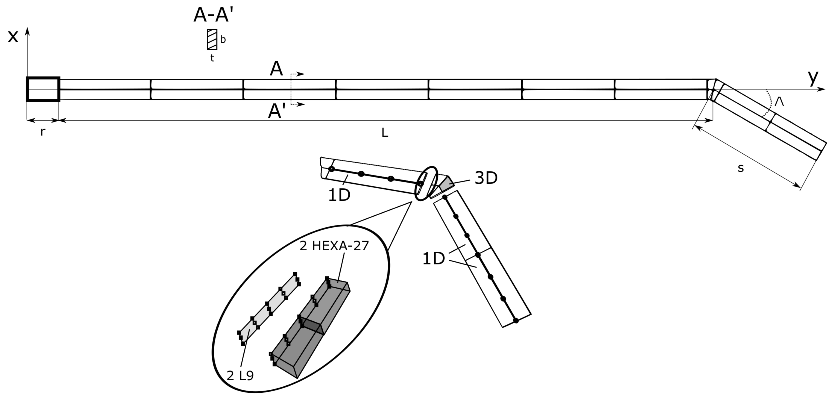


Figure 2: The swept-tip blade and a detail of the connection region. Figures taken from Ref. [3].

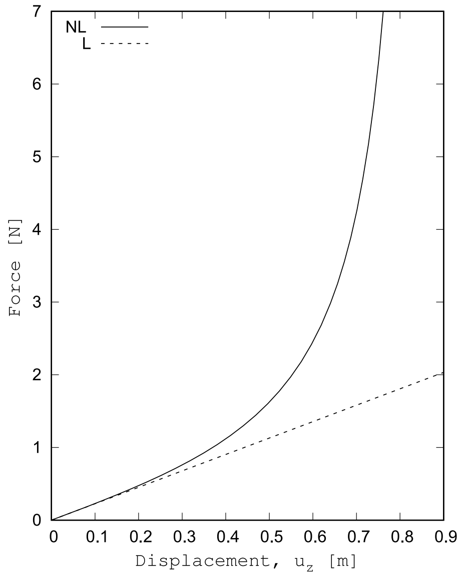


Figure 3: Comparison between linear (L) and nonlinear (NL) formulations.


[2] Filippi, M.; Azzara, R.; Carrera, E.: Variable Kinematic Shell Finite Elements for Dynamic Analyses of Rotating Structures. Proceedings of the ASME 2022 International Mechanical Engineering Congress and Exposition. Volume 5: Dynamics, Vibration, and Control. Columbus, Ohio, USA. October 30–November 3, 2022.

[3] Filippi, M.; Zappino, E.; Carrera, E.: Multidimensional Models for Double-Swept Helicopter Blades. AIAA Journal, Vol. 57, No. 6, pp. 1–8, 2019.

[4] Filippi, M.; Zappino, E.; Carrera, E.; Castanié, B.: Effective Static and Dynamic Finite Element Modeling of a Double Swept Composite Rotor Blade. Journal of the American Helicopter Society, Vol. 65, No. 3, pp. 1-12(12), 2020.

# Flow-Induced Vibrations of Rotated Square Tube Arrays

**Amro Elhelaly [*], Marwan Hassan [*], David Weaver [†], Jovica R. Riznic [#], Soha Moussa [*]**

[*] University of Guelph
Guelph, Ontario, Canada, N1G 2W1
[amro, mhassan, smoussa]@ uoguelph.ca

[†] McMaster University
Hamilton, Ontario, Canada, L8S 4L7
weaverds@mcmaster.ca

[#] Canadian Nuclear Safety Commission
Ottawa, Ontario, Canada, K1P 5S9
jovica.riznic@cnsc-ccsn.gc.ca

**Abstract**

Fluidelastic instability (FEI) is widely recognized as a mechanism which can cause rapid failure of tubes in shell and tube heat exchangers. Thus, predicting the onset of instability has been the subject of intensive research for the past five decades. The majority of these investigations were aimed for inline and triangular arrays, with very few investigations available for rotated square arrays to date due to is complexity. This paper provides a systematic investigation of the array geometrical impact (effect of pitch ratio and array flexibility level) on the onset of instability for both transverse and streamwise directions independently.

## 1. Introduction

Heat exchangers, became a common place for flow-induced vibration (FIV). The Fluidelastic instability (FEI) is by far the most important FIV excitation mechanism. If not mitigated, this phenomenon may lead to tube failure and may necessitate the shutdown of the plant due to the expensive vibration amplitudes. Recent catastrophic failure of the steam generator (SG) at the San Onofre Nuclear Generating Station (SONGS) is one of the prime examples of this phenomeon [1]. The streamwise fluidelastic instability (SFEI)—a phenomenon that was discovered for the first time in an operational SG—was the cause of the failure. As a result, there have been considerable efforts dedicated to understand this phenomenon. While significant progress has been achieved, there are still unresolved issues.

There are four basic tube array configurations: parallel triangle, normal trinagle, inline, and rotated square array. The later array is not well researched due to its complex behaviour. The work of Hartlen [2] is the earliest experimental work on rotated square array (RS). In contrast to the square and normal triangle pattern, it was found that the tube array always remains stable in the transverse direction and only becomes unstable in the streamwise direction due to the change of the flow channel in the RS array. In summary, RS array continues to be challenging and is not completely understood. To further understand the fluidelastic behaviour of this array layout, an experimental research program has been initiated at University of Guelph. The research described here aims to study the dynamic behaviour and geometrical effect of RS array on the onset of FEI in both transverse and streamwise directions.

## 2. Experimental procedure

The reported experiments were carried out in an open loop wind tunnel facility. The test section was designed to accommodate tube arrays with various pitch ratio (in this study P/D of 1.25, 1.4, 1.5, and 1.7 were investigated). In order to control the number of flexible tubes, the test section was designed to allow each tube to be altered from flexible to rigid. Figure 1 depicts the (7 x 5) rotated square array configurations that were tested. All tubes were constructed from a straight acrylic tube that was mounted on a thin flexible rectangular cantilever beam. This allowed the tubes to be flexible just in the preferred direction, either streamwise or transverse, while maintaining full rigidity in the other direction. For the three tubes marked U (upstream), C (center), and D (downstream), strain gauges are utilized to track tube vibration signal (Fig. 1). A pitot tube connected to a digital differential pressure transducer and located 155 mm upstream of the tube array was used to monitor the flow velocity. The average tube mass damping parameter ($m\delta\ /\ \rho D^2$) was found to be 4.0.

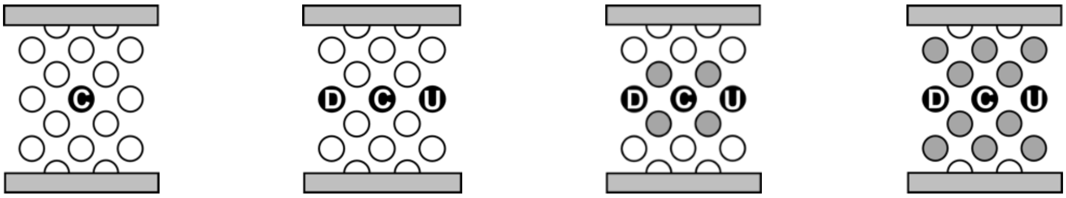


(a) (b) (c) (d)

**Figure 1**. Rotated square configurations: a) single flexible tube, b) flexible column of 3 tubes, c) kernel of 7 flexible tubes, and d) fully flexible array: ○ fixed tube, ◉ flexible tube, ● instrumented flexible tube.

## 3. Modelling

Modelling of the system requires the accounting for the fluid excitation and the structural response. The structural response is obtained by the temporal integrating the second order equation of tube structure. The fluid excitation is modelled by utiliziling the unsteady model for fluidelastic instability of tube arrays in cross flow by Hassan and Weaver [1]. In this model, the flow inside the tube bundle is idealized as being unsteady, incompressible and inviscid flow. The coupling results from the tube motion influencing the flow channel width. The change in the flow channel due to the tube motion does not take place instantaneously. The delayed flow response is incorporated by introducing time delay due to the flow redistribution. The flow pressure is integrated over the tube/flow interface resulting in the FEI force which is included in the structural model.

## 4. Results

For the kernel configuration of the tube array with a pitch ratio of 1.25, Fig. 2 illustrates the rms responses for the three monitored tubes in transverse and streamwise directions against the reduced flow velocity ($U_r = U/fD$). Both the transverse and streamwise orientations exhibit similar overall tube response pattern up to a critical value. The rms amplitudes grow gradually with the flow velocity; after that threshold, the amplitudes rapidly increase with the flow velocity. The experiment was promptly interrupted to prevent damage to the tubes since once the flow velocity exceeds certain limits, the tube amplitudes grow to unacceptable levels. From the results in Fig. 2, the critical reduced velocities were estimated to be 23 and 51, respectively, for the streamwise and transverse directions.
It was found that the stability threshold in transverse direction (Fig. 3a) was sensitive to the flexibility level of the array as single and column configuration remains stable and the tube becomes unstable only in case of kernel and full flexible configurations. Also, the streamwise FEI was found to be sensitive to the number of flexible tubes (Fig. 3b) for all examined P/D. Due to the lack of tube-to-tube interaction, single and partially flexible arrays exhibit delayed instability development.

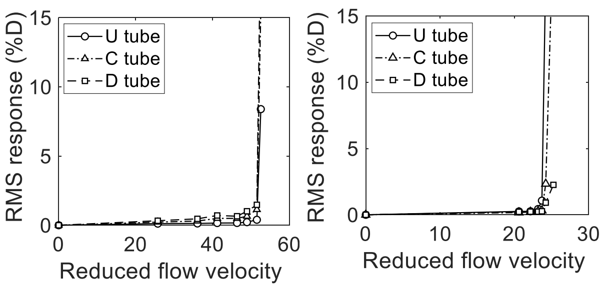


(a)Transverse (b)Streamwise

**Figure 2.** Tube response versus reduced flow velocity for P/D =1.25 (kernel configuration)

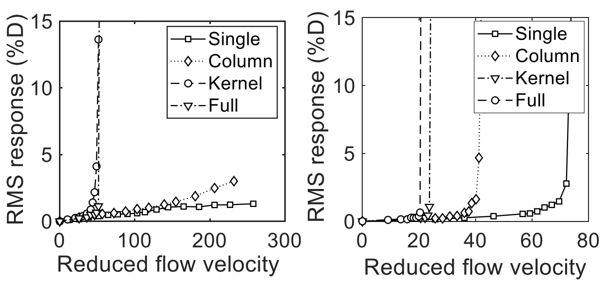


(a)Transverse (b)Streamwise

**Figure 3.** Effect of the number of flexible tubes on the FEI for P/D =1.25

Figures 4 and 5 depict the effects of the pitch ratio on the transverse and streamwise response for the kernel configuration. It is clear, that transverse and streamwise directions have the same behaviour.

No significant effect was recorded for smaller P/D arrays; however the critical velocity ($U_{cr}$) was sensitive to P/D greater than 1.4 as $U_{cr}$ increases with increasing the P/D. Figure 6 shows a comparison between the model prediction of the present work and data from the literature for both transverse and streamwise directions. The current experimental data was including in both the transverse and streamwise directions. The expermintal data from the present work follows the same trend as those of the previous experimental data. The model prediction agrees well with the bulk of the expermintal work.

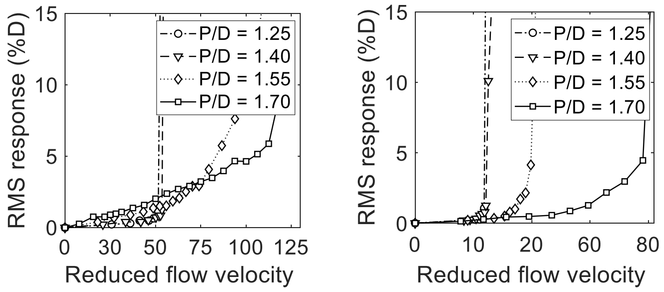

(a)Transverse (b)Streamwise

**Figure 4.** Effect of the P/D ratio on the response

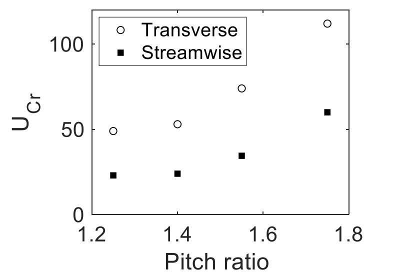

**Figure 5.** The effect of the tube pitch ratio, P/D, on the stability threshold

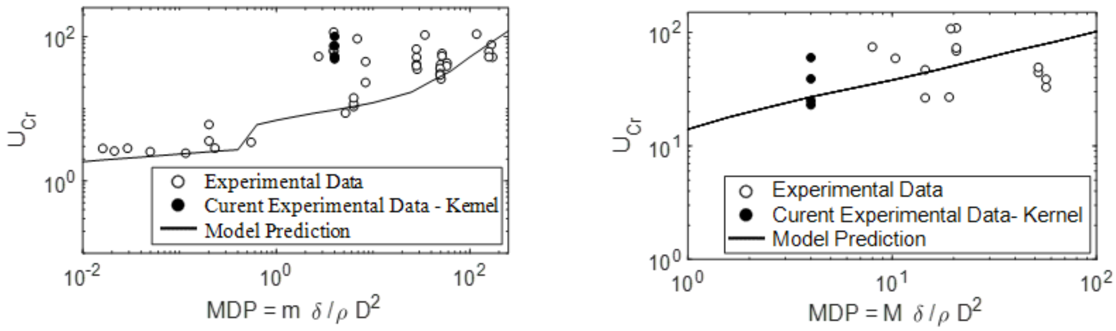

(a) Transverse (b) Streamwise

**Figure 6.** Stability map of the FEI comparing the current results to the available experimental data.

## Conclusion

Fluidelastic stability in rotated square array with 4 different pitch ratios was experimentally investigated in both transverse and streamwise directions. The results show that the number of flexible tubes significantly impacts the onset of FEI at the same MDP for both transverse and streamwise. Also, the stability threshold was found to be sensitive to the pitch ratio, generally the FEI stability threshold decreases with decreasing pitch ratio. In fact, these findings confirm that FEI in RS array was driven by the stiffness-controlled excitation and tube-to-tube coupling is very essential for the array to become unstable either in transverse or streamwise directions.

## References


[1] Hassan, M., and Weaver, D. (2021). "Pitch and Pattern Effects on Streamwise Fluidelastic Instability in Tube Arrays." ASME. J. Pressure Vessel Technol. 144(4): 041403. https://doi.org/10.1115/1.4052399

[2] Hartlen, R., 1974. Wind-tunnel determination of fluid-elastic-vibration thresholds for typical het-exchanger tube patterns. Ontario Hydro Research Division.

# Dynamic Response of Composite Laminates on Linear and Nonlinear Elastic Foundations with Delamination

**Bin Huang**[*], **Yan Guo**[*], **Ji Wang**[*]

[*] Piezoelectric Device Laboratory,
Faculty of Mechanical Engineering & Mechanics, Ningbo University
818 Fenghua Road, Jiangbei District, Ningbo, 315211 Zhejiang, China
Email: huangbin@nbu.edu.cn

## Summary

Composite structures are on some occasions surrounded or supported by elastic or viscoelastic media in serving environment. With supporting foundations, dynamic characteristics change since the foundations provides additional constraints. The interaction between the foundations and composites can be linear, nonlinear or viscoelastic. In this work, we aim to build the mathematical model for delaminated composite plates, as shown in Figure 1, resting on various foundations by means of the improved layerwise theory and finite element implementation for free vibration- and dynamic response analysis. The displacement fields are assumed by the following equation:

$$
\begin{aligned}
U_1^k(x,y,z,t) &= u_1(x,y,t)+\phi_1(x,y,t)z+\theta_1^k(x,y,t)g(z)+\psi_1^k(x,y,t)h(z)+\sum_{j=1}^{N-1}\bar{u}_1^j(x,y,t)H(z-z_j)\\
U_2^k(x,y,z,t) &= u_2(x,y,t)+\phi_2(x,y,t)z+\theta_2^k(x,y,t)g(z)+\psi_2^k(x,y,t)h(z)+\sum_{j=1}^{N-1}\bar{u}_2^j(x,y,t)H(z-z_j) \qquad (1)\\
U_3^k(x,y,z,t) &= w(x,y,t)+\sum_{j=1}^{N-1}\bar{w}^j(x,y,t)H(z-z_j)
\end{aligned}
$$

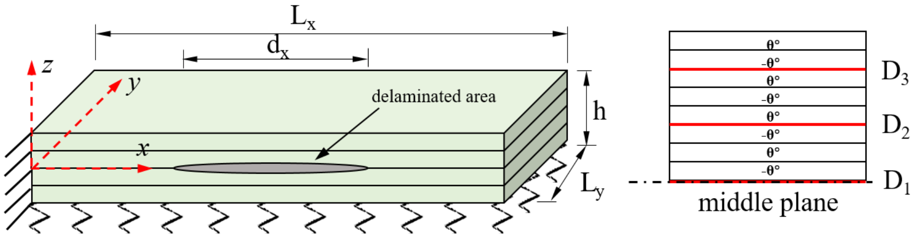


**Figure 1.** Geometry of delaminated composite laminate on elastic foundation, and three interfacial delamination locations

The proposed model takes into account three foundation models, such as two-parameter foundation, three-parameter nonlinear model and visco-Pasternak foundation model to investigate their effect on the dynamic characteristics of delaminated plates. (LF: two-parameter linear foundation; NF: three-parameter nonlinear foundation; VF: visco- Pasternak foundation):

$$
p = k_0 w - k_1\left(\frac{\partial^2 w}{\partial x^2}+\frac{\partial^2 w}{\partial y^2}\right) \qquad \text{(LF)}
$$

$$
p = k_0 w + k_1 w^3 - k_2\left(\frac{\partial^2 w}{\partial x^2}+\frac{\partial^2 w}{\partial y^2}\right) \qquad \text{(NF)} \qquad (2)
$$

$$P = k_w w - k_p\left(\frac{\partial^2 w}{\partial x^2} + \frac{\partial^2 w}{\partial y^2}\right) + k_d\dot{w} \qquad \text{(VF)}$$

The equations of motion are obtained from Hamilton's principle. The details of Hamilton's principle can be expressed by the following equations for the three foundation cases:

$$\int_{t_0}^{t_1}\left(\frac{1}{2}\delta\left(\int_v \boldsymbol{\varepsilon}^T\boldsymbol{\sigma} - \rho\dot{\mathbf{u}}^T\dot{\mathbf{u}}\right)dV + \frac{1}{2}\delta\int_A\left(\mathbf{W}^T k_0\mathbf{W} + \boldsymbol{\gamma}^T k_1\boldsymbol{\gamma}\right)dxdy - \int_\Gamma \mathbf{u}^T\mathbf{t}\,d\Gamma\right)dt = 0 \qquad \text{(LF)}$$

$$\int_{t_0}^{t_1}\left(\frac{1}{2}\delta\left(\int_v \boldsymbol{\varepsilon}^T\boldsymbol{\sigma} - \rho\dot{\mathbf{u}}^T\dot{\mathbf{u}}\right)dV + \frac{1}{2}\delta\int_A\left(\mathbf{W}^T k_0\mathbf{W} + \mathbf{W}^T\left(\mathbf{W}^T\right)^2 k_1\mathbf{W} + \boldsymbol{\gamma}^T k_2\boldsymbol{\gamma}\right)dxdy - \delta\int_\Gamma \mathbf{u}^T\mathbf{t}\,d\Gamma\right)dt = 0 \qquad \text{(NF)} \quad (3)$$

$$\delta\int_{t_0}^{t_1}\left(\frac{1}{2}\int_v \boldsymbol{\varepsilon}^T\boldsymbol{\sigma}dV + \frac{1}{2}\int_A \mathbf{W}^T k_w\mathbf{W}dxdy + \frac{1}{2}\int_A \boldsymbol{\gamma}^T k_p\boldsymbol{\gamma}dxdy + \frac{1}{2}\int_A k_d\mathbf{W}^T\dot{\mathbf{W}}dxdy - \frac{1}{2}\int_v \rho\dot{\mathbf{u}}^T\dot{\mathbf{u}}dV - \int_\Gamma \mathbf{u}^T\mathbf{t}\,d\Gamma\right)dt = 0 \qquad \text{(VF)}$$

Substituting all the strain-stress relation, geometric relaitons, performing integration by parts and applying boundary conditions, the governing equations can be obtained in the following matrix form, for the three foundation cases:

$$\mathbf{M}\ddot{\mathbf{d}} + \mathbf{K}\mathbf{d} = 0 \qquad \text{(LF)}$$

$$\mathbf{M}\ddot{\mathbf{d}} + \left(\mathbf{K}_{L\varepsilon} + \mathbf{K}_{L0} + \mathbf{K}_{NL1} + \mathbf{K}_{L2}\right)\mathbf{d} = 0 \qquad \text{(NF)} \qquad (4)$$

$$\mathbf{M}\ddot{\mathbf{d}} + \mathbf{K}_{Ld}\dot{\mathbf{d}} + \mathbf{K}\mathbf{d} = \mathbf{F} \qquad \text{(VF)}$$

For free vibration, the first four natural frequencies are shown in Figure 2, for a cross-ply ($[0/90]_{4s}$) composite plate with various delamination locations on two-parameter elastic foundation. We can observe the delamination effect on the natural frequencies especially for the delamination located at the middle plane of the laminate. The impact response of the equations of motion is solved by the Newmark time integration method. The displacement, velocity and acceleration are approximated by the Taylor's expansion and only terms up to the second derivative. The results are shown in Figure 3. The slight difference due to delamination on transient history can be observed and the PSD result also shows some difference at the high frequency peaks.

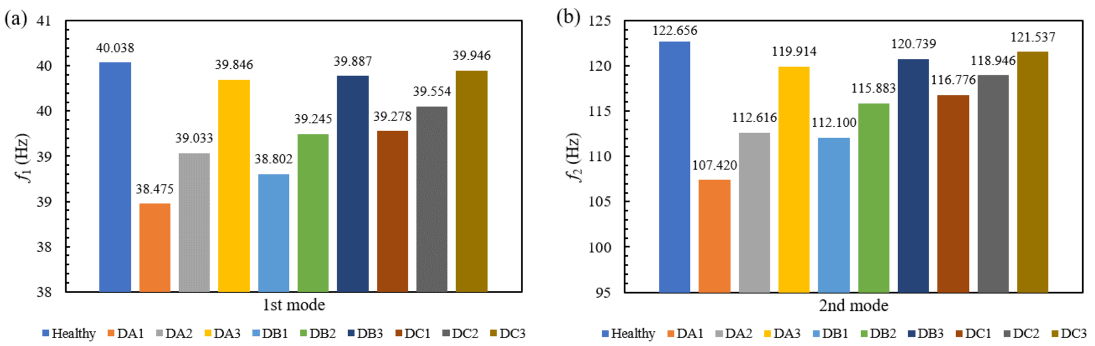

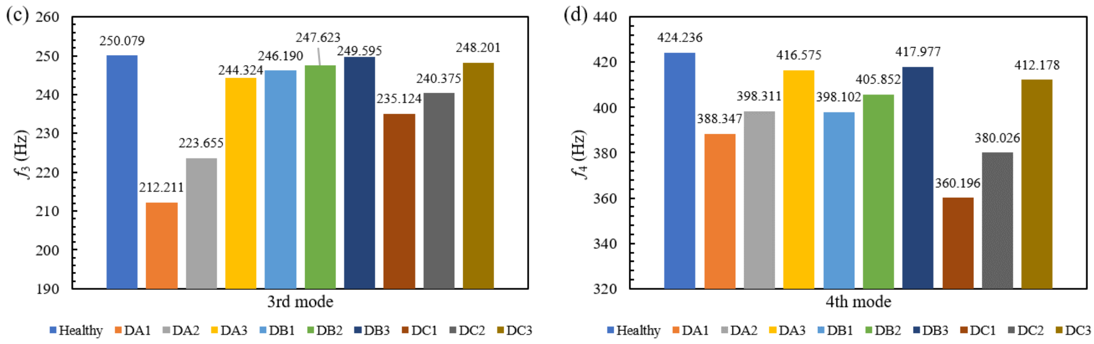


**Figure 2.** Natural frequencies of the first four modes for cross-ply ($[0/90]_{4s}$) composite plate with various delamination locations

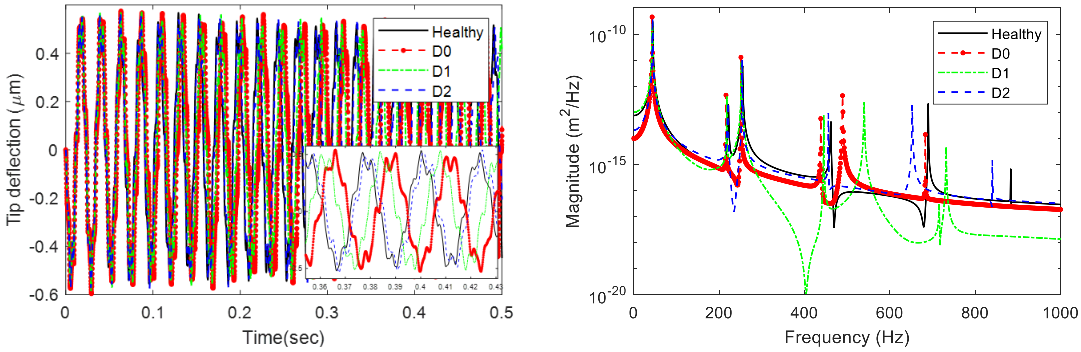


**Figure 3.** Transient history and PSD of healthy and delaminated clamped-free plate with $k_d$= 0.002 under 1N impact load at the tip center with the time duration of 1ms

Understanding the dynamic behaviour of composite structures on elastic foundations is very important for structural applications. Moreover, the existence of delamination affects the higher frequencies dramatically which may further help identify delamination locations in composite plates resting on various foundations for structural health monitoring.

## References


[1] Bin Huang, Ji Wang, Yan Guo, Investigation of delamination effect on nonlinear vibration behaviors of a composite plate resting on nonlinear elastic foundation, Composite Structures, Vol. 280, 114897, 2022.

[2] Yan Guo, Bin Huang, Licheng Hua, Jianbin Chen, Ji Wang, Modeling of partially delaminated composite plates resting on two-parameter elastic foundation with improved layerwise theory, Mechanics of Advanced Materials and Structures, DOI:10.1080/15376494.2022.2044571, 2022.

[3] Chen Yang, Bin Huang, Yan Guo, Ji Wang, Characterization of delamination effects on free vibration and impact response of laminated composite plates resting on visco-Pasternak foundations, International Journal of Mechanical Sciences, Vol. 212, 106833, 2021.

# Natural Frequencies of Cracked Rectangular Plates: An Energy Approach

**Farhad Masoudian*, Akshay A. Satpute*, David Kennedy*, Carol A. Featherston*, Sinniah Ilanko#**

* School of Engineering
Cardiff University
Queen's Buildings, The Parade,
Cardiff CF24 3AA, United Kingdom
[MasoudianFN, SatputeAA, KennedyD, FeatherstonCA]@cardiff.ac.uk

# School of Engineering
University of Waikato
Private Bag 3105, Hamilton 3240,
New Zealand
Ilanko@waikato.ac.nz

## Summary

Plates and stiffened panels provide low mass solutions in many engineering applications, including aircraft, road and rail vehicles, ships and bridges. Initial imperfections, cracks, delaminations and other forms of damage reduce their stiffness and load carrying capacity. Damage is often difficult to detect visually, particularly in built-up structures such as aircraft wings and fuselage panels. Non-destructive testing can identify changes in vibration behaviour, and can be carried out with minimal instrumentation if attention is confined to the natural frequencies rather than the vibration modes [1]. The location and extent of damage in beams and frame structures have been identified from observed degradations in their natural frequencies in conjunction with a dynamic stiffness model which represents a crack by a rotational spring [2-4]. Such models for plates commonly assume longitudinal invariance, which is violated by the presence of a crack, and instead finite element and hybrid models have been employed [5].

Consider a thin rectangular plate of thickness $h$, covering the area $0 \leq x \leq a$, $0 \leq y \leq b$ and simply supported on all four sides. The plate is made from an isotropic material with Young's modulus $E$, Poisson's ratio $\nu$ and density $\rho$, and vibrates at a natural frequency $\omega_{mn0}$ with a mode shape given by

$$w(x,y) = w_{mn} \sin\left(\frac{m\pi x}{a}\right) \sin\left(\frac{n\pi y}{b}\right) sin(\omega_{mn0} t) \tag{1}$$

At zero displacement the strain energy is zero, while the kinetic energy takes its maximal value

$$T_0 = \frac{1}{2}\rho h \omega_{mn0}^2 w_{mn}^2 \int_0^a \int_0^b \sin^2\left(\frac{m\pi x}{a}\right) \sin^2\left(\frac{n\pi y}{b}\right) dy\, dx \tag{2}$$

At peak displacement the kinetic energy is zero, while the strain energy takes its maximal value

$$U_0 = \frac{1}{2} D w_{mn}^2 \pi^4 \left(\frac{m^2}{a^2} + \frac{n^2}{b^2}\right)^2 \int_0^a \int_0^b \sin^2\left(\frac{m\pi x}{a}\right) \sin^2\left(\frac{n\pi y}{b}\right) dy\, dx\,;\; D = \frac{Eh^3}{12(1-\nu^2)} \tag{3}$$

Conservation of energy requires that $T_0 = U_0$ and so

$$\omega_{mn0}^2 = \frac{D\pi^4}{\rho h}\left(\frac{m^2}{a^2} + \frac{n^2}{b^2}\right)^2 \tag{4}$$

A crack running from $(x_1, y_1)$ to $(x_2, y_2)$ is modelled as a rotational spring with compliance $C$ per unit length calculated as in [3]. The strain energy associated with discontinuous rotation along the length of the crack is

$$U_d = \frac{1}{2} C D^2 w_{mn}^2 \pi^4 l \int_0^l \left\{ \left[ \left( \frac{m^2}{a^2} + \nu \frac{n^2}{b^2} \right) \cos^2\varphi + \left( \nu \frac{m^2}{a^2} + \frac{n^2}{b^2} \right) \sin^2\varphi \right] \sin\alpha_x \sin\alpha_y + \left[ 2(1-\nu) \frac{mn}{ab} \sin\varphi\cos\varphi \right] \cos\alpha_x \cos\alpha_y \right\}^2 ds\,; \quad (5)$$

$$\alpha_x = \frac{m\pi(x_1 + s\sin\varphi)}{a}\,;\ \alpha_y = \frac{n\pi(y_1 + s\cos\varphi)}{b}$$

where $l$ is the length of the crack and $\varphi$ is its orientation to the positive $y$ axis. The cracked plate vibrates with a reduced natural frequency $\omega_{mnc}$ and at zero displacement has kinetic energy

$$T_c = \frac{1}{2} \rho h \omega_{mnc}^2 w_{mn}^2 \int_0^a \int_0^b \sin^2\left(\frac{m\pi x}{a}\right) \sin^2\left(\frac{n\pi y}{b}\right) dy\, dx \quad (6)$$

Conservation of energy requires that $T_c = U_0 - U_d$ and so $\omega_{mnc}^2 = \omega_{mn0}^2 - \delta_{mn}$ where

$$\delta_{mn} = \frac{2U_d}{\rho h w_{mn}^2 \int_0^a \int_0^b \sin^2\left(\frac{m\pi x}{a}\right) \sin^2\left(\frac{n\pi y}{b}\right) dy\, dx} \quad (7)$$

Table 1 shows the lowest six natural frequencies of a simply supported rectangular plate of length $a = 0.12$m, width $b = 0.10$m and thickness $h = 0.001$m with Young's modulus $E = 110\text{GNm}^{-2}$, Poisson's ratio $\nu = 0.3$ and density $\rho = 4480\text{kgm}^{-3}$, before and after the introduction of a crack of depth $d = 0.1h$ running parallel to the $x$ axis from $(x_1, y_1) = (0.02, 0.03)$m to $(x_2,\ y_2) = (0.06, 0.03)$m. The degradations $\delta_{mn}$ in the squares of natural frequencies calculated from Equation (7) show good agreement with finite element results using a mesh of $48 \times 20$ rectangular shell elements with 12 degrees of freedom taken from [6]. The degradations $\delta_{mn}$ may be regarded as components of a vector $\boldsymbol{\delta}$ which, when normalised to a unit vector $\bar{\boldsymbol{\delta}}$, can be used to locate the crack [3]. The normalised components $\bar{\delta}_{mn}$ are shown in Table 1 for this example, and also for variants in which the crack depth, location or length are altered as shown. It is seen that the $\bar{\delta}_{mn}$ are independent of the crack depth but vary a little with the length of the crack. They vary much more with the crack location because the energy calculation of Equation (5) depends on the curvatures of the different mode shapes along the crack. Note that, in common with much previous research, the analysis has ignored the small changes in mode shape due to the crack, resulting in some inaccuracy for larger cracks.

**Table 1**. Natural frequencies of a simply supported rectangular plate, degradations $\delta_{mn}$ in their squares due to a crack**,** and normalised degradations $\bar{\delta}_{mn}$. Key to variants: deep crack $d = 0.2h$; short crack $(x_1, x_2) = (0.03, 0.05)$m; $x$ shift $(x_1, x_2) = (0.01, 0.05)$m; $-y$ shift $y_1 = y_2 = 0.015$m; $+y$ shift $y_1 = y_2 = 0.045$m.

| $(m,n)$ | $\omega_{mn0}$ (rad s$^{-1}$) | $\omega_{mnc}$ (rad s$^{-1}$) | $\delta_{mn}$ (rad$^2$ s$^{-2}$) | Error vs FE (%) | $\bar{\delta}_{mn}$ | $\bar{\delta}_{mn}$ deep crack | $\bar{\delta}_{mn}$ short crack | $\bar{\delta}_{mn}$ $x$ shift | $\bar{\delta}_{mn}$ $-y$ shift | $\bar{\delta}_{mn}$ $+y$ shift |
|---|---|---|---|---|---|---|---|---|---|---|
| (1,1) | 2507.7 | 2506.7 | 5140.6 | 0.84 | 0.037 | 0.037 | 0.035 | 0.027 | 0.004 | 0.021 |
| (2,1) | 5590.9 | 5590.0 | 10102.8 | 0.44 | 0.073 | 0.073 | 0.077 | 0.088 | 0.007 | 0.041 |
| (1,2) | 6947.5 | 6941.3 | 86169.6 | 1.12 | 0.620 | 0.620 | 0.590 | 0.452 | 0.137 | 0.025 |
| (2,2) | 10030.7 | 10025.9 | 97039.6 | 0.88 | 0.699 | 0.699 | 0.744 | 0.843 | 0.154 | 0.028 |
| (3,1) | 10729.6 | 10728.6 | 20588.2 | 1.52 | 0.148 | 0.148 | 0.049 | 0.153 | 0.014 | 0.084 |
| (1,3) | 14347.3 | 14345.7 | 43556.0 | 1.42 | 0.314 | 0.314 | 0.298 | 0.229 | 0.978 | 0.995 |

**Table 2**. Natural frequencies of a simply supported square plate and degradations $\delta_{mn}$ in their squares due to a short crack running from $(0.054, 0.0385)$m to $(0.056, 0.0415)$m. Key to variants: medium crack running from $(0.050, 0.0325)$m to $(0.060, 0.0475)$m; long crack running from $(0.035, 0.010)$m to $(0.075, 0.070)$m.

| $(m, n)$ | $\omega_{mn0}$ (rad $s^{-1}$) | $\omega_{mnc}$ (rad $s^{-1}$) | $\delta_{mn}$ (rad$^2$ $s^{-2}$) | Error vs [7] (%) | $\bar{\delta}_{mn}$ | $\bar{\delta}_{mn}$ medium crack | $\bar{\delta}_{mn}$ long crack |
|---|---|---|---|---|---|---|---|
| (1,1) | 2959.9 | 2957.1 | 16489.4 | -45.39 | 0.033 | 0.035 | 0.037 |
| (2,1) | 7399.7 | 7399.4 | 5359.8 | -66.84 | 0.011 | 0.027 | 0.196 |
| (1,2) | 7399.7 | 7398.1 | 23497.3 | -71.24 | 0.048 | 0.060 | 0.158 |
| (2,2) | 11839.6 | 11835.8 | 89746.3 | 396.83 | 0.182 | 0.162 | 0.304 |
| (3,1) | 14799.5 | 14783.6 | 469457.6 | -8.49 | 0.950 | 0.941 | 0.744 |
| (1,3) | 14799.5 | 14795.3 | 121578.1 | -64.26 | 0.246 | 0.286 | 0.538 |

Table 2 shows the lowest six natural frequencies of a simply supported square plate with sides $a = b = 0.1$m, thickness $h = 0.001$m, Young's modulus $E = 110\text{GNm}^{-2}$, Poisson's ratio $\nu = 0.3$ and density $\rho = 4480\text{kgm}^{-3}$, before and after the introduction of a short crack of depth $d = 0.5h$. The degradations $\delta_{mn}$ in the squares of natural frequencies differ substantially from those of [7], where the energy calculations use the curvatures in the mode shape at the midpoint of the crack, whereas here they are integrated along the crack length and are therefore more accurate. Also Equation (5) is more accurate than its equivalent in [7], allowing for the effects of twist on the compliance of arbitratily aligned cracks.

The proposed energy approach can be applied to plates with different boundary conditions by replacing the sinusoidal mode shapes in Equation (1) by appropriate deflection functions. Built-up structures can be handled by first using the dynamic stiffness method to find the natural frequencies and mode shapes of the uncracked structure. The mode shapes then supply the boundary conditions for each of the component plates.

It is proposed to apply the understanding gained from this analysis to inverse problems involving the identification of cracks in plate structures. This is a more challenging task than for beams and frame structures [3] and will be tackled using advanced optimisation techniques.

## References


[1] Salawu, O.S.: Detection of structural damage through changes in frequency: a review. Engineering Structures, Vol. 19, No. 9, pp. 718–723, 1997.

[2] Caddemi, S.; Caliò, I.: Exact solution of the multi-cracked Euler-Bernoulli column. International Journal of Solids and Structures, Vol. 45, No. 5, pp. 1325–1351, 2008.

[3] Labib, A.; Kennedy, D.; Featherston, C.A.: Crack localisation in frames using natural frequency degradations. Computers and Structures, Vol. 157, pp. 51–59, 2015.

[4] Ilanko, S.; Mochida, Y.; De Los Rios, J.; Kennedy, D.: Separating the effect of crack severity and location in a skeletal structure with a single crack. ISVCS 2019 - Proceedings of 12th International Symposium on Vibrations of Continuous Systems, pp. 59–61, 2019.

[5] Luo, Y.; Featherston, C.A.; Kennedy, D.: A hybrid model for modelling arbitrary cracks in isotropic plate structures. Thin-Walled Structures, Vol. 183, Paper 110345, 2023.

[6] Przemieniecki, J.S.: Theory of Matrix Structural Analysis. Dover Publications Inc., New York, 1985.

[7] Kannappan, L.; Shankar, K.: Non destructive inspection of plates using frequency measurements. ACAM 2007 – Proceedings of 5th Australasian Congress on Applied Mechanics, pp. 215–220, 2007.

# A mixed finite element method for free vibration analysis of composite periodic beams

**Jiaqing Jiang***, **Weiqiu Chen#**

* Department of Engineering Mechanics, Zhejiang University, No. 38, Zheda Road, Hangzhou, China. jiangjq@zju.edu.cn

# Department of Engineering Mechanics, Zhejiang University, No. 38, Zheda Road, Hangzhou, China. chenwq@zju.edu.cn

## 1. Introduction

Multi-layered composite structure exhibits complex shear deformation characteristics. The periodic concept of material arrangement in metamaterial design can provide structures with different dynamic properties and create new resonance characteristics [1], while also presenting challenges on vibration analysis.

Based on different shear deformation theories, scholars derived a variety of analytical solutions for dynamic analysis of composite beams [1-3]. As for numerical analysis, different beam elements were proposed [4-6]. These studies were all based on one-dimensional beam theory. If a composite beam is treated as a two-dimensional structure, then there is no need to assume the distribution of deformation or stress on the cross-section [7, 8].

The state-space method has a unique advantage in analysing multi-layer composite structures because it treats displacement and its energy-conjugated stress components as basic unknowns [8, 9]. Based on this, a mixed finite element method for the dynamic analysis of periodic composite structures is proposed in this paper. It has the advantage of accurately analysing dynamic characteristics of composite structures.

## 2. Governing equations and solutions

Consider the free vibration problem of a periodic composite beam. The vibration frequency of the beam is denoted by $\omega$, and the Lagrangian function of the two-dimensional system can be expressed as:

$$\mathcal{L} = \frac{1}{2}\begin{Bmatrix} \mathbf{u},_x \\ \mathbf{u},_y \end{Bmatrix}^{\mathrm{T}} \begin{bmatrix} \mathbf{C}_{xx} & \mathbf{C}_{xy} \\ \mathbf{C}_{yx} & \mathbf{C}_{yy} \end{bmatrix} \begin{Bmatrix} \mathbf{u},_x \\ \mathbf{u},_y \end{Bmatrix} - \frac{1}{2}\omega^2 \mathbf{u}^{\mathrm{T}} \boldsymbol{\rho} \mathbf{u}, \tag{1}$$

where $\mathbf{u} = [u \quad v]^{\mathrm{T}}$ is the displacement vector in which $u$ and $v$ represents displacements in $x$ and $y$ direction, the subscript comma followed by the coordinate indicates the partial derivative with respect to this coordinate. $\mathbf{C}_{xx}, \mathbf{C}_{xy}, \mathbf{C}_{yx}, \mathbf{C}_{yy}$ are matrices of elastic coefficients of orthotropic material in plane stress problem [9], $\boldsymbol{\rho}$ is the material density matrix. Choosing $y$-direction as the transfer direction, the following Hamilton function is obtained by the Legendre transformation

$$H_y(\mathbf{u}, \boldsymbol{\sigma}_y) = \frac{1}{2}\boldsymbol{\sigma}_y^{\mathrm{T}} \mathbf{C}_{yy}^{-1} \boldsymbol{\sigma}_y - \boldsymbol{\sigma}_y^{\mathrm{T}} \mathbf{C}_{yy}^{-1} \mathbf{C}_{yx} \mathbf{u},_x - \frac{1}{2}\mathbf{u},_x^{\mathrm{T}} \bar{\mathbf{C}}_{xx} \mathbf{u},_x + \frac{1}{2}\omega^2 \mathbf{u}^{\mathrm{T}} \boldsymbol{\rho} \mathbf{u}, \tag{2}$$

where $\boldsymbol{\sigma}_y = [\sigma_{yx} \quad \sigma_{yy}]^{\mathrm{T}}$ is the stress vector in which $\sigma_{yx}$, $\sigma_{yy}$ is the shear and normal stress in the plane normal to the direction parallel to the $x$-axis, and

$$\bar{\mathbf{C}}_{xx} = \mathbf{C}_{xx} - \mathbf{C}_{xy} \mathbf{C}_{yy}^{-1} \mathbf{C}_{yx}. \tag{3}$$

The finite element discretization is performed in the $x$-direction, that is, the following assumptions are made for the displacements and stresses in element $e$

$$\mathbf{u}_e(x, y) = e^{i\omega t} \mathbf{N}(x) \mathbf{d}_e(y), \tag{4a}$$

$$\boldsymbol{\sigma}_{ye}(x,y) = e^{i\omega t}\mathbf{P}(x)\mathbf{s}_e(y). \tag{4b}$$

where $e^{i\omega t}$ represents the time-varying functions of displacement and stress at frequency $\omega$. $\mathbf{u}_e$ and $\boldsymbol{\sigma}_{ye}$ denote the displacement and stress components inside an element, $\mathbf{d}_e$ and $\mathbf{s}_e$ denote the displacement and stress components at the nodes of the element, and $\mathbf{N}(x)$ and $\mathbf{P}(x)$ denote the interpolated shape functions of the displacement and stress inside the element. The mixed energy functional of the system becomes

$$\Pi_1 = \int_0^H \left(\sum_{e=1}^{m} \int_{x_e}^{x_{e+1}} [\boldsymbol{\sigma}_y^{\mathrm{T}}\mathbf{u},_y - H_y(\mathbf{u},\boldsymbol{\sigma}_y)]\,\mathrm{d}x\right)\mathrm{d}y \tag{5}$$

where $H$ is the whole beam height, $m$ is the number of elements in $x$-direction, and $\left[x_e, x_{e+1}\right]$ are the interval occupied by the $e$-th element. Substituting Eq. (4) into Eq. (5), we obtain

$$\Pi_1 = e^{2i\omega t}\int_0^H (\mathbf{s}^{\mathrm{T}}\mathbf{D}\mathbf{d},_y - \frac{1}{2}\mathbf{s}^{\mathrm{T}}\mathbf{H}\mathbf{s} + \mathbf{s}^{\mathrm{T}}\mathbf{G}\mathbf{d} + \frac{1}{2}\mathbf{d}^{\mathrm{T}}\mathbf{K}\mathbf{d} - \frac{\omega^2}{2}\mathbf{d}^{\mathrm{T}}\mathbf{D}\mathbf{R}\mathbf{d})\,\mathrm{d}y, \tag{6}$$

where **d** and **s** denote the global vectors of displacements and stresses, and **D**, **G**, **H**, **K, R** and **J** denote the global matrices assembled from their element counterparts. Taking the variation of equation (6) and non-dimensionalizing it, we obtain

$$\frac{\mathrm{d}\boldsymbol{\Delta}}{\mathrm{d}\zeta} = \mathbf{A}\boldsymbol{\Delta},\ \zeta \in [0,1]. \tag{7}$$

where

$$\mathbf{d} = \frac{L}{m}\bar{\mathbf{d}},\ \mathbf{s} = E\bar{\mathbf{s}},\ y = \zeta H, \tag{8}$$

$$\boldsymbol{\Delta} = \begin{Bmatrix} \bar{\mathbf{d}} \\ \bar{\mathbf{s}} \end{Bmatrix},\ \mathbf{A} = \begin{bmatrix} -\mathbf{D}^{-1}\mathbf{G}H & \mathbf{D}^{-1}\mathbf{H}^{\mathrm{T}}Em\dfrac{H}{L} \\ \mathbf{D}^{-\mathrm{T}}(\mathbf{K}^{\mathrm{T}} - \omega^2\mathbf{D}^{\mathrm{T}}\mathbf{R})\dfrac{LH}{mE} & \mathbf{D}^{-\mathrm{T}}\mathbf{G}^{\mathrm{T}}H \end{bmatrix}. \tag{9}$$

For different sizes of the **A** matrix, different methods can be used for accurate solution, such as matrix exponential function, DQM method, and matrix eigenvalue decomposition, which can be referred to the works of Sheng et al. [11], Xu et al. [12] and Jiang et al. [9].

## 3. Numerical example

The steel-concrete composite beam works together through periodically distributed shear connectors. Consider a steel-concrete experimental composite beam with a span of 2m (figure 1). Two methods were considered here for shear connectors. One is to consider the actual spaced periodic distribution of stiffness, and the other is to equivalent it to a uniform distribution. Table 1 provides the natural frequency results of the composite beam under the two methods, which are compared with the finite element numerical results and test results of Zhang et al. [13]. Results using method (I) match well with the experimental measurements, with an error of only 0.64%. In contrast, results using method (II) are lower than the experimental measurements. This is because the equivalent method that uniformly distributes the shear strength over the entire beam length reduces the connection stiffness at the ends, leading to a decrease in the natural frequency of the composite beam.

**Table 1.** Natural frequency of periodic composite beam

| Method | Present (I) | Present (II) | FEM | Test |
|---|---|---|---|---|
| $f$ (Hz) | 56.48 | 55.12 | 56.55 | 56.12 |
| Error (%) | 0.64 | -1.78 | 0.76 | / |

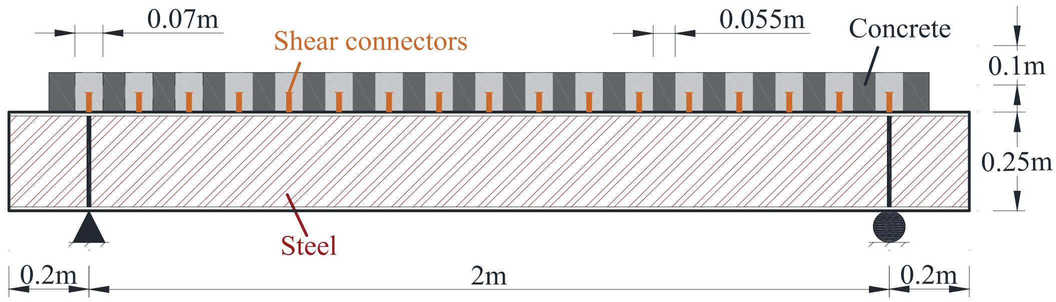


**Figure 1.** Schematic diagram of a composite beam with periodic shear connectors.

## References


[1] Wang, Y.-F., et al.: Tunable and active phononic crystals and metamaterials. Applied Mechanics Reviews, Vol. 72, No. 4, pp. 040801, 2020.

[2] Carrera, E.; Filippi, M.; Zappino, E.: Free vibration analysis of laminated beam by polynomial, trigonometric, exponential and zig-zag theories. Journal of Composite Materials, Vol. 49, No. 19, pp. 2299-2316, 2014.

[3] Xu, R.; Wu, Y.: Static, dynamic, and buckling analysis of partial interaction composite members using Timoshenko's beam theory. International Journal of Mechanical Sciences, Vol. 49, No. 10, pp. 1139-1155, 2007.

[4] Vo, T.P.; Lee, J.: Free vibration of axially loaded thin-walled composite Timoshenko beams. Archive of Applied Mechanics, Vol. 81, No. 9, pp. 1165-1180, 2011.

[5] Chakrabarti, A., et al.: Dynamic response of composite beams with partial shear interaction using a higher-order beam theory. Journal of Structural Engineering, Vol. 139, No. 1, pp. 47-56, 2013.

[6] Li, J.; Hu, X.; Li, X.: Free vibration analyses of axially loaded laminated composite beams using a unified higher-order shear deformation theory and dynamic stiffness method. Composite Structures, Vol. 158, pp. 308-322, 2016.

[7] Chen, W.Q.; Lü, C.F.; Bian, Z.G.: Elasticity solution for free vibration of laminated beams. Composite Structures, Vol. 62, No. 1, pp. 75-82, 2003.

[8] Lim, C.W., et al.: On new symplectic elasticity approach for exact free vibration solutions of rectangular Kirchhoff plates. International Journal of Engineering Science, Vol. 47, No. 1, pp. 131-140, 2009.

[9] Jiang, J., et al.: Two-dimensional model for composite beams and its state-space based mixed finite element solution by DQM. Composite Structures, Vol. 304, pp. 116442, 2023.

[10] Courant, R.; D. Hilbert: Methods of mathematical physics: partial differential equations. John Wiley & Sons, 2008.

[11] Sheng, H.Y.; Ye, J.Q.: A semi-analytical finite element for laminated composite plates. Composite Structures, Vol. 57, No. 1-4, pp. 117-123, 2002.

[12] Xu, R., et al.: Numerically Stable Solutions to the State Equations for Structural Analyses. Journal of Engineering Mechanics, Vol. 146, No. 3, pp. 04019136, 2020.

[13] Zhang, Y., et al: Natural frequency and mode of vibration of steel-concrete composite beam. Journal of Jilin University (Engineering and Technology Edition), Vol. 50, No. 2, pp. 581-588, 2020.

# A highly accurate and efficient hybrid dynamic stiffness method for vibro-acoustic problems within a wide frequency range

**Xueyi Zhao***, **Xiang Liu***

*High-speed Train Research Center
School of Traffic & Transportation Engineering
Central South University, Changsha 410075, China
xiangliu06@gmail.com

## Introduction

This summary presents a highly accurate and efficient hybrid modelling technique for the broadband 2D vibro-acoustic analysis. The structures are modelled by dynamic stiffness method (DSM) [1] using particular solutions of general acoustic and distributed force excitations. The acoustic cavities are modelled by the spectral DSM [2] with arbitrary BCs. The vibro-acoustic coupling is modelled analytically in the form of the modified Fourier series with very rapid convergence rate by enforcing the velocity continuity. As a result, the hybrid method exhibits a predominant advantage over the finite element method (FEM) [3] in terms of accuracy and computational efficiency.

## 1 Problem definition

A typical 2D vibro-acoustic system can be characterized by two physical variables: the acoustic pressure $p(\boldsymbol{r})$ at a position $\boldsymbol{r}(x,y)$ inside the acoustic domain $\Omega_a$ and the transverse deformation $w(\boldsymbol{r}')$ at a position $\boldsymbol{r}'(x',y')$ on the structure $\Gamma_s$. On parts $\Gamma_p$, $\Gamma_v$ and $\Gamma_Z$ the prescribed pressure, normal velocity and normal impedance can be specified respectively.

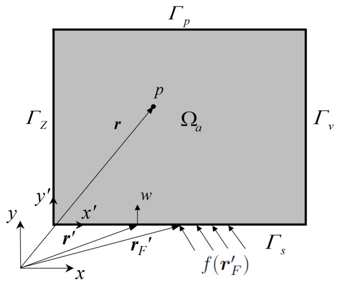


Figure 1: The model of a 2D coupled vibro-acoustic system.

The acoustic cavity $\Omega_a$ is filled with an acoustic fluid (density $\rho_0$ and sound speed $c_0$). The steady-state acoustic pressure $p(\boldsymbol{r})$ inside the cavity is governed by the Helmholtz equation

$$\nabla^2 p(\boldsymbol{r}) + k_a^2 p(\boldsymbol{r}) = 0, \quad \forall \boldsymbol{r} \in \Omega_a \tag{1}$$

where $k_a = \omega/c_0$ denotes the acoustic wave number, $\omega$ is the circular frequency.

The structure $\Gamma_s$ can be treated as a beam assembly, which has a density $\rho_s$ and Young's modulus $E$. The steady-state transverse displacement $w(\boldsymbol{r}')$ of the beam assembly is governed by the Euler-Bernoulli theory

$$\left(\nabla^4 - k_b^4\right) w\left(\boldsymbol{r}'\right) = \frac{f(\boldsymbol{r}'_F)}{EI}, \quad \forall \boldsymbol{r}' \in \Gamma_s \tag{2}$$

where $k_b = \sqrt[4]{\frac{\rho_s A \omega^2}{EI}}$ is the bending wavenumber, $EI$ is the bending stiffness and $A$ is the cross-sectional area of a beam. $f(\boldsymbol{r}'_F)$ is the distributed force or acoustic excitation at the position $\boldsymbol{r}'_{\boldsymbol{F}}(x'_F, y'_F)$.

Here, a light-fluid approximation is made: the normal velocity continuity condition needs to be satisfied along the structural-acoustic coupling interface $\Gamma_s$

$$\frac{\mathrm{j}}{\rho_0 \omega} \frac{\partial p(\boldsymbol{r})}{\partial n} = \mathrm{j}\omega w(\boldsymbol{r}\prime), \quad \boldsymbol{r} \in \Gamma_s \tag{3}$$

where $\mathrm{j} = \sqrt{-1}$ is the imaginary unit and $n$ is the surface outward normal.

## 2 Spectral dynamic stiffness (SDS) formulations for vibro-acoustic analysis

The interior acoustic cavity is first constructed by the SDS model [2] using the modified Fourier series (MFS) with a favourable convergence rate. The acoustic pressure is expanded into a sum of two series solutions by using modified Fourier basis functions (MFBF) [2], which satisfies exactly the Helmholtz equation and is given by

$$P(x,y) = \sum_{\substack{m \in \mathbb{N} \\ k \in \{0,1\}}} \mathscr{T}_k(\alpha_{km} x) P_{km}(y) + \sum_{\substack{n \in \mathbb{N} \\ j \in \{0,1\}}} P_{jn}(x) \mathscr{T}_j(\beta_{jn} y) \tag{4}$$

and $\mathscr{T}_k(\alpha_{km}x)$ and $\mathscr{T}_j(\beta_{jn}y)$ are MFBF defined in the united form as

$$\mathscr{T}_l(\gamma_{ls}\xi) = \begin{cases} \cos(\gamma_{ls}\xi) & l=0 \\ \sin(\gamma_{ls}\xi) & l=1 \end{cases}, \quad \gamma_{ls} = (s + \frac{l}{2})\frac{\pi}{L} \tag{5}$$

where $\gamma_{ls}$ refers to either $\alpha_{km}$ or $\beta_{jn}$, $\xi$ refers to $x$ or $y$ and $L$ is half the boundary length of the acoustic cavity.

Next, the SDS matrix for an acoustic cavity can be developed analytically based on the above general solution and boundary conditions, which can be written in the form

$$\boldsymbol{v} = \boldsymbol{K}\boldsymbol{p} \tag{6}$$

where $\boldsymbol{K}$ is the SDS matrix of the acoustic cavity, $\boldsymbol{v}$ and $\boldsymbol{p}$ are respectively the modified Fourier coefficient vector of the normal velocity and the acoustic pressure. The modified Fourier coefficients $V_{ls}$ of the normal velocity vector $\boldsymbol{v}$ can be given by

$$V_{ls} = \int_{-L}^{L} \mathrm{j}\omega w(\xi) \frac{\mathscr{T}_l(\gamma_{ls}\xi)}{\sqrt{\zeta_{ls} L}} \mathrm{d}\xi \tag{7}$$

with

$$w(\xi) = \boldsymbol{N}_F(\xi, \omega)\boldsymbol{d}_F + w_F^*(\xi), \quad \boldsymbol{d}_F = \boldsymbol{K}_F^{-1}\boldsymbol{f}_F \tag{8}$$

where $\boldsymbol{N}_F(\xi, \omega)$ is the shape function, $\boldsymbol{K}_F$ is the DS matrix which relates the force vector $\boldsymbol{f}_F$ and displacement vector $\boldsymbol{d}_F$ of the beam. $w_F^*(\xi)$ is the particular solution of an external excitation.

## 3 Results

An I-shaped beam frame coupled with two acoustic cavities is given to illustrate the superior performance of the proposed method. The vibro-acoustic system is subjected to an incident plane wave with an oblique incident angle of $\alpha = 30°$, as shown in Figure 2. The dimensions of each acoustic cavity are $2L_1 = 1.25$ mm and $2L_2 = 1.6$ mm. The vibro-acoustic response up to 1000 Hz under the acoustic excitation is computed by the present methods and FEM, as shown in Table 1. The DoFs for both the structural and acoustic part is 86 in total, while only 5 structural elements and 2 acoustic elements are used in the proposed method. However, 6988 elements are obtained during the FE discretization in which the element size is not larger than 2.5 mm and thus 29118 DoFs are used in the FEM. Thus, the proposed method shows a big potential in reducing the computational cost.

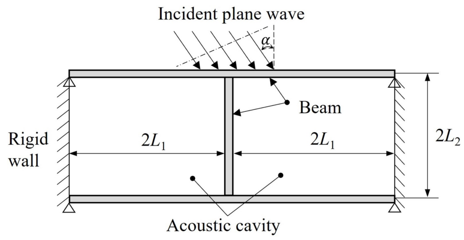


Figure 2: The vibro-acoustic system consist of beams and cavities under acoustical excitation.

Table 1: Vibro-acoustic response of an I-shaped beam frame coupled with two acoustic cavities under the acoustical excitation at 70 Hz, 400 Hz and 1000 Hz.

| Method | 70 Hz | 400 Hz | 1000 Hz |
|---|---|---|---|
| Present method | 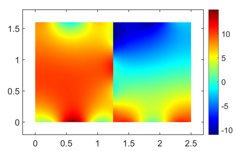 | 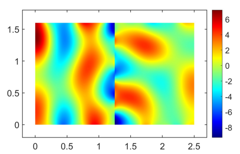 | 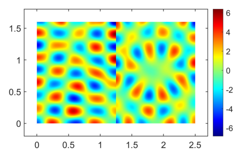 |
| FEM | 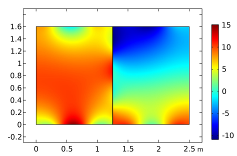 | 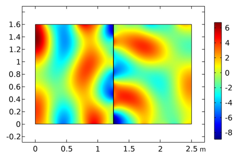 | 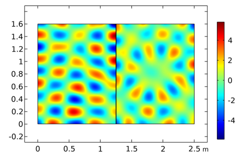 |

## References


[1] J. R. Banerjee: Review of the dynamic stiffness method for free-vibration analysis of beams. Transportation Safety and Environment, Vol. 1, No. 2, pp. 106–116, 2019.

[2] Liu, X., Zhao, X., Liu, X.: A highly accurate spectral dynamic stiffness method for efficient broadband modal and dynamic response analysis of membranes assemblies with arbitrary boundary conditions. Computers & Structures, Vol. 267, 2022.

[3] Ph. Bouillard, F. Ihlenburg: Error estimation and adaptivity for the finite element method in acoustics: 2D and 3D applications. Computer Methods in Applied Mechanics and Engineering, Vol. 176, No. 1, pp.147–163, 1999.

# Vibrational Characteristics of Rotating Soft Cylinders

**Chaofeng Lü[*#], Kecheng Li[*], Yinnan Zhang[#], He Zhang[#]**

[*] Faculty of Mechanical Engineering
Ningbo University
818 Fenghua Road, Ningbo
315211, PR China
lucf@zju.edu.cn

[#] Department of Civil Engineering
Zhejiang University
866 Yuhangtang Road, Hangzhou
310058, PR China
zjuzhanghe@zju.edu.cn

In the field of soft or stretchable manufacturing, rotating structures are always the core components of sensors, pumps, and actuators that are designed for specific functions and complicated working scenarios [1-3]. Moreover, rotating structures are also used to generate various prescribed patterns [3]. For soft cylinders, the effects of the rotation on both static and dynamic behaviour are more obvious. Ertepinar [4] studied the vibration characteristics of a rotating cylinder using the theory of small motions superposed on the large deformation, while Haughton and Ogden [5] presented the bifurcation analysis of a rotating thick-walled soft cylinder with finite length.

Here, we investigate the effects of the centrifugal and Coriolis forces on the dynamic behaviour of a rotating soft cylinder based on the nonlinear elasticity and linear incremental theories [6]. The large deformation of the soft cylinder induced by centrifugal force causes initial tension and makes the material anisotropic. The cylinder is then assumed to undergo small perturbation superposed on the large deformation. Numerical results are finally presented to explain the differences of dynamic behaviour between the rotating and stationary soft cylinders.

Consider a stationary infinitely long soft cylinder with arbitrary thickness in a reference coordinate system $\left(R,\Theta,\mathrm{Z}\right)$ . Under a uniform rotating speed $\varPhi$ along its axis, the cylinder undergoes an axisymmetric deformation to a deformed state in the initial coordinate system $\left(r,\theta,z\right)$ . Then, the deformation gradient can be described as $\mathbf{F}=\mathrm{diag}\left(\lambda_r,\lambda_\theta,\lambda_z\right)$ $=\mathrm{diag}\left(\mathrm{d}r/\mathrm{d}R,r/R,1\right)$ . For an incompressible neo-Hookean solid with the strain energy density $\Omega=\mu\left(\lambda_r^2+\lambda_\theta^2+\lambda_z^2-3\right)/2$ , the Cauchy stresses can be writen as $\tau_{rr}=\mu\lambda_\theta^{-2}-p$ and $\tau_{\theta\theta}=\mu\lambda_\theta^2-p$ with $p$ denoting the hydrostatic pressure. The Cauchy stresses in the cylinder then satisfy the equilibrium equation

$$\frac{\partial\tau_{rr}}{\partial r}+\frac{\tau_{rr}-\tau_{\theta\theta}}{r}+\rho\varPhi^2 r=0\,. \tag{1}$$

Combine with the boundary conditions at the outer and inner surfaces $r=r_\mathrm{i},r_\mathrm{o}$ , the above equation finally gives the inner radius $r_\mathrm{i}$ of the deformed cylinder. Once the inner radius of the deformed cylinder has been determined, the initial stresses can be obtained.

Theoretical predictions show that the principal hoop stretch at the inner surface $\overline{r}_\mathrm{i}=r_\mathrm{i}/R_\mathrm{i}$ increases with the rotating speed $\overline{\varPhi}=\varPhi R_\mathrm{o}\sqrt{\rho/\mu}$ for various initial tube sizes, and tends to infinity at a certain rotating speed $\overline{\varPhi}_\mathrm{max}$ (Fig. 1a). The rotation is also expected to induce inhomogeneous deformation in the rotating cylinder (Fig. 1b) with the dimensionless equivalent elastic moduli defined as $\bar{A}_{0rr} = \lambda_\theta^{-2} + \bar{p}$ and $\bar{A}_{0\theta\theta} = \lambda_\theta^2 + \bar{p}$.

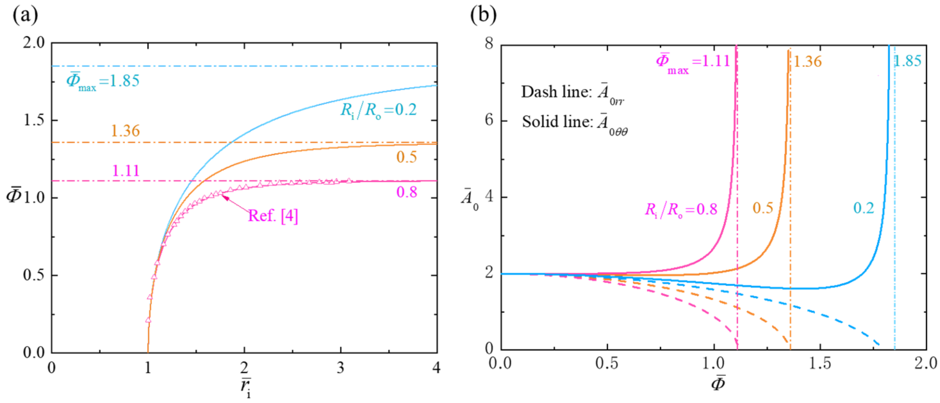


**Figure 1.** (a) Deformed inner radius of the soft cylinder due to rotating speed for various initial radius ratios. (b) Variations of the equivalent elastic moduli at the deformed middle surface versus the rotating speed.

For the dynamic characteristics of the deformed soft cylinder, the incremental displacement vector is $\mathbf{u} = u_r \mathbf{e}_r + u_\theta \mathbf{e}_\theta$, where $\mathbf{e}_r, \mathbf{e}_\theta$ are the unit base vectors corresponding to the deformed configuration. According to the linear incremental theory [6], the governing equations are

$$\begin{aligned} &\frac{\partial \tilde{T}_{0rr}}{\partial r} + \frac{1}{r}\frac{\partial \tilde{T}_{0\theta r}}{\partial \theta} + \frac{\tilde{T}_{0rr} - \tilde{T}_{0\theta\theta}}{r} + \rho \Phi^2 u_r + 2\rho\Phi \frac{\partial u_\theta}{\partial t} = \rho \frac{\partial^2 u_r}{\partial t^2} \\ &\frac{\partial \tilde{T}_{0r\theta}}{\partial r} + \frac{1}{r}\frac{\partial \tilde{T}_{0\theta\theta}}{\partial \theta} + \frac{\tilde{T}_{0\theta r} + \tilde{T}_{0r\theta}}{r} + \rho \Phi^2 u_\theta - 2\rho\Phi \frac{\partial u_r}{\partial t} = \rho \frac{\partial^2 u_\theta}{\partial t^2} \end{aligned} \tag{2}$$

where $\tilde{T}_0$ is the incremental Lagrangian stress. The incremental field problem governed by Eqs. (2) may be solved using the state space method [7].

For the rotating cylinder, the dimensionless natural frequency $\bar{\omega} = \omega R_o \sqrt{\rho / \mu}$ is no longer symmetric due to Coriolis force. A significant difference lies between the fequencies of the waves propagating along the rotating direction (forward) and those propagating along the anti-rotating direction (backward) as shown in Fig. 2a.

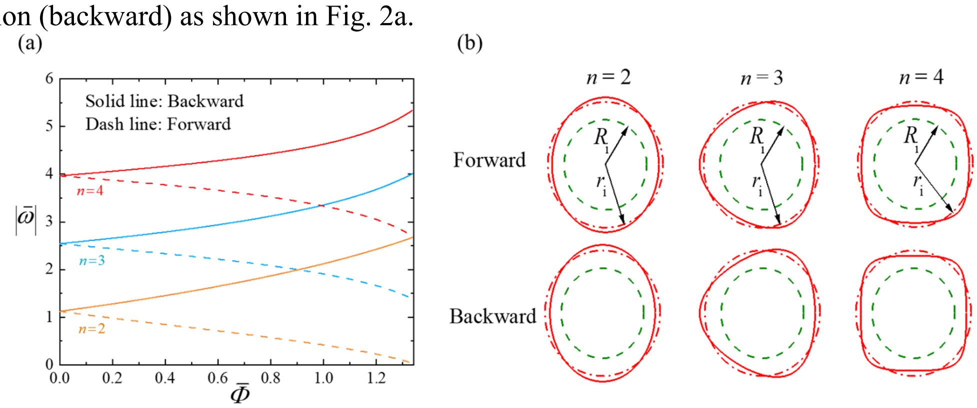


**Figure 2.** (a) The natural frequencies of vibration modes $n = 2,\ 3,\ 4$ versus the rotating speed. (b) Vibration modes at rotating speed $\bar{\Phi} = 1$.

We further investigate the snap-through instability of rotating tubes with Ogden model, which results in jump phenomenon of frequency. As shown in Fig.3(a), the rotating soft tube expands suddenly from point $P_1$ to point $P_2$, corresponding to a sudden jump in the frequencies, see Fig.3(b). Interestingly, for a thin tube, the negative frequencies of first- and second-order almost meet together when the snap-through instability occurs, and the first-order negative frequency is nearly unchanged before and after the snap-through instability as indicated by the point $P_3$.

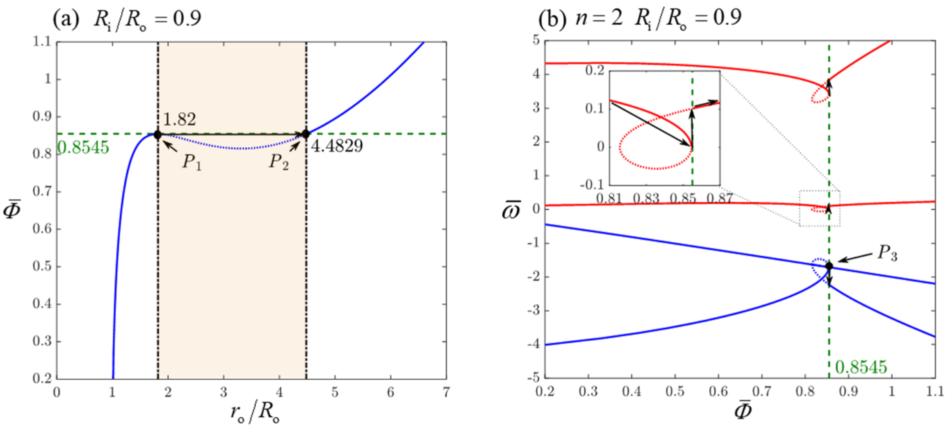


**Figure 3.** (a) The snap-through instability of rotating Ogden tubes. (b) The natural frequencies jump suddenly as the rotating speed increases.

In conclusion, the soft cylinder expands nonlinearly with the increasing rotating speed. The natural frequencies of the cylinder are no longer symmetric due to the presence of Coriolis force induced by the rotation. The soft cylinder may suffer snap-though instability with high rotating speed, leading to the suddenly jump of natural frequencies. This work demonstrates that the centrifugal and Coriolis forces might have significant effects on the vibrational characteristics of the cylinder. The results will benefit the design and control of novel engineering systems with rotating soft cylinders or shafts.

## References


[1] Chen, W.Q.; Lee, K.Y.: Stresses in Rotating Cross-Ply Laminated Hollow Cylinders with Arbitrary Thickness. The Journal of Strain Analysis for Engineering Design, Vol. 39, No. 5, pp. 437-445, 2004.

[2] Clement G.: International Roadmap for Artificial Gravity Research. npj Microgravity, Vol. 3, No. 1, pp. 29, 2017.

[3] Mora S., Richard F.: Buckling of a Compliant Hollow Cylinder Attached to a Rotating Rigid Shaft. International Journal of Solids and Structures, Vol. 167, pp. 142-155, 2019.

[4] Ertepinar, A.: Stability and Vibrations of Spinning Tubes Subjected to Uniform Radial Pressure. Journal of Sound and Vibration, Vol. 86, No. 3, pp. 343-351, 1983.

[5] Haughton, D.M.; Ogden, R.W.: Bifurcation of Rotating Thick-Walled Elastic Tubes. J. Mech. Phys. Solids, Vol. 28, No. 1, pp. 59-74, 1980.

[6] Dorfmann, A.; Ogden, R.W.: Nonlinear Electroelastic Deformations. Journal of Elasticity, Vol. 82, No. 2, pp. 99-127, 2006.

[7] Wu, B.; Su, Y.P.; Chen, W.Q.; et al.: On Guided Circumferential Waves in Soft Electroactive Tubes Under Radially Inhomogeneous Biasing Fields. J. Mech. Phys. Solids, Vol. 99, pp. 116-145, 2017.

# Voxel-Based Method for Determining Effective Cross-Section Properties of Sandwich Beams with Porous Cores in Natural Frequency Analysis

**Yunhua Luo**[*], **Prajjayini Chakma**[*], and **Jonghyun Kim**[*]

[*] Department of Mechanical Engineering
University of Manitoba
75A Chancellor's Circle, R3T 2N2, Winnipeg, Canada
Yunhua.Luo@umanitoba.ca

**Summary**

Sandwich beams with porous cores have extensive application in engineering structures due to their advantageous characteristics, including lightweight design, high strength-to-weight ratio, and enhanced vibration damping. Accurately determining the effective elastic properties of these sandwich beams is essential for understanding their dynamic behaviour, particularly in relation to natural frequencies. Presently, methods for determining these properties typically involve a two-step process. Initially, the effective elasticity modulus of the porous core is determined, often through the use of analytical formulas or numerical techniques based on homogenization theories. Subsequently, this modulus is employed to calculate the effective cross-section stiffness, encompassing axial, bending, shear, and torsional stiffness, by considering the material and geometric properties of both the core and face sheets. However, this approach is subject to certain limitations. The analytical formulas or numerical techniques often rely on simplified assumptions when deriving the effective elasticity modulus. These assumptions involve idealized geometric configurations, uniform pore distributions, and isotropic material behaviour. Furthermore, in the calculation of cross-section stiffness, material properties such as Young's modulus and shear modulus, along with cross-section geometric parameters like cross-section area and bending moment of inertia, are frequently treated separately for the sake of simplicity, despite their integrated contributions to the cross-section stiffness. These simplifications may introduce substantial errors into the effective properties of the sandwich beam, thereby affecting the accuracy of the calculated natural frequencies.

To overcome these limitations and to align with the emerging technology of voxel-based 3D printing [1], we are developing a voxel-based method for accurately determining the effective cross-section stiffness of sandwich beams with porous cores, the new method is based on our previous work [2, 3]. If the assumptions of Euler-Bernoulli or Timoshenko beam theory are adopted, this approach employs the definitions of beam cross-section stiffness, as illustrated in Figure 1(a) and expressed in the equations below.

$$\begin{aligned} EA &= \int_A E(x,y)dA, \quad EI_x = \int_A E(x,y)\, y^2 dA, \\ GA &= \int_A G(x,y)dA, \quad JA = \int_A G(x,y)\,(x^2+y^2)dA \end{aligned} \tag{1}$$

In the above expressions $EA$, $EI_x$, $GA$ and $JA$ are respectively the axial, bending, shear and torsional stiffness of the beam. $E(x,y,z)$ and $G(x,y,z)$ are Young's modulus and shear modulus of the material. $A$ is the area of the cross-section.

We assume that the size of the pores is not sufficiently small compared to the cross-sectional

dimensions. Therefore, it is necessary to treat the porous core as a heterogeneous material with varying effective material properties across the area. To calculate the effective stiffness for the cross-section depicted in Figure 1(a) and defined in Equation (1), we began by voxelizing the beam, as shown in Figure 1(b). Subsequently, the beam cross-section was partitioned into cells for numerical integration, as illustrated in Figure 1(c). In order to determine the effective material properties at a Gaussian point, we employed a representative volume element (RVE), Figure 1(d), located at that point and performed finite element characterization.

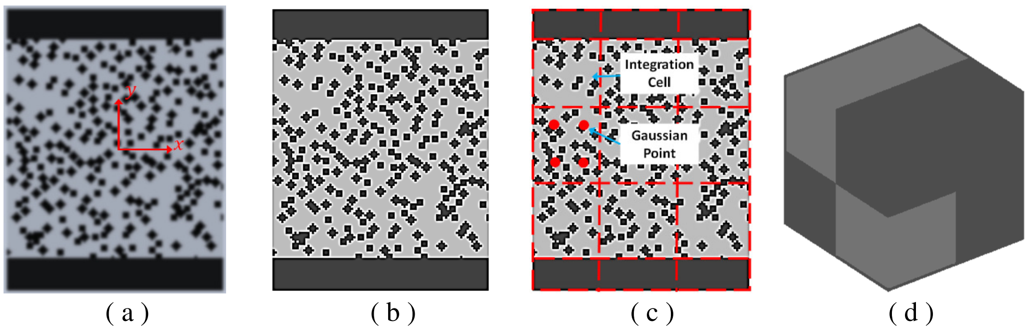


**Figure 1.** Voxel-based method for determining effective stiffness of sandwich beam with porous core. (a) A cross-section of the sandwich beam; (b) Voxelization of the phase materials; (c) Integration cells and Gaussian points; (d) a RVE taken at a Gaussian point.

The determined cross-section stiffness properties are subsequently employed in the analysis of natural frequencies using beam elements. It is noted that the voxel-based method exhibits computational complexity. However, there are several approaches available to enhance its computational efficiency. For instance, prior to conducting finite element characterization, it is possible to examine the material composition within the representative volume element (RVE). If the RVE comprises a single material phase, the material properties can be directly used without conducting finite element characterization, thereby saving computational time.

During the conference presentation, we intend to share the following results as they become available:

1) The impact of various factors such as voxel size, the number of integration cells, and the size of the representative volume element (RVE) on the computed natural frequencies.
2) Given the scarcity of experimental data on natural frequencies for sandwich beams with porous cores in existing literature, we will compare the natural frequencies obtained through beam elements with those computed directly from the voxel-based finite element model.
3) The relation between porosity in the core and the natural frequencies of the beam.

## References

[1] Kokkinis, D.; Bouville, F. and Studart, A.R. : 3D printing of materials with tunable failure via bioinspired mechanical gradients. Adv. Mater., Vol. 30, e1705808, 2018.

[2] Luo, Y.: An accuracy comparison of micromechanics models of particulate composites against microstructure-free finite element modeling. Materials, Vol. 15, No. 4021, 2022.

[3] Luo,Y.: Voxel-based design and characterization of functionally graded materials. Results in Materials, Vol. 17, No. 100375, 2023.

# Energy transmission through finite periodic structures

**Brian R. Mace***, **Jean P. Carneiro Junior#**, **Donovan du Toit***, **Paulo J. P. Gonçalves#**, **Vladislav S. Sorokin***, **Michael J. Brennan#**, **Vinicius G. Cleante†**

*Acoustics Research Centre,
Department of Mechanical and
Mechatronics Engineering,
The University of Auckland,
Auckland, New Zealand
b.mace@auckland.ac.nz
v.sorokin@auckland.ac.nz
ddut037@aucklanduni.ac.nz

# State University of São Paulo,
UNESP,
Faculty of Engineering,
Bauru, Brazil
jeancarneirojr@gmail.com
paulo.paupitz@unesp.br
mjbrennan0@btinternet.com

† Division of Mechanical Engineering,
Aeronautics Institute of Technology Institute of Mechanics
São José dos Campos, Brazil
cleante@ita.br

**Summary**

This paper concerns the transmission of time-harmonic vibrations through a system comprising two, one-dimensional uniform waveguides, such as a rod or beam, between which is a finite periodic structure (Figure 1(a)). An example is the continuous waveguide with periodic attachments shown in Figure 1(b). It is well known that wave propagation in infinite periodic structures exhibits pass and stop bands due to Bragg scattering: these are frequency bands in which waves propagate freely over long distances or attenuate rapidly with distance. Wave transmission through finite periodic structures has been less extensively considered (e.g. [1,2]) and the behaviour is more complicated. The aim here is to predict the amplitudes of the net transmitted waves $\mathbf{b}^+$ given incident waves $\mathbf{a}^+$ and what affects this transmission: these are the result of wave reflection, transmission and propagation in various parts of the overall structure.

Figure 1(a) also shows the vectors of wave amplitudes at relevant locations. There are $N$ cells in the periodic segment. There may be a number of waves which travel in both the positive and negative $x$-directions: for example, there is one wave for a rod undergoing axial vibration, two for a thin beam in flexural vibration. In the continuous waveguides waves propagate in the positive $x$-direction as $\exp i(\omega t - kx)$ at frequency $\omega$, with $k$ being the wavenumber ($k = \omega\sqrt{E/\rho}$ for a rod, $E$ and $\rho$ being the elastic modulus and density). The time dependence will henceforth be suppressed. In the periodic segment waves propagate as Bloch waves, each wave varying as $\lambda = \exp(\mu)$ from one periodic cell to the next, $\mu$ being the propagation constant (imaginary in the pass band, complex with a negative real part in the stop bands). Thus at the ends of the periodic segment the Bloch waves are related by the propagation relations

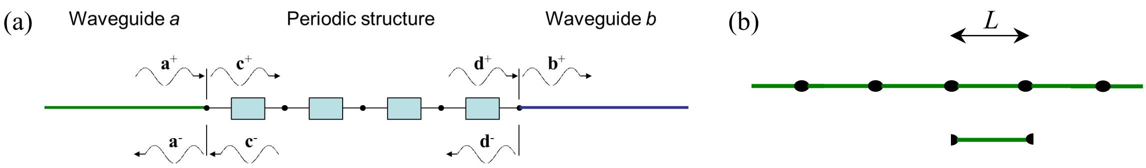


**Figure 1.** (a) Waveguides with finite periodic array ($N = 4$). Wave amplitudes at various locations shown. (b) Uniform waveguide with $N + 1$ periodic attachments and periodic cell.

$$\mathbf{d}^+ = diag\left(\lambda^N\right)\mathbf{c}^+, \quad \mathbf{c}^- = diag\left(\lambda^N\right)\mathbf{d}^- \tag{1}$$

where *diag*(.) denotes a diagonal matrix. The propagation constants can be found in various ways.

The discontinuities between the uniform waveguides and the periodic segment cause incident waves to be reflected and transmitted. The outgoing waves from these discontinuities are

$$\mathbf{c}^+ = \mathbf{T}_1\mathbf{a}^+ + \mathbf{R}_1\mathbf{c}^-,\ \mathbf{d}^- = \mathbf{R}_2\mathbf{d}^+,\ \mathbf{b}^+ = \mathbf{T}_2\mathbf{d}^+ \tag{2}$$

where $\mathbf{R}_{1,2}$ and $\mathbf{T}_{1,2}$ are matrices of reflection and transmission coefficients, which can be found from equilibrium and continuity conditions at junctions 1 and 2. It follows that

$$\mathbf{c}^+ = \left[\mathbf{I} - \mathbf{R}_1 diag\left(\lambda^N\right)\mathbf{R}_2 diag\left(\lambda^N\right)\right]^{-1}\mathbf{T}_1\mathbf{a}^+. \tag{3}$$

Thus $\mathbf{b}^+ = \mathbf{T}_{tot}\mathbf{a}^+$ where the total transmission matrix $\mathbf{T}_{tot}$, which defines the transmission of waves $\mathbf{a}^+$ through the finite periodic segment, is given by

$$\mathbf{T}_{tot} = \mathbf{T}_2 diag\left(\lambda^N\right)\left[\mathbf{I} - \mathbf{R}_1 diag\left(\lambda^N\right)\mathbf{R}_2 diag\left(\lambda^N\right)\right]^{-1}\mathbf{T}_1. \tag{4}$$

The total transmission depends on three factors. The first (the $\lambda$ terms) relates to the pass/stop band structure of the periodic segment: in a stop band typically $\lambda$ is small and wave transmission is small while in a pass band $|\lambda| = 1$. The second concerns entrance/exit effects ($\mathbf{T}_{1,2}$) because of impedance discontinuities at the two junctions: the wave and Bloch wave mode shapes and impedances are different – there are changes in the waveguide properties. There may also be an attached impedance at the junction. The third, the matrix inverse in square brackets, represents internal resonance effects: the wavefield within the periodic segment comprises successive reflections of the Bloch waves from the junctions which may interfere constructively or destructively, leading to large and small transmission respectively. The net effect is that the energy transmission is centred on the pass bands where it varies very rapidly with frequency.

As an example, consider axial waves in a uniform rod with $N$+1 masses spaced equal distances $L$ apart (Figure 1(b)). There is 1 DOF, the axial displacement $u$, and the corresponding internal force is the tension $P = EA\,\partial u/\partial x$. Thus **q**, **f**, the wave amplitude vectors and reflection and transmission matrices become scalars. The choice of the periodic cell is somewhat arbitrary, but is here chosen to be a rod segment with half of the attachment at each end (Figure 1(b)), so that there are $N$ cells. The transmission coefficient for a single mass is [3]

$$t = Te^{i\phi_t}, \quad T = 1/(1+i\mu), \quad \mu = (m/2\rho AL)kL, \quad \phi_t = -\tan^{-1}\mu \tag{5}$$

while $R_{1,2} = R\,\mathrm{e}^{-i\phi_r}, T_1T_2 = T^2$. The propagation constant and $T_{tot}$ are

$$\cosh\mu = \cos(kL - \phi_t)/\cos\phi_t, \quad T_{tot} = T^2\lambda^N\Big/\left(1 - R^2\lambda^{2N}e^{-i2\phi_r}\right). \tag{6}$$

In a stop band $|\lambda| < 1$ and the transmitted power is $\tau = \left|T_{tot}^2\right| \approx T^4\lambda^{2N}$, and is small. In a pass band

$$\lambda = e^{-i\phi}, \quad T_{tot} = T^2 e^{-iN\phi} \Big/ \left(1 - R^2 e^{-i(2N\phi + 2\phi_r)}\right). \tag{7}$$

Internal resonances occur when $N\phi + \phi_r = n\pi$ where $|T_{tot}| = 1$. There are thus $N$ internal resonances in each pass band at which energy flows freely through the periodic segment. Between these are antiresonances, where destructive interference occurs. It can be shown that the frequency average energy transmission is less than $T^4$, so that the periodic insert decreases the net energy flow, even in the pass bands. Figure 2(a) shows the propagation constant as a function of dimensionless frequency $\Omega = kL/\pi$ for the case where $m = 0.2\rho AL$. The width of the pass bands decreases as frequency increases, with the start of each pass band occurring for integral $\Omega$. The transmitted power $\tau$ is shown in Figures 2(b,c) for the cases where there are $N = 0,1,2,10$ periodic cells, hence 1,2,3,11 masses. Transmission is very small in the stop bands but strongly modulated in the pass bands, with there being resonances where $\tau = 1$ in each pass band. The results can be extended to include the effects of damping, determine frequency average transmission etc.

**Acknowledgements** The authors gratefully acknowledge the financial support provided by ENZ, New Zealand and FAPESP, Brazil.

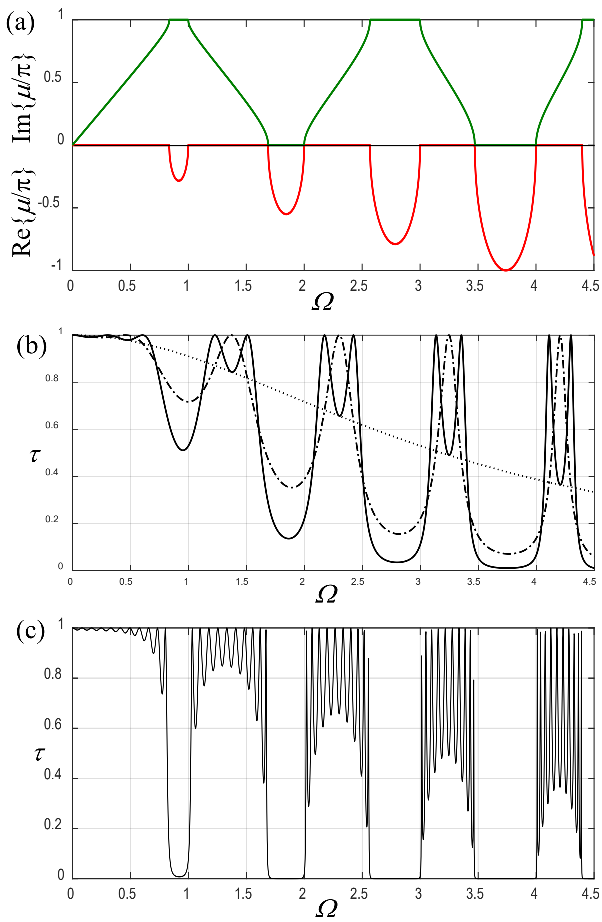


**Figure 2.** Rod with added masses: (a) Propagation constant; (b) Transmitted power, … 1 mass, - · - · 2 masses, ___ 3 masses; (c) 11 masses ($N$=10).

## References


[1] Santos, R.B.; Berres, G; Inman, D.J.; Gonsalez-Bueno, C.G.; Bueno, D.D.: A Practical Approach to Evaluate Periodic Rods Composed of Cells with Geometric and Material Periodicity. Journal of Sound and Vibration, 553. doi.org/10.1016/j.jsv.2023.117646, 2020.

[2] Gonçalves, P.J.P.; Brennan, M.J.; Cleante, V.G.: Predicting the stop-band behaviour of finite mono-coupled periodic structures from the transmissibility of a single element. Mechanical Systems and Signal Processing, 154, doi.org/10.1016/j.ymssp.2020.107512, 2021.

[3] Rughunanan, L.; Mace, B.R.; Sorokin, V.; du Toit, D.: On the behaviour of infinite, periodic, mono-coupled waveguides using a transmission coefficient phase method. Mechanical Systems and Signal Processing **135**, doi.org/10.1016/j.ymssp.2019.106409, 2020.

# Natural Frequency Estimation for an Euler-Bernoulli Beam Carrying a Mass with Rotary Inertia

**Xutao Sun, Yusuke Mochida, Sinniah Ilanko**

The School of Engineering, The University of Waikato

Gate 1 Knighton Road Private Bag

3105 Hamilton 3240 New Zealand

BrianSun2018@hotmail.com, yusuke@waikato.ac.nz, ilanko@waikato.ac.nz

## Summary

An Euler-Bernoulli beam carrying a mass with rotary inertia is shown in Figure 1. The governing equation of motion of the beam can be expresses as

$$\bar{m}\ddot{u}(x,t) + EIu''''(x,t) = \left[-M\ddot{q}_M(t) - J\ddot{\theta}(t)\right]\delta(x - x_0) \tag{1}$$

where $\bar{m}$ is mass per unit length, $EI$ is flexural rigidity, $x_0$ is the coordinate of the mass location, and $u(x,t)$ is the deflection of the beam. The overdot represents the derivative with respect to time and the prime represents the derivative with respect to $x$. $M$ and $J$ denote the translational inertia and rotary inertia of the mass, respectively. $q_M(t)$ and $\theta(t)$ are the vertical displacement and rotation of the mass, respectively. The mass is rigidly attached to the beam. For the $n$th mode, the motion of the mass can be written as

$$q_M(t) = u_n(x,t)|_{x_0} = u_n(x_0,t) \tag{2}$$

and

$$\theta(t) = u_n'(x,t)|_{x_0} = u_n'(x_0,t) \tag{3}$$

where $u_n(x,t)$ is the beam deflection for the $n$th mode.

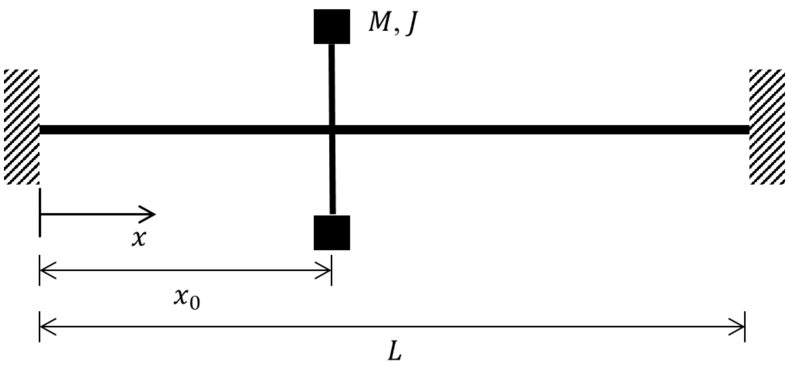


**Figure 1. A beam carrying a roving mass with rotary inertia.**

When $M$ and $J$ are small enough, the influence of the mass is insignificant. Therefore, assuming the mode shape stays the same after attaching the mass to the beam, $u_n(x,t)$ can be expressed as (assuming harmonic oscillation)

$$u_n(x,t) = \phi_n(x)e^{i\omega_n t} \tag{4}$$

where $\omega_n$ is the $n$th natural frequency of the beam carrying the mass, and $\phi_n(x)$ is the $n$th mode shape of the beam found by solving the following equation

$$EI\phi_n''''(x) - \bar{m}\omega_{bn}^2\phi_n(x) = 0 \tag{5}$$

where $\omega_{bn}$ is the $n$th natural frequency of the bare beam (i.e. the beam without carrying a mass). Substituting Equations (2)-(4) into Equation (1) and multiplying $\phi_n(x)$ on both sides and integrating over the whole beam yields

$$\begin{aligned} -\omega_n^2 \int_0^L \bar{m}\phi_n(x)\phi_n(x)dx + \int_0^L EI\phi_n(x)\phi_n''''(x)dx = \\ \omega_n^2 \int_0^L \phi_n(x)[M\phi_n(x_0) + J\phi_n'(x_0)]\delta(x - x_0)dx \end{aligned} \tag{6}$$

Considering the orthogonal property of mode shapes

$$\int_0^L \phi_n(x)\phi_m(x)dx = \begin{cases} 0 & (n \neq m) \\ \psi_n & (n = m) \end{cases} \tag{7}$$

the first term on the left-hand side of Equation (6) can be simplified as

$$-\omega_n^2 \int_0^L \bar{m}\phi_n(x)\phi_n(x)dx = -\omega_n^2\bar{m}\psi_n \tag{8}$$

Considering Equation (5) and Equation (7), the second term on the left-hand side of Equation (6) can be written as

$$\int_0^L EI\phi_n(x)\phi_n''''(x)dx = \bar{m}\omega_{bn}^2\psi_n \tag{9}$$

Using Equation (7) and the sifting property of $\delta$ function, the right-hand side of Equation (6) can be expressed as

$$\omega_n^2 \int_0^L \phi_n(x)[M\phi_n(x_0) + J\phi_n'(x_0)]\delta(x - x_0)dx = \omega_n^2\phi_n(x_0)[M\phi_n(x_0) + J\phi_n'(x_0)] \tag{10}$$

Therefore, rearranging and rewriting Equation (6) gives

$$\bar{m}\omega_{bn}^2\psi_n - \omega_n^2\{\bar{m}\psi_n + \phi_n(x_0)[M\phi_n(x_0) + J\phi_n'(x_0)]\} = 0 \tag{13}$$

The $n$th natural frequency of the beam carrying a mass at $x_0$ can be written as

$$\omega_n^2(x_0) = \frac{\omega_{bn}^2}{1 + \dfrac{M\phi_n^2(x_0) + J\phi_n(x_0)\phi_n'(x_0)}{\bar{m}\psi_n}} \tag{14}$$

To verify the accuracy of Equation (14), the natural frequency of a simply supported steel beam carrying a mass with rotary inertia is calculated using the dynamic stiffness method (DSM). The dimension of the beam and the mass location are shown in Figure 2. For the beam material: $\rho$=7850kg/m$^3$, E=200GPa, and $\nu$=0.28. For the mass: $\tau = M/M_{beam}$ and $\varphi = J/J_{beam}$ where $J_{beam}$=1.1307kg·m$^2$ is the rotary inertia about the central axis $O'$ of the beam.

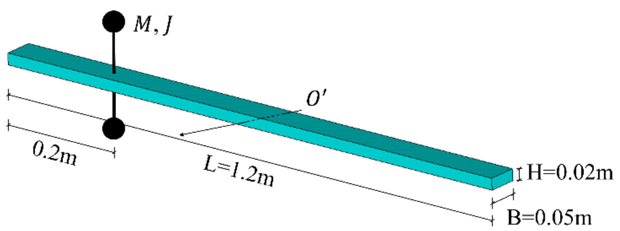


**Figure 2. The geometry of the simply supported beam carrying a mass with rotary inertia.**

When maintaining $\tau$ (or $\varphi$) equal to zero and adjusting $\varphi$ (or $\tau$), the relative frequency error is evaluated by the ratio between absolute frequency error and DSM frequency result, i.e.

$$\gamma = \frac{\left|\omega_{DSM} - \omega_{equation(14)}\right|}{\omega_{DSM}} \tag{15}$$

Figure 3 shows the variation of $\gamma$ against $\varphi$ (or $\tau$) plotted in logarithm for the first five natural frequencies. The magnitude of $\gamma$ is found to be very small when $\varphi$ and $\tau$ are small, which means the assumption that the mode shape stays the same after attaching the mass to the beam does not cause significant error when $\varphi$ and $\tau$ are small. In that case, Equation (14) gives very good natural frequency estimates. It is worth noting that in Figure 3(a), the magnitude of $\gamma$ for $\omega_3$ is consistently close to zero. This is because the mass is located at the extreme point of $\phi_3(x)$ featuring zero beam rotation. Hence the effect of rotary inertia is nullified.

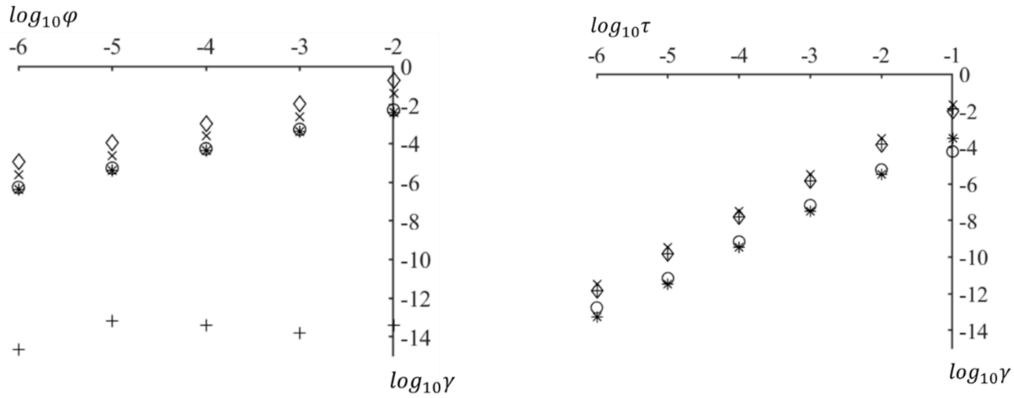


(a) when $\tau$=0 and $\varphi \neq$0 (b) when $\varphi$=0 and $\tau \neq$0

* $\omega_1$ ○ $\omega_2$ + $\omega_3$ × $\omega_4$ ◇ $\omega_5$

**Figure 3. The development of relative frequency error as $\varphi$ (or $\tau$) increases.**

Similar equations for natural frequency estimation were found in [1-3], however, no explanation is given on the assumption for the approximation. The derivation in this summary addresses this issue. Equation (14) offers a straightforward way to estimate the natural frequency of a beam carrying a mass, especially for beams with standard boundary conditions of which the mode shape expressions are readily available in textbooks [4]. It is possible to generalise Equation (14) to consider the situation when multiple masses are distributed on the beam. In addition, Equation (14) also explicitly shows how $M$ and $J$ affect the natural frequency. The effect of a roving $J$ has been discussed in a cracked beam scenario in [5]. From Equation (14), as $J$ is engaged by multiplying $\phi_n(x_0)$ and $\phi_n'(x_0)$, the discontinuity in $\phi_n'(x_0)$ caused by a crack leads to a shift in $\omega_n$, which can be used for crack detection.

**References**


[1] Y. Zhang, L. Wang, S.T. Lie, Z. Xiang, Damage detection in plates structures based on frequency shift surface curvature. J. Sound Vibr. 332 (25), 6665-6684, 2013.

[2] Y. Zhang and Z. Xiang, Frequency shift curve based damage detection method for beam structures. Computers, Materials, & Continua, 2011. 26(1): p. 19-35.

[3] X. Sun, Y. Mochida, I. Sinniah, The natural frequency estimation for a system composed of a beam and a spring-mass system, Noise and Vibration: Emerging Methods (NOVEM), Auckland, New Zealand, 2023.

[4] R.D. Blevins and R. Plunkett, Formulas for Natural Frequency and Mode Shape. Journal of Applied Mechanics, 1980. 47(2): p. 461-462.

[5] F. Cannizzaro, J. De Los Rios, S. Caddemi, I. Caliò, S. Ilanko, On the use of a roving body with rotary inertia to locate cracks in beams. J. Sound Vibr. 425, 275-300, 2018.

# Vibration Analysis of Doubly Curved Shallow Shells Elastically Constrained Along Parts of the Edges

**Y. Narita***

* Hokkaido University (Professor Emeritus)
N-13 W-8, 060-8628 Sapporo, Japan
ynarita@eng.hokudai.ac.jp

## Introduction

A large number of engineering structures, such as airplanes and automobiles, use thin shallow open shells as structural components. It is therefore important to evaluate natural frequencies to avoid resonance. For shell vibration problems under known material property and dimension, choices of boundary conditions for these shells affect significantly values of the natural frequencies. Boundary conditions, e.g., free edge, supported edge and clamped edge, are mathematically idealized, and in practical situations however the edge constraint should be modelled as elastically constrained.

Based on this premise, this paper presents an analytical approach to study free vibration of thin shallow shells elastically constrained along edges by translational and rotational springs. In the previous literature, there exist many papers dealing with vibration of shallow shells under uniform classical boundary conditions, but there are few papers considering elastic constraints on the edges. Furthermore, the present paper considers more complicated problem of shallow shells constrained along parts of the edges, and to the author's knowledge, there are no papers on shallow shells with mixed boundary conditions. In numerical studies, after convergence characteristics of the solution is tested, the effects of degree in elastic constraint are discussed.

## Outline of the analysis

An analytical procedure is briefly stated. Shell curvature is modelled in the coordinates by

$$\phi(x,y) = -(1/2)\left(x^2/R_x + y^2/R_y\right) \tag{1}$$

Dimension of the shell planform is $a$ and $b$, and the thickness is given by $h$. $R_x$ and $R_y$ are curvature radius in $x$ and $y$ direction, respectively. For $1/R_x = 1/R_y$ =(finite), the shell has spherical shape and for $1/R_x = -1/R_y$ =(finite) it has hyperbolic paraboloidal shape.

Based on Donnell-type shallow shell theory and standard lamination theory, stiffness matrices

$$[A] = \begin{bmatrix} A_{11} & A_{12} & A_{16} \\ A_{12} & A_{22} & A_{26} \\ A_{16} & A_{26} & A_{66} \end{bmatrix}, \ [B] = \begin{bmatrix} B_{11} & B_{12} & B_{16} \\ B_{12} & B_{22} & B_{26} \\ B_{16} & B_{26} & B_{66} \end{bmatrix}, \ [D] = \begin{bmatrix} D_{11} & D_{12} & D_{16} \\ D_{12} & D_{22} & D_{26} \\ D_{16} & D_{26} & D_{66} \end{bmatrix} \tag{2}$$

are derived for in-plane (stretching) motion, in-plane and out-of-plane coupling motion, and out-of-plane (bending) motion, respectively. For isotropic material, these are reduced to $A_{ij} = h\,Q_{ij}$, $B_{ij} = 0$, $D_{ij} = (h^3/12)Q_{ij}$ (i,j=1,2,6) in terms of $Q_{11} = Q_{12} = E/(1-\nu^2)$, $Q_{12} = \nu\,Q_{11}$ and $Q_{66} = G$. Here, $E$ is Young's modulus, $G = E/2(1+\nu)$ is shear modulus and $\nu$ is Poisson's ratio.

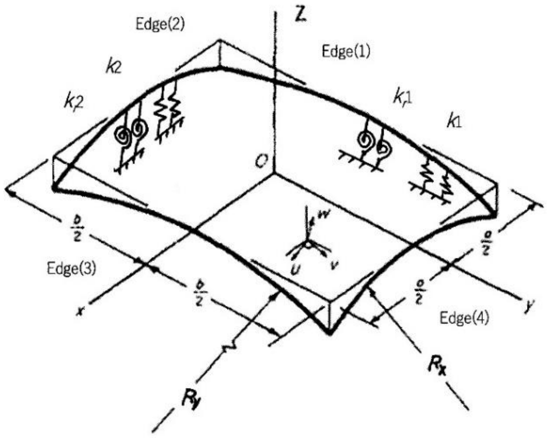


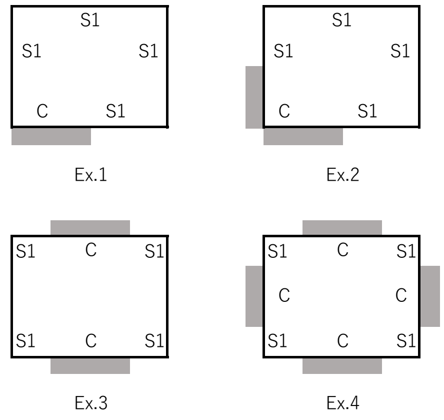


**Figure 1**. Doubly curved shallow shell under partial elastic constraints.

**Figure 2.** Numerical examples.

The energy functional of a vibrating shallow shell is given by

$$L = T - \left\{ \left( V_s + V_{bs} + V_b \right) + \left( V_t + V_r \right) \right\} \tag{3}$$

where $V_s$, $V_{bs}$, $V_b$ are strain energies due to in-plane, in-plane and out-of-plane coupling, and out-of-plane motions, respectively, and $T$ is kinetic energy. In addition to these energies, one can add the potential energy $V_t$ stored in translational springs with coefficients $k_i$ (i=1,2,3,4) and the potential energy $V_r$ stored in rotational springs with coefficients $k_{ri}$ (i=1,2,3,4) as

$$V_t = \frac{1}{2}\left\{ \int_{-b/2}^{b/2} k_1 w^2\left(-\frac{a}{2}, y\right) dy + \int_{-a/2}^{a/2} k_2 w^2\left(x, -\frac{b}{2}\right) dx + \int_{-b/2}^{b/2} k_3 w^2\left(\frac{a}{2}, y\right) dy + \int_{-a/2}^{a/2} k_4 w^2\left(x, \frac{b}{2}\right) dx \right\}$$

$$\begin{aligned} V_r = \frac{1}{2}\Bigg[ & \int_{-b/2}^{b/2} k_{r1} \left\{ \frac{\partial w}{\partial x}\left(-\frac{a}{2}, y\right) \right\}^2 dy + \int_{-a/2}^{a/2} k_{r2} \left\{ \frac{\partial w}{\partial y}\left(x, -\frac{b}{2}\right) \right\}^2 dx \\ & + \int_{-b/2}^{b/2} k_{r3} \left\{ \frac{\partial w}{\partial x}\left(\frac{a}{2}, y\right) \right\}^2 dy + \int_{-a/2}^{a/2} k_{r4} \left\{ \frac{\partial w}{\partial y}\left(x, \frac{b}{2}\right) \right\}^2 dx \Bigg] \end{aligned} \tag{4a,b}$$

The upper and lower bounds in these integrals are modified to meet with ranges of constraints in the numerical examples. Next, the following series solutions are assumed for *u, v, w* (ξ=2*x/a*, η=2*y/b*) as

$$u(\xi,\eta) = \sum_{i=0}^{M-1}\sum_{j=0}^{N-1} P_{ij}\xi^i (1+\xi)^{Bu1}(1-\xi)^{Bu3} \times \eta^j (1-\eta)^{Bu2}(1-\eta)^{Bu4} \tag{5a}$$

$$v(\xi,\eta) = \sum_{k=0}^{M-1}\sum_{l=0}^{N-1} Q_{kl}\xi^k (1+\xi)^{Bv1}(1-\xi)^{Bv3} \times \eta^l (1-\eta)^{Bv2}(1-\eta)^{Bv4} \tag{5b}$$

$$w(\xi,\eta) = \sum_{m=0}^{M-1}\sum_{n=0}^{N-1} R_{mn}\xi^m (1+\xi)^{Bw1}(1-\xi)^{Bw3} \times \eta^n (1-\eta)^{Bw2}(1-\eta)^{Bw4} \tag{5c}$$

where $P_{ij}$, $Q_{kl}$, $R_{mn}$ are undetermined coefficients, and $B_{u1}$, ⋯, $B_{w4}$ are boundary index to prescribe kinematical boundary condition. Use of the boundary index is explained in previous studies. When elastic springs are not included, in-plane displacements *u* and *v* can be zero or stress free, and out-of-plane displacement *w* can take free, simple supported or clamped condition. The energy functional is minimized with the coefficients, and this process yields a frequency equation

$$det\left(\left[K\right]-\Omega^2\left[M\right]\right)=0 \tag{6}$$

where $\Omega$ is a frequency parameter defined by $\Omega=\omega a^2\sqrt{\rho h/D}$ ($D=Eh^3/12\left(1-\nu^2\right)$).

**Numerical results and discussions**

Numerical results are given here for frequency parameters of spherical shallow shells ($1/R_x=1/R_y=1/R$). The shell has a thickness ratio ($h/a$=0.01) with square planform ($a/b$=1) and relatively small curvature ($a/R$=0.2). The in-plane boundary condition is set to be S-1 condition on the four straight edges, namely, the in-plane displacements perpendicular to the edges are free, but displacements along edges are fixed. The out-of-plane displacements (deflection) can be simply supported and practically clamped (with high rotational stiffness) simultaneously along the edges.

Figure 2 shows four numerical examples Ex.1,.., Ex.4, where a square spherical shell with the S1-S1-S1-S1 edge condition is used as a base shell additionally with distributed rotational springs. Specifically, Ex.1 is a shell with a part from one corner on Edge(2) constrained by a spring. When the stiffness value $k_{r1}^*=(a/D_0)k_{r1}$ is increased, that part of the edge gradually becomes nearly clamped and the edge has mixed boundary condition. Variations of frequency parameters approach to certain values as the stiffness becomes more than $k_r^*=10^3$ and can be regarded as practically clamped at $k_r^*=10^4$. Similarly, Ex.2, Ex.3 and Ex.4 have mixed boundary conditions at a corner, a pair of opposite edges and two pairs of opposite edges, respectively.

Table 1 presents convergence study of frequency parameters in Ex.1 and Ex.2, when the number of series terms in the assumed solution (5) is increased from 6×6 to 14×14. Since the assumed solution satisfies the kinematical boundary conditions exactly, they show monotonical decrease from above and clearly reveal fast convergence.

Table 2 gives comparison with previous results for square *flat* plates (i.e., no curvature) with mixed boundary conditions, since there are no previous results available for shallow shells with mixed boundary conditions. The present results under assumption of $a/R$=0 agree well with those of plates cited from the past references.

**Table 1**. Convergence of frequency parameters for spherical shallow shells with partially clamped edges ($k_r^*=10^4$, $a/b$=1, $a/R$=0.2, $a/h$=100).

| $M$x$N$ | $\Omega_1$ | $\Omega_2$ | $\Omega_3$ | $\Omega_4$ | $\Omega_5$ | $\Omega_6$ |
|---|---|---|---|---|---|---|
| Ex.1 | | | | | | |
| 6×6 | 23.06 | 50.59 | 56.93 | 83.11 | 101.2 | 111.7 |
| 8×8 | 22.92 | 50.38 | 56.61 | 82.73 | 99.79 | 108.9 |
| 10×10 | 22.83 | 50.27 | 56.41 | 82.57 | 99.75 | 108.5 |
| 12×12 | 22.78 | 50.19 | 56.27 | 82.48 | 99.74 | 108.2 |
| 14×14 | 22.73 | 50.14 | 56.17 | 82.43 | 99.73 | 108.0 |
| Ex.2 | | | | | | |
| 6×6 | 70.75 | 86.58 | 89.92 | 108.9 | 131.2 | 132.6 |
| 8×8 | 70.64 | 85.52 | 89.21 | 108.0 | 127.8 | 128.7 |
| 10×10 | 70.57 | 85.18 | 89.09 | 107.7 | 127.6 | 128.0 |
| 12×12 | 70.53 | 84.96 | 89.00 | 107.6 | 127.5 | 127.6 |
| 14×14 | 70.49 | 84.81 | 88.94 | 107.5 | 127.3 | 127.4 |

**Table 2**. Comparison of frequency parameters for square plates with partially clamped edges ($k_r^*=10^4$, $a/b$=1, $a/R$=0).

| | $\Omega_1$ | $\Omega_2$ | $\Omega_3$ | $\Omega_4$ | $\Omega_5$ |
|---|---|---|---|---|---|
| Ex.1 | | | | | |
| Present | 22.73 | 50.14 | 56.17 | 82.43 | 99.73 |
| Narita(2006) | 22.49 | 49.84 | 55.62 | 81.85 | 99.43 |
| Wei (2001) | 22.42 | 49.88 | 55.54 | 82.26 | 99.67 |
| Shu (1999) | 22.42 | 49.93 | 55.51 | 82.32 | 99.64 |
| Mizusawa (1990) | 22.71 | 50.10 | 56.13 | 82.37 | 99.73 |
| Narita (1981) | 22.63 | 50.04 | 55.95 | 82.34 | 99.71 |
| Ex.3 | | | | | |
| Present | 28.62 | 53.87 | 68.37 | 91.70 | 101.0 |
| Narita(2006) | 28.37 | 52.26 | 67.64 | 89.74 | 100.2 |
| Wei (2001) | 28.36 | 53.29 | 67.60 | 89.87 | 100.4 |
| Narita (1981) | 28.44 | 53.49 | 67.85 | 90.50 | 100.6 |

# Small amplitude free vibration of soft materials and structures by high order finite elements

**A. Pagani*, P. Chiaia, E. Carrera**

Mul[2] Lab, Department of Mechanical and Aerospace Engineering
Politecnico di Torino, 10129 Turin, Italy
* Corresponding author: alfonso.pagani@polito.it

## Summary

In the recent years, applications of soft material are widely spread in many mechanical, aeronautical, robotics engineering and biological applications. Many experimental and numerical studies have been conducted on hyperelastic media under various static and dynamics loads. Vibrations of hyperelastic materials have become more and more important due to their extreme elastic behavior: in this framework both geometrical and material non-linearities must be taken into account, leading to strongly nonlinear governing equations that result in a lack of closed-form solutions for vibrations problems. Studies in the last decade rely on FEM (Finite Element Method), that allow a wide range of investigations in terms of material properties and geometries, topology and weight optimization, frequency analysis and design phase of components.

In this work, finite element models for hyperelasticity and vibrations around nonlinear equilibrium states are based on Carrera Unified Formulation (CUF): the primary unknown variables are expressed by a polynomial expansion of kinematic models and arbitrary cross-section function/thickness functions (Node-Dependent Kinematics) [1]. Under the CUF formulation, the nonlinear governing equations in weak form are obtained adopting an index notation that allows the definitions of fundamental nuclei of physical quantities independently of the chosen polynomial expansion of the displacement field:

$$\text{Beam 1D models: } \mathbf{u}(x,y,z) = F_\tau(x,z)N_i(y)\mathbf{q}_{\tau\mathbf{i}} \quad i = 1,2,..,N_n \tag{1}$$

$$\text{Plate 2D models: } \mathbf{u}(x,y,z) = F_\tau(z)N_i(x,y)\mathbf{q}_{\tau\mathbf{i}} \quad i = 1,2,..,N_n \tag{2}$$

$$\text{Solid 3D models: } \mathbf{u}(x,y,z) = N_i(x,y,z)\mathbf{q}_{\mathbf{i}} \quad i = 1,2,..,N_n \tag{3}$$

Recently, CUF models for geometrical nonlinear analysis of linear elastic structures [2, 3] have been extended to including material non-linearities, in particular hyperelasticity, obtaining higher-order displacement-based models for nearly-incompressible and compressible soft materials [4].

To show the capabilities of the present implementation of hyperelastic models, we present here the nonlinear static analysis of a thick hollow sphere subjected to internal uniform pressure. In this case study, the analytic solution is known: radial displacement distribution obtained via parabolic hexahedral models is compared with the analytic reference, for various load conditions. The geometry, boundary conditions and material model and constants are taken from Jiang et al.[5]. Figure 1(a) shows the comparison of radial displacement distribution between analytical and numerical results, whereas Fig.1(b) shows the deformed configuration when $p$ = 1 Pa.

Afterwards, as done in Carrera et.al [6], we derive the governing equation of the free vibration problem (or undamped vibration problem) for hyperelastic structures by means of the principle of virtual displacements (PVD), written as:

$$\delta\mathscr{L}_{int} + \delta\mathscr{L}_{ine} = 0 \tag{4}$$

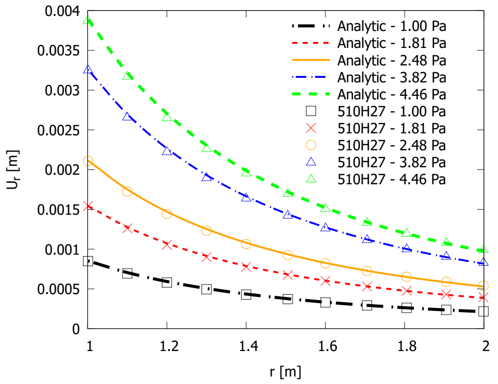


(a) Equilibrium curve

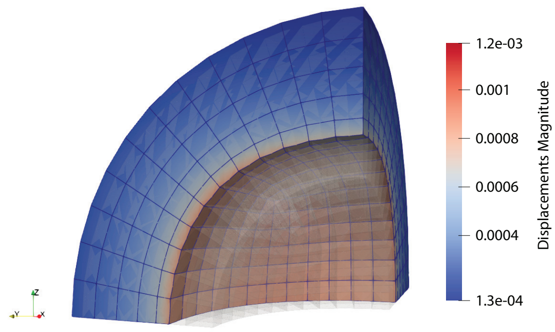


(b) Deformed configuration

Figure 1: Thick hollow sphere: equilibrium curve and deformed configurations.

where $\mathscr{L}_{int}$ is the internal work, $\mathscr{L}_{ine}$ is the work done by inertia forces and $\delta$ denotes the virtual variation. Adopting the same index notation for the full Green-Lagrange strain tensor, we can derive the FNs (fundamental nuclei) of internal forces vector, mass matrix and tangent stiffness matrix by linearization of the virtual variation of internal work:

$$\delta \mathscr{L}_{int} = \delta \mathbf{q}_{sj}^T \mathbf{F}_{int}^{\tau sij} \tag{5}$$

$$\delta \mathscr{L}_{ine} = \delta \mathbf{q}_{sj}^T \mathbf{M}^{\tau sij} \ddot{\mathbf{q}}_{\tau i} \tag{6}$$

$$\delta(\delta \mathscr{L}_{int}) = \delta \mathbf{q}_{sj}^T \mathbf{K}_T^{\tau sij} \delta \mathbf{q}_{\tau i} \tag{7}$$

All these FNs have the property that they are independent of the polynomial expansion chosen: higher-order model are rapidly defined by considering the summation over the indices. The proposed method solves the undamped vibration problem around a nonlinear equilibrium states computing first the static equilibrium problem by means of a Newton-Raphson iterative procedure coupled with the arc-length procedure [7], then solving the simplified equations of motion (the classical linear eigenvalue problem) adopting the tangent stiffness matrix at the point of interest:

$$(\mathbf{K}_T^{\tau sij} - \omega^2 \mathbf{M}^{\tau sij}) \mathbf{q}_{\tau i} = 0 \tag{8}$$

In this way, normal mode frequencies and shapes can be obtained. Contrary to the case of linear elastic material, for which low amplitude vibrations were observed (thus, linearization of the problem around a non-trivial equilibrium condition is legitimate), hyperelastic materials undergo large amplitude vibrations: even so, the small-amplitude behaviour under prestressed conditions represents an interesting research problem thanks to its various practical applications.

In this last paragraph, we report the actual numerical results obtained for an undamped vibration problem regarding the thick hyperelastic hollow sphere considered before, around the trivial equilibrium condition. Regarding the mass matrix definition, density is fixed at the classical value of natural rubber $\rho$ = 1340 kg/m$^3$. Results from the present model are compared with reference results obtained by the commercial finite element code ABAQUS. In Table 1 we report the comparison between reference results and numerical values of the first ten natural frequencies obtained by the present model, whereas in Fig.2 undamped vibration configurations are shown.

| Mode | 3D ABQ | CUF | Mode | 3D ABQ | CUF |
|---|---|---|---|---|---|
| 1 | 0.0795 | 0.0798 | 6 | 0.1837 | 0.1848 |
| 2 | 0.0795 | 0.0798 | 7 | 0.2083 | 0.2091 |
| 3 | 0.1519 | 0.1519 | 8 | 0.2185 | 0.2190 |
| 4 | 0.1837 | 0.1848 | 9 | 0.2185 | 0.2190 |
| 5 | 0.1837 | 0.1848 | 10 | 0.2484 | 0.2489 |

Table 1: Thick hollow sphere: Natural frequencies [Hz]

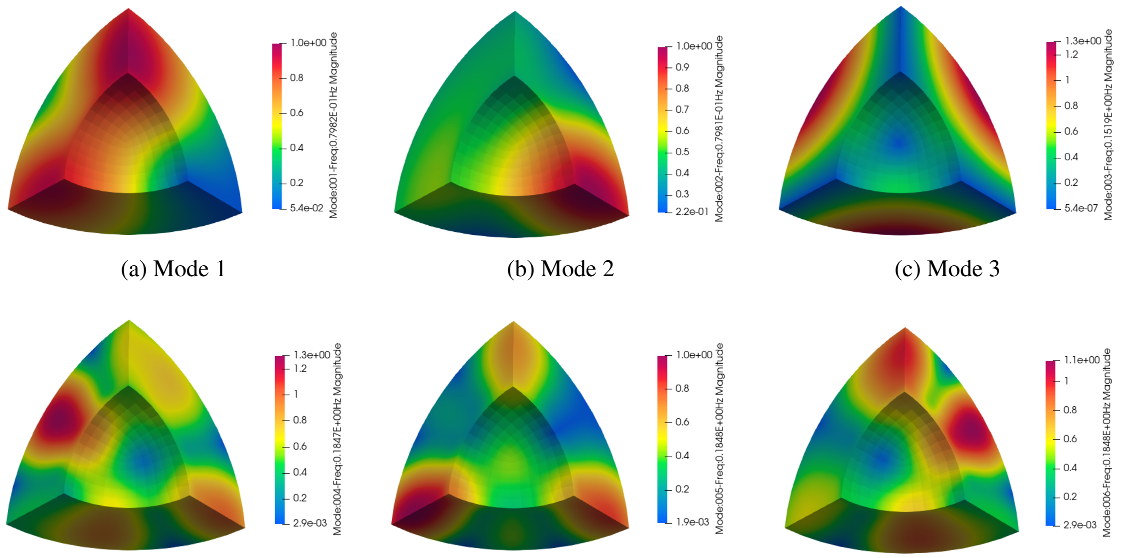

(a) Mode 1 (b) Mode 2 (c) Mode 3

(d) Mode 4 (e) Mode 5 (f) Mode 6

Figure 2: Thick hollow sphere: snapshots of normal modes of vibration.

## References


[1] Carrera, E.; Cinefra, M.; Zappino, E.; Petrolo, M.: *Finite Element Analysis of Structures Through Unified Formulation*. Wiley, 2014.

[2] Pagani, A.; Carrera, E.: "Unified formulation of geometrically nonlinear refined beam theories". In: *Mechanics of Advanced Materials and Structures* 25.1 (2016), pp. 15–31.

[3] Wu, B.; Pagani, A.; Filippi, M.; Chen, W.Q.; Carrera, E.: "Large-deflection and post-buckling analyses of isotropic rectangular plates by Carrera Unified Formulation". In: *International Journal of Non-Linear Mechanics* 116 (2019), pp. 18–31.

[4] Pagani, A.; Carrera, E.: "Unified one-dimensional finite element for the analysis of hyperelastic soft materials and structures". In: *Mechanics of Advanced Materials and Structures* 30.2 (2021), pp. 342–355.

[5] Jiang, C.; Zhang, Z.Q.; Liu, G.R.; Han, X.; Zeng, W.: "An edge-based/node-based selective smoothed finite element method using tetrahedrons for cardiovascular tissues". In: *Engineering Analysis with Boundary Elements* 59 (2015), pp. 62–77.

[6] Carrera, E.; Pagani, A.; Azzara, R.; Augello, R.: "Vibration of metallic and composite shells in geometrical nonlinear equilibrium states". In: *Thin-Walled Structures* 157 (2020), p. 107131.

[7] Carrera, E.: "A study on arc-length-type methods and their operation failures illustrated by a simple model". In: *Computers & Structures* 50.2 (1994), pp. 217–229.

# Experiments on Non-Newtonian Fluid-Structure Interaction

**Francesco Pellicano*, Antonio Zippo*, Giovanni Iarriccio#**

* Dept. of Engineering Enzo Ferrari
Centre InterMech MoRe
University of Modena and Reggio Emilia
V. P. Vivarelli 10, 41125 Modena, Italy
[francesco.pellicano,antonio.zippo]@unimore.it

# Dept. of Engineering Enzo Ferrari
University of Modena and Reggio Emilia
V. P. Vivarelli 10, 41125 Modena, Italy
giovanni.iarriccio@unimore.it

## Summary

Fluid structure interaction (FSI) phenomena are of interest for several engineering fields as well as in medical science and in bioengineering or biomechanics. One can find countless examples of FSI problems in engineering, e.g. flutter of airplane wings, galloping in powerlines and bridge cables, supersonic panel flutter, pipes flutter, fully or partially filled tanks, heat exchangers. In the field of Medical Sciences an important example is the human aorta, where the fluid is highly viscous and non-Newtonian and the artery wall is hyper-elastic, this is a combination of exceptionally difficult problems.
In order to have a comprehensive description of fluid structure interaction phenomena, models and applications, the reader is suggested to read the monumental work of Paidoussis [1], [1]; in such treatises the main fluid-interaction models are described as well as methods of analysis. Another interesting paper to be mentioned is a review published in 2003 by Amabili and Païdoussis [3], where more than 300 papers on the topic of nonlinear vibrations of shells with or without FSI were listed; among the deep and interesting comments on the literature the authors pointed out the attention on two aspects, we report their full sentences: "only 23 of the more than 350 papers discussed in the present review give experimental data on large-amplitude vibrations of complete shells", "most of the papers reviewed are dedicated to various theoretical aspects of the problem, with very few experimental results, although more experimental data are available for supersonic flutter of shells".
In 2012 Girchenko et al studied numerically the interaction of a nonlinear viscous fluid, having a pseudoplastic nature, with a helical shell. They combined two commercial software FlowVision (finite volumes) and Simulia ABAQUS (finite elements). They showed the differences between Newtonian and Non-Newtonian flows in terms of stresses caused on the helical structure. Another study regarding FSI and non-Newtonian fluid was focused on arterial bypass [4], the effects of wall elasticity and non Newtonian rheology were investigated numerically through the commercial software ANSYS.
An experimental study on the rheology and processing of solvent-free core shell "polymer opals", see Ref. [5], analyzed an elastic shell grafted to hard colloidal polymer core particles in order to study the optical properties under deformation.
In 2019 Wu et al. [6] presented a numerical study on interaction between elastic multilayered spheres and a non-Newtonian fluid. They analyzed gold nanospheres immersed in water and calculated theoretically the natural frequencies and the quality factors.
The bibliographic analysis clearly shows that, even though a huge number of publications can be found about FSI problems, and many papers are available about non-Newtonian fluids, the interactions between vibrating structures and non-Newtonian fluids appear to be an almost unexplored field.

This paper presents the results of an extensive experimental campaign focused on the analysis of the dynamic interactions between an elastic structure and a non-Newtonian fluid. The structure is a circular cylindrical shell clamped at one end to a shaking table and at the other end to a heavy rigid disc. The shell has been investigated both in presence and absence of fluid. The fluid is a mixture of water and corn starch flour, commonly called Oobleck. The experiments were carried out at low and high vibration energy, in order to clarify the influence of the fluid in different conditions: changing of modal properties, onset of complex dynamics when the fluid-solid transitions take place in the fluid.

**Experimental setup and specimen definition**

The system is a polyethylene terephthalate (PET) shell, vertically placed, wedged in an aluminum base rigidly connected to the shaker at the bottom, and constrained at the top by a C-40 steel disc, which is called top mass.

The internal face of the shell was fixed to the external face of both the top mass and the basement by means of an instant cyano-acrylic glue. In addition, the lower end of the shell was secured to the basement via an aluminum ring, lying on the basement and tightened to it with screws. This ring was inserted to guarantee the interlocking constraint. In this setup, the lower end of the shell is rigidly connected to the shaker, since the basement is anchored to the shaker horizontal plate with screws; conversely, the top mass induces a rigid body motion at the upper end of the shell, preventing this end a free deformation.

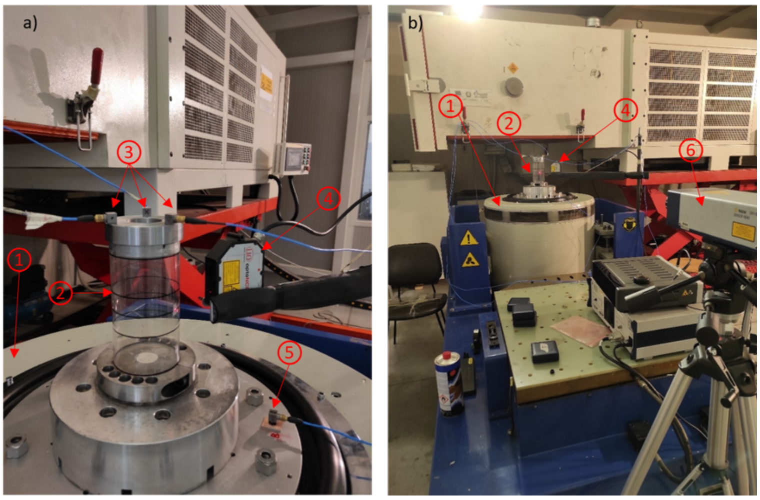


**Figure 1** – a) Setup: (1) shaker, (2) shell, (3) measurement accelerometers, (4) telemeter and (5) control accelerometer on the shaker plate. b) Overall experimental setup.

**Nonlinear dynamic scenario**

Experiments are now carried out considering an empty and a fluid filled shell. The shell is now excited from the base, the excitation signal provided to the amplifier is harmonic with different amplitudes (0.01-0.08V) and frequencies (150-310Hz for the empty shell and 150-270Hz for the fluid filled shell).

Figure 2 shows a bifurcation diagram obtained from Poincaré sections obtained by using a single signal (lateral displacement). The dynamic scenario is extremely rich, we observed different sub-harmonic responses: ½, 1/3, ¼, 1/8 as well as quasiperiodic and chaotic dynamics in a very wide frequency range. For the sake of brevity bifurcation diagrams obtained by the other signals (accelerometers, Laser Doppler) and by changing the excitation levels are not reported.

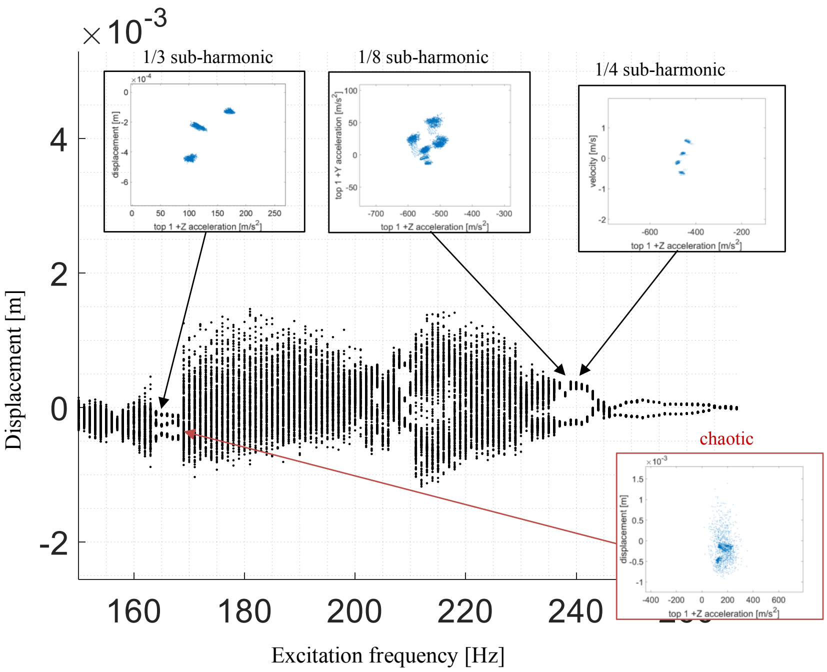


**Figure 2**: Bifurcation diagram of Poincaré maps: excitation 0.06V, downward frequency sweep.

## Conclusions

In this paper an extensive experimental champaign, focused on the analysis of the dynamic interactions between an elastic structure and a non-Newtonian fluid, is presented. When tests are carried out at high excitation intensity and close to the resonance conditions of the shell, the high amplitudes of vibration induced in the structure cause strong waves propagation in the fluid and the onset of complex dynamics when the fluid-solid transitions take place. The analysis of the dynamic scenario reveals an exceptional complexity with alternance of harmonic, sub-harmonic, quasiperiodic and chaotic responses.

## References


[1] Païdoussis, M.P. : Fluid-Structure Interactions, Volume 1: Slender Structures and Axial Flow, Second Edition, ISBN: 9780123973122, Academic Press, 2014.

[2] Païdoussis, M.P.: Fluid-Structure Interactions, Volume 2: Slender Structures and Axial Flow, Second Edition, ISBN: 9780123973122, Academic Press, 2016.

[3] Amabili, M. and Païdoussis, M.P. : Review of studies on geometrically nonlinear vibrations and dynamics of circular cylindrical shells and panels, with and without fluid-structure interaction, ASME Applied Mechanics Review Vol. 56(4), 2003.

[4] Kabinejadiana, F., Ghista, D. N.: Compliant model of a coupled sequential coronary arterial bypass graft: Effects of vessel wall elasticity and non-Newtonian rheology on blood flow regime and hemodynamic parameters distribution. *Medical Engineering & Physics* Vol. 34, 860–872, 2012.

[5] Wong, H. S. Mackley, M. Butler, S. Baumberg, J. Snoswell, D. Finlayson, C. and Zhao, Q. The rheology and processing of "edge sheared" colloidal polymer opals, J. Rheol. Vol. 58(2), 397-409, 2014.

[6] Wu, B. Gan, Y. Carrera E. and Chen W. Q., Three-dimensional vibrations of multilayered hollow spheres submerged in a complex fluid, J. Fluid Mech., Vol. 879, 682–715, 2019.

# Some recent advances in the dynamic analysis of parametrically excited continuous rotor systems

**A. De Felice**[†], **S. Sorrentino**[†]

[†] Department of Engineering Enzo Ferrari
University of Modena and Reggio Emilia
Via Vivarelli 10, 41125 Modena, Italy
[alessandro.defelice, silvio.sorrentino]@unimore.it

## Summary

Dynamic analysis of parametrically excited rotors is a research field of great interest and practical importance, since instability and resonant behavior can cause issues ranging from anomalous noise and wear to catastrophic failures.

An overview is presented of some advances recently proposed by the authors on the dynamic analysis of parametrically excited continuous rotor systems, including results regarding stability analysis (parametric resonances) and preliminary insights into resonant behavior in the asymptotically stable domain, due to unbalance (external resonances).

An axisymmetric shaft described by a spinning Timoshenko beam is studied, loaded by oscillating axial end thrust and twisting moment, carrying additional inertial elements like discs. Both isotropic and anisotropic supports are considered, as well as gyroscopic effects and different kinds of damping distributions (both external and internal), which represents a model including all the general features of slender rotors which are relevant for their dynamic analysis.

Stability is studied after discretization of the equations of motion into a set of coupled ordinary differential Mathieu-Hill equations. Stability maps in the form of Ince-Strutt diagrams are discussed to highlight the occurrence of simple and combination critical solutions [1], as well as the influence of angular speed, damping, and anisotropy in the supports.

Steady-state response is studied in the asymptotically stable domain under the effect of unbalance, yielding an additional external harmonic load, acting on flexural deflection [2]. As a first insight into this problem, to study the effects of angular speed independently to variations of natural frequencies and to facilitate decoupling of the equations of motion, the Timoshenko model is simplified into the Euler-Bernoulli model, neglecting the gyroscopic effects, additional discs, anisotropy in the supports and twisting moment at the ends of the shaft.

*Stability analysis*

Regarding parametric resonances, it has been found that, through gyroscopic actions, the angular speed induces on isotropic rotors peculiar interactions between pairs of closely separated modes, affecting the stability thresholds. This ‘splitting’ of otherwise coincident eigenfrequencies can be determined in any case by the angular speed itself, yielding forward and backward modal pairs, and also by the additional presence of anisotropy in the supports [2]. On the contrary, well separated flexural modes do not interact in determining the stability thresholds, at least for relatively low amplitudes of parametric excitation. Gyroscopic actions generate combination critical solutions [3] (in general, represented by non-periodic functions of time), instead of simple critical solutions (represented by periodic functions of time).

In the presence of principal stiffness anisotropy in the supports, increasing the angular speed has the effect of getting the stability thresholds progressively closer to those computed in isotropic conditions. On the other hand, in the presence of principal damping anisotropy in the supports, raising the angular speed has a moderate stabilizing effect, whilst an increasing part of the stability threshold results by combination critical solutions, both effects due to gyroscopic actions [4]. This can be seen in Fig. 1, diplaying stability maps computed in an example-case, where $\delta$ is the frequency parameter and $\varepsilon$ is the (parametric) axial force amplitude parameter (both normalized and defined following the conventional representation of Ince-Strutt diagrams [3]). In particular, Fig. 1*a* shows the growth of combination Arnold tongues (labelled C) due to increasing angular speed, in the presence of stiffness anisotropy in the supports, while Fig. 1*b* shows the progressive conversion of stability thresholds into combination critical solutions (labelled C), due to increasing angular speed and damping anisotropy in the supports.

With respect to internal damping, the counteracting effects due to angular speed and principal stiffness anisotropy in the supports have opposite directions: raising the angular speed is destabilizing, while increasing the stiffness anisotropy is stabilizing. More in detail, while external damping affects mainly the tips of unstable tongues (producing smoothing and contractions, with stabilizing effects), internal damping acts significantly on their lateral borders (producing 'merging' of unstable tongues, as can be seen in Fig. 2*a* with destabilizing effects induced by angular speed [3]). Stiffness anisotropy in the supports counteracts the 'merging' between adjacent combination tongues due to internal damping, playing a stabilizing role on the parametrically excited system [4]. This can be noticed in Fig. 2*b*, where the straight line representing the stability threshold would get closer and closer to the ε = 0 axis by reducing the degree of stiffness anisotropy in the supports, until it would coincide with the ε = 0 axis in case of pure isotropy.

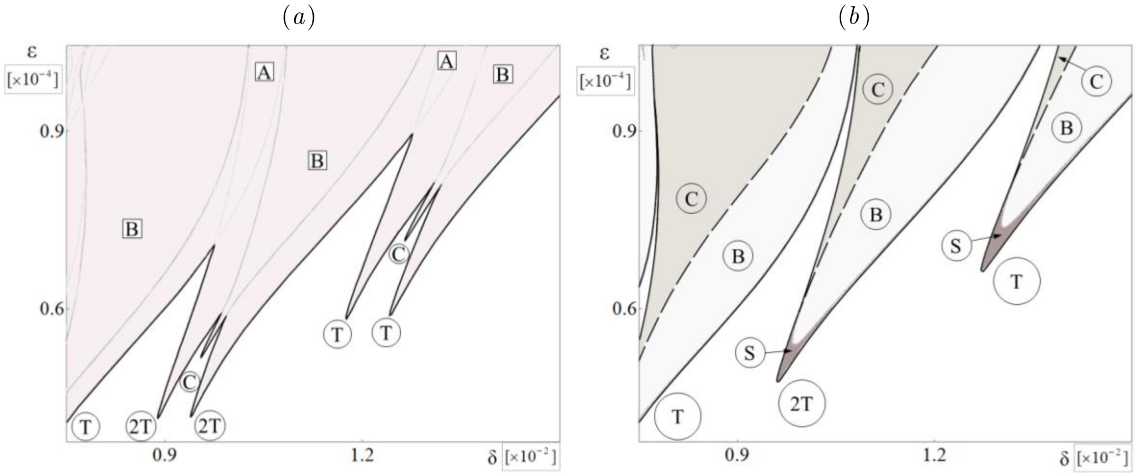


**Figure 1.** Stability maps in presence of anisotropy in the supports: (*a*) effect of stiffness anisotropy at 116.8 rpm (subcritical; T = single period tongue; 2T = double period tongue; C = combination tongue; A = unstable region with 2 real multipliers out of the unit circle, in opposite directions; B = unstable region with 2 multipliers out of the unit circle, in the same half-plane); (*b*) effect of damping anisotropy at 155.84 rpm S = unstable sub-region with 1 real multiplier out of the unit circle; B = unstable sub-region with 2 real multipliers out of the unit circle, in the same direction; C = unstable combination sub-region with 2 complex-conjugate multipliers out of the unit circle).

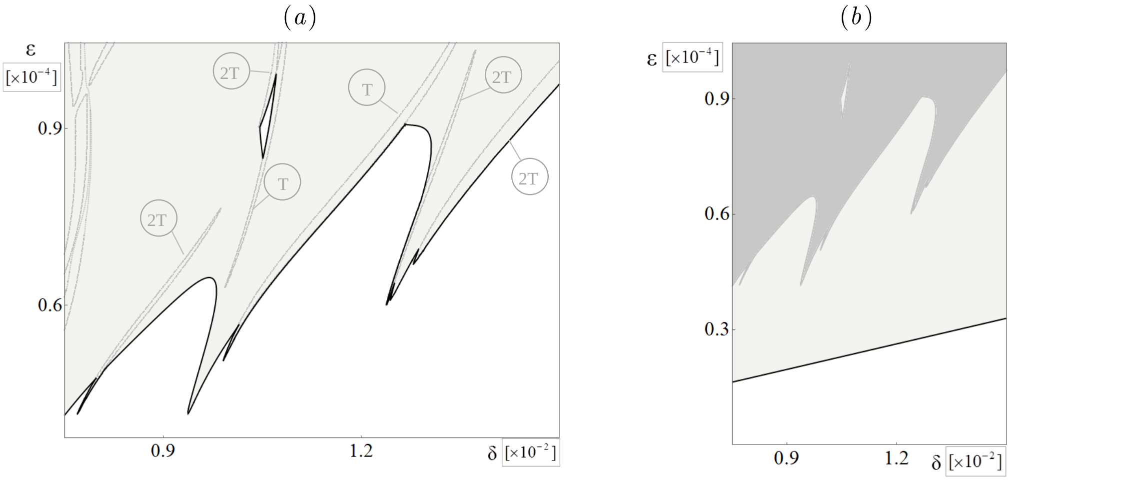


**Figure 2**. Example of stability map showing the effect of stiffness anisotropy in the supports at 3896 rpm (subcritical) in the presence of distributed internal damping along the shaft: (*a*) residual single-period T and double-period 2T tongues; (*b*) stability threshold obtained at 3896 rpm superimposed to the one (black line) obtained at 6818.8 rpm (first forward critical speed of the rotor).

### *Steady-state response of the non-homogeneous asymptotically stable system*

Regarding the steady-state response of the system to unbalance, it has been studied after decoupling of the equations of motion, reducing the problem to the analysis of a non-homogeneous single-degree-of-freedom damped Mathieu equation, and cast in dimensionless form. This allows the study of the modal frequency response in terms of four governing parameters: normalized frequency of the unbalance excitation (depending on the angular speed of the rotor), normalized frequency of the parametric excitation, normalized modal amplitude of the parametric excitation, and modal damping factor.

It has been found that the steady-state response of the asymptotically stable system is aperiodic unless the parametric excitation frequency and the unbalance frequency are commensurate [5]. The relative amplitudes of the frequency components of the response are determined directly by the governing parameters, and by the characteristic exponents of the parametrically excited system. An approximated analytical expression has been derived, yielding the infinite sequence of resonances generated on each modal coordinate by the combination of parametric and external excitation frequencies.

Of particular importance is the result that in presence of parametric excitation, resonances can occur at lower frequencies than the related natural frequency, as it can be noticed in Fig. 3. Hence, in a parametrically excited (stable) rotor, the first flexural critical speed can occur at a lower value than in the non-parametrically excited system.

The amplitudes of the frequency responses in resonance conditions are strongly dependent on both external damping and parametric excitation (frequency and amplitude). Therefore, a correlation is found between resonances and working points on the Ince-Strutt diagrams, as shown in Fig. 3.

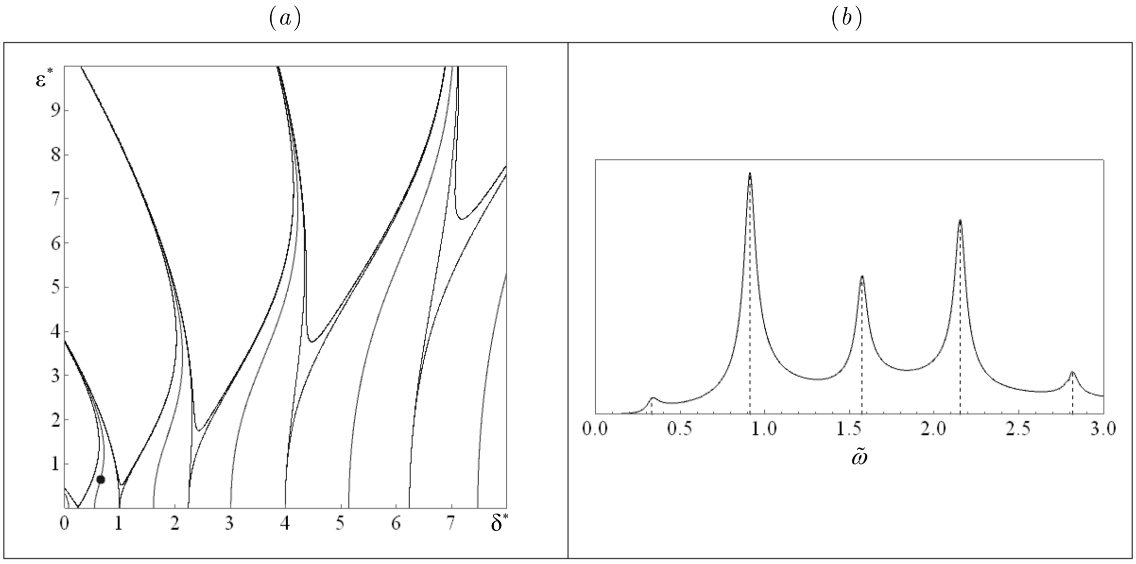


**Figure 3**. Effects of unbalance: (*a*) Ince-Strutt diagram for the modal Mathieu equation (black dot: selected parameters for computing the steady-state response due to unbalance for figure *b*); (*b*) amplitude of modal flexural displacement, as a function of the ratio $(\tilde{\omega})$ between angular speed and modal natural frequency. Notice the presence of a large resonance peak at a normalized frequency of about 0.9.

## References


[1] Yakubovich, V.A., Starzhinskii, V.M.: Linear differential equations with periodic coefficients. Parts I and II. Wiley, 1975.

[2] Dimentberg, F.M.: Flexural vibrations of rotating shafts, Butterworth, 1961.

[3] De Felice, A., Sorrentino, S.: Damping and gyroscopic effects on the stability of parametrically excited continuous rotor systems, Nonlinear Dynamics Vol. 103, No. 4, pp. 3529-3555, 2021.

[4] De Felice, A., Sorrentino S.: Effects of anisotropic supports on the stability of parametrically excited slender rotors. Nonlinear Dynamics, published online 28 May 2022.

[5] D'Angelo, H. : Linear Time Varying Systems: Analysis and Synthesis. Allyn and Bacon, 1970.

# Vibrations of a flexible rod partially sliding in a rigid sleeve: finite element and semi-analytical solutions for the the dancing rod problem

**Yury Vetyukov**

Institute of Mechanics and Mechatronics
Technische Universitaet Wien
Getreidemarkt 9, 1060 Vienna, Austria
yury.vetyukov@tuwien.ac.at

## Introduction

A flexible rod, partially sliding in a rigid sleeve (channel) may exhibit complicated vibration scenarios in its free part, whose material length is varying over time; see the discussion of the "flying spaghetti problem" in [1]. Recently, the role of configurational forces in the dynamics of such structures has been investigated by the authors of [2, 3] on the example of a "dancing rod problem". One considers a flexible rod, partially injected into an inclined sleeve in the field of gravity. Letting the rod fall and slide into the sleeve, we also initiate vibrations in its free part. The frequency of vibrations grows with axial motion as the free part is getting shorter, which in the absence of damping results into a resistance force at the tip of the sleeve. Under the action of this configurational force, the injection eventually changes to ejection, such that the rod may even completely fly out of the sleeve. In the present talk, we discuss a simple mathematical model, which allows for the efficient finite element analysis of the dynamics of the dancing rod. At small vibrations we present a semi-analytical solution in form of a system of two nonlinear differential equations, which may easily be integrated numerically and allow obtaining some of the characteristics of the dynamic process in a closed form.

## Mathematical model

The mechanical system under consideration is depicted in Figure 1. A flexible, shear underformable and inextensible rod of the length $l$ is moving in the plane $x, y$, being partially injected in the rigid sleeve. We assume frictionless contact between the rod and the sleeve, and the gap within the sleeve is very close to the thickness of the rod: the injected part remains straight and may move along the $x$ axis. The angle between the sleeve and the vertical direction is $\alpha$, such that a rigid rod would just slide into the sleeve with acceleration. A flexible rod, however, would develop oscillations, which prevent it from falling completely into the sleeve.

We denote the material length of the free part of the rod as $\eta(t)$, and the length of the part in the sleeve is $l - \eta$. Furthermore, we parametrize the free part of the rod by a dimensionless non-

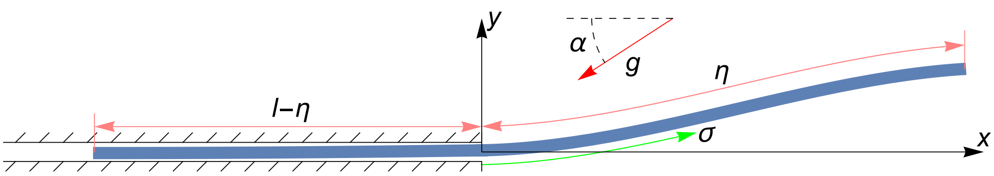


Figure 1: Flexible rod, partially sliding in a sleeve and partially moving free in the field of gravity.

material coordinate $\sigma$ with $\sigma = 0$ corresponding to the material particle presently at the tip of the sleeve and $\sigma = 1$ corresponding to the free end. Introducing a material coordinate $s$ varying from $s = 0$ to $s = l$ from left to right, for a material particle in the free segment we find a linear mapping

$$s = l - \eta + \eta\sigma, \quad \sigma = 1 - (l - s)/\eta. \tag{1}$$

The total time derivative of the material coordinate vanishes: $\dot{s} = 0$, from which we obtain the total time derivative of the normalized coordinate in a material particle:

$$\dot{\sigma} = \frac{(l-s)\dot{\eta}}{\eta^2} = \frac{(1-\sigma)\dot{\eta}}{\eta}. \tag{2}$$

As mentioned earlier, we parametrize the position vector of a particle of the free part of the rod

$$\mathbf{x}(\sigma,t) = x(\sigma,t)\mathbf{e}_x + y(\sigma,t)\mathbf{e}_y \tag{3}$$

as a function of the normalized coordinate and time. The equations of structural mechanics require the first and the second order derivatives of the position vector with respect to the material coordinate, namely

$$\partial_s\mathbf{x} = \partial_\sigma\mathbf{x}\,\partial_s\sigma = \frac{1}{\eta}\partial_\sigma\mathbf{x}, \quad \partial_s^2\mathbf{x} = \frac{1}{\eta^2}\partial_\sigma^2\mathbf{x}. \tag{4}$$

For the transient analysis we also need the material velocity of a particle

$$\dot{\mathbf{x}} = \partial_t\mathbf{x}|_{s=\mathrm{const}} = \partial_t\mathbf{x}|_{\sigma=\mathrm{const}} + \dot{\sigma}\,\partial_\sigma\mathbf{x}. \tag{5}$$

Introducing further a $C^1$ continuous global Ritz or finite element approximation for $\mathbf{x}$ as function of $\sigma$, we obtain the strain energy of bending of the rod $U$ (possibly with a penalty term for the inextensibility constraint), the kinetic energy of both parts of the rod $T$ and the potential energy in the field of gravity $W$ as functions of the generalized degrees of freedom $q$ and their time derivatives. For a cubic finite element approximation, $q$ comprises the nodal position vectors $\mathbf{x}_i$, nodal derivatives $(\partial_\sigma\mathbf{x})_i$ and the additional unknown $\eta$. The boundary conditions at the tip of the sleeve read

$$x(0,t) = y(0,t) = 0, \quad \partial_\sigma y(0,t) = 0. \tag{6}$$

The dynamics of small and large vibrations of the rod coupled with the axial motion $\eta(t)$ is governed by Lagrange's equations of motion of the 2nd kind. Such a non-material analysis scheme for axially moving structures is in line with the mixed Eulerian-Lagrangian simulation framework, previously used in [4, 5], see also review article [6]. It is interesting to note, that the configurational force, which acts against the injection being work conjugate to $\eta$, is related to the release rate of potential energy and is proportional to the curvature of the rod at the tip of the sleeve. In the sense of Newtonian mechanics, this force appears as the longitudinal component of the contact force at the tip of the sleeve because of the small but inevitable inclination of the rod: the gap of the sleeve must be slightly larger than the thickness of the rod, see again Figure 1.

### Semi-analytical solution and comparison

When the vibration amplitude is small, it makes sense to use linear beam theory for the free part and just a single term in the Ritz approximation. The position vector is sought in the form

$$\mathbf{x}(\sigma,t) = \sigma\eta(t)\mathbf{e}_x + \gamma(t)w(\sigma)\mathbf{e}_y. \tag{7}$$

The shape function $w(\sigma)$ corresponds to the first vibration mode of a cantilever beam with $w(1) = 1$, such that the generalized coordinate $\gamma$ is the transverse deflection of the tip of the beam. The

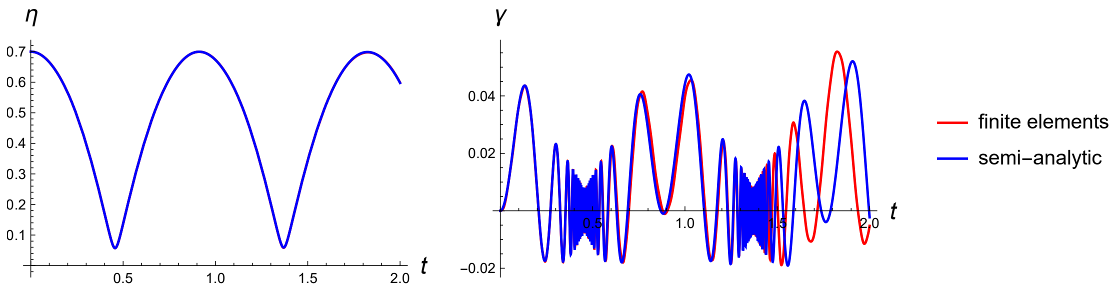


Figure 2: Computed transient dynamics for FE and 2 d.o.f. models.

axial motion of each particle is governed by the second generalized coordinate $\eta$. Integrating over $0 \leq s \leq l$, we obtain the energy expressions

$$\begin{gathered} U = ak_U\gamma^2/\eta^3, \quad W = \rho g(l(l-2\eta)\cos\alpha - 2k_W\gamma\eta\sin\alpha)/2, \\ T = \rho(\eta\dot{\gamma}^2 + \gamma\dot{\gamma}\dot{\eta} + 4(2k_T\gamma^2 + l\eta)\dot{\eta}^2/\eta)/8 \end{gathered} \tag{8}$$

with $a$ being the bending stiffness, $\rho$ the mass density per unit length, $g$ the free fall acceleration and three numerical coefficients following after the integration: $k_U = 1.5453$, $k_T = 0.094385$, $k_W = 0.39150$. The two nonlinear differential equations of motion are difficult to approach by analytical methods, but they can easily be integrated numerically. We consider the rod of the length $l = 1$, thickness $h = 2 \cdot 10^{-3}$, Young's modulus $E = 2 \cdot 10^{11}$ and volumetric density $\rho_3 = 7800$ (SI units). The gravity force acts in the diagonal direction: $g = 9.8$, $\alpha = \pi/4$. We compare the simulation results to the converged finite element solution in Figure 2. One observes alternating injection and ejection of the rod with rapid changes in the vibration frequency $\omega$. The coefficients at $\gamma^2$ in $U$ and at $\dot{\gamma}^2$ in $T$ in Equation (8) provide an estimate $\omega = 2\sqrt{2ak_U/\rho}/\eta^2$, which matches very good with the observations from numerical experiments.

## References


[1] Humer, A.; Steinbrecher, I.; Vu-Quoc, L: General sliding-beam formulation: A non-material description for analysis of sliding structures and axially moving beams. Journal of Sound and Vibration, Vol. 480, 115341, 2020.

[2] Armanini, C.; Dal Corso, F.; Misseroni, D.; Bigoni, D: Configurational forces and non-linear structural dynamics. Journal of the Mechanics and Physics of Solids, Vol. 130, pp. 82–100, 2019.

[3] Han, S.; Bauchau, O.A.: Configurational forces in variable-length beams for flexible multi-body dynamics. Multibody System Dynamics, pp. 1–24, 2022.

[4] Vetyukov, Y.: Non-material finite element modelling of large vibrations of axially moving strings and beams. Journal of Sound and Vibration, Vol. 414, pp. 299–317, 2018.

[5] Kocbay, E.; Scheidl, J.; Riegler, F.; Leonhartsberger, M.; Lamprecht, M.; Vetyukov, Y.: Mixed Eulerian–Lagrangian modeling of sheet metal roll forming. Thin-Walled Structures, Vol. 186, 110662, 2023.

[6] Scheidl, J.; Vetyukov, Y.: Review and perspectives in applied mechanics of axially moving flexible structures. Acta Mechanica, Vol. 234(4), pp. 1331–1364, 2023.

# The Approximate Solutions and Modal Identification of Coupled Overtone Nonlinear Vibrations of a Cantilever Beam with the Extended Galerkin Method

Ji Wang, Baochen Meng, Chencheng Lian, Rongxing Wu
Piezoelectric Device Laboratory, School of Mechanical Engineering & Mechanics, 818 Fenghua Road, Ningbo, 315211 Zhejiang, China
Email: wangji@nbu.edu.cn

The nonlinear vibrations of large amplitudes of elastic beams are frequently encountered as the elastica problem, with complications in various applications. As the continuation of the analysis of the large deformation of an elastica, the nonlinear vibration equation of a cantilever beam in the rotation angle of the cross-section is utilized for approximate solutions. Using the linear solutions, the nonlinear equation with the inertia effect and couplings of higher-order vibration modes have been solved with the newly suggested extended Galerkin method (EGM). The solutions to the vibration problem of an elastic cantilever beam are compared with the exact solutions known in elliptic functions, including frequencies and mode shapes of the first three modes, with good agreement. The results also proved that the nonlinear vibration modes are close to the linear ones. And the mode identification can be done effectively with both kinetic and strain energy proportions calculated from vibration solutions. This is a perfect combination of the EGM for solutions of nonlinear vibrations and the utilization of energy proportion for the identification of coupled vibration modes.

The cantilever beam is shown in Figure 1, with $L$ as the length, $EI$ as the flexural stiffness, $\xi$ as the tangential coordinate, $s$ as the arc length, and $m$ as the unit mass, respectively. The nonlinear free vibration equation and boundary conditions of a cantilever beam in the rotation angle of a cross-section from the beam equation [1] is

$$\frac{\partial^2}{\partial s^2}\left[EI\frac{\partial\theta(s,t)}{\partial s}\right]+m\ddot{w}(x,t)=0, \sin\theta=\frac{dw}{ds},$$
$$\theta(0,t)=0,\ \theta'(1,t)=0,\ \theta''(1,t)=0 \tag{1}$$

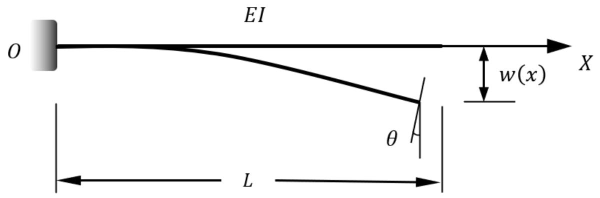


**Figure 1**. The cantilever beam model.

To this problem, the trial solution is taken from linear solutions as [2]

$$\theta(\xi,t)=\sum_{i=1}^{N}A_i\varphi_i(\xi)\cos\omega_i t\,,\xi=\frac{s}{L}$$
$$\varphi_i(\xi)=C_1\cos\lambda_i\xi+C_2\sin\lambda_i\xi+C_3\cosh\lambda_i\xi+C_4\sinh\lambda_i\xi \tag{2}$$

where $A_i$ are undetermined amplitudes, $\omega_i$ is the $i$th-order frequency, $\lambda_i$ are the characteristic values from the mode shape solutions of the linear Euler-Bernoulli beam equation [2], and $C_j(j = 1,2,3,4)$ are obtained from linear vibrations with boundary conditions in Eq. (1) and incorporated into $A_i$ as unknowns. Differentiating Eq. (1) with respect to $\xi$, followed by a series expansion, then applying the EGM [3] with the solution in Eq. (2), one obtains

$$\int_0^{\frac{2\pi}{\omega}}\int_0^1 \left\{\alpha\frac{d^4\theta}{d\xi^4} + \left[\ddot{\theta}\left(1-\frac{\theta^2}{2}\right) - \dot{\theta}^2\theta\right]\right\}\delta\theta d\xi dt = 0,\ \alpha = \frac{EI}{mL^4} \quad (3)$$

with $\omega$ as the vibration frequency and $\delta\theta$ as the variation of rotation in Eq. (2). The initial condition in Eq. (2) is

$$\theta(1, t = 0) = A$$

Since there are $N$ components of parameters of vibrations from Eq. (2), the integration in Eq. (3) is performed separately as

$$\begin{aligned}
&N_i(A_1, A_2, \cdots, A_N, \lambda_1, \lambda_2, \cdots, \lambda_N, \omega_1, \omega_2, \dots, \omega_N, \alpha; \lambda_i, \omega_i)\\
&\quad = \int_0^{\frac{2\pi}{\omega_i}}\int_0^1 \left\{\alpha\frac{d^4\theta}{d\xi^4} + \left[\ddot{\theta}\left(1-\frac{\theta^2}{2}\right) - \dot{\theta}^2\theta\right]\right\}\varphi_i\cos\omega_i t d\xi dt\\
&N_1(A_1, A_2, \cdots, A_N, \lambda_1, \lambda_2, \cdots, \lambda_N, \omega_1, \omega_2, \dots, \omega_N, \alpha; \lambda_1, \omega_1) = 0\\
&N_2(A_1, A_2, \cdots, A_N, \lambda_1, \lambda_2, \cdots, \lambda_N, \omega_1, \omega_2, \dots, \omega_N, \alpha; \lambda_2, \omega_2) = 0\\
&\vdots\\
&N_N(A_1, A_2, \cdots, A_N, \lambda_1, \lambda_2, \cdots, \lambda_N, \omega_1, \omega_2, \dots, \omega_N, \alpha; \lambda_N, \omega_N) = 0\\
&A_1 + A_2 + \cdots + A_N = A
\end{aligned} \quad (4)$$

The frequency solutions in Table 1 are from the following iterative procedure

1. Assuming the $A_j^k = 0$ with $j \geq 1$ and $k > 1$ in equation $N_j$ in Eq. (4) for the approximate solutions $(\omega_j, A)$ with known $(\omega_i, A)$ for $i \leq j$.
2. Substituting known $(\omega_i, A_i), i = 1, 2, \cdots, k$ pairs with $A_{k+1} = A - \sum_{i=1}^{N} A_i, k \geq 1$ into $N_{k+1}$ equations in Eq. (4) and obtain $(\omega_i, A_i), i = k+1, \cdots, N$ in $A$.

**Table 1.** The frequencies of a cantilever beam with different amplitudes

| Amplitude $A$(m) | Parameters $\frac{EI}{mL^4}$ $(\frac{\text{N}}{\text{kg}\cdot\text{m}^2})$ | Nonlinear $\omega_1$ $(\frac{\text{rad}}{\text{s}})$ | Lian et al. [4] | Nonlinear $\omega_2(\frac{\text{rad}}{\text{s}})$ | Lian et al. [4] | Nonlinear $\omega_3(\frac{\text{rad}}{\text{s}})$ | Lian et al. [4] |
|---|---|---|---|---|---|---|---|
| 0.001 | 5000 | 248.6188 | 248.5929 | 1558.0799 | 1558.103 | 4362.7002 | 4362.921 |
| 0.001 | 10000 | 351.6000 | 351.5634 | 2203.4577 | 2203.363 | 6169.7898 | 6170.103 |
| 0.001 | 20000 | 497.2375 | 497.1858 | 3116.1597 | 3116.011 | 8725.4004 | 8725.842 |
| 0.4 | 5000 | 250.6767 | 248.6345 | 1580.3624 | 1558.537 | 4515.6503 | 4362.011 |
| 0.4 | 10000 | 354.5103 | 351.6223 | 2234.9700 | 2204.104 | 6386.0938 | 6168.816 |
| 0.4 | 20000 | 501.3533 | 497.2691 | 3160.7246 | 3117.075 | 9031.3005 | 8724.023 |
| 0.6 | 5000 | 253.3224 | 250.9881 | 1609.4097 | 1588.287 | 4702.7158 | 4352.588 |
| 0.6 | 10000 | 358.2520 | 354.9508 | 2276.0490 | 2246.177 | 6650.6445 | 6155.489 |
| 0.6 | 20000 | 506.6448 | 501.9762 | 3218.8193 | 3176.572 | 9405.4316 | 8705.177 |

For the examination of energy distribution in the vibrations of a beam, with the neglect of coupled terms, the strain energy $U$ and kinetic energy $T$ of the $i$th-mode are [5]

$$U = \int_0^{\frac{2\pi}{\omega_i}}\sum_{i=1}^{N}\int_0^1 \frac{EIA_i^2}{2}\left[\frac{\partial^2\varphi_i(\xi,t)}{\partial\xi^2}\cos\omega_i t\right]^2 d\xi dt, T = \int_0^{\frac{2\pi}{\omega_i}}\sum_{i=1}^{N}\int_0^1 \frac{mA_i^2}{2}[\omega_i\varphi_i(\xi,t)\cos\omega_i t]^2 d\xi dt \quad (5)$$

In the calculation, the modal functions of linear vibrations have been used as an approximate solution of the governing equation in Eq. (4) to calculate the higher-order frequency solutions by the EGM. Then Eq. (4) can be used again to find amplitudes $A_1, A_2, A_3$ of each mode with known frequencies, thus enabling the evaluation of all modes. From Eq. (5), the maximum energies of the *i*th-mode in Tables 2 and 3 are

$$V_{\varphi_i} = \int_0^1 \frac{1}{2} EI(A_i \varphi_i'')^2 \, d\xi, T_{\varphi_i} = \int_0^1 \frac{1}{2} m(\omega_i A_i \varphi_i)^2 \, d\xi \tag{6}$$

**Table 2.** Energies of each mode at the second-order frequency

| Amplitude | 1st strain energy | 1st kinetic energy | 2nd strain energy | 2nd kinetic energy |
|---|---|---|---|---|
| $A$(m) | $V_{\varphi_1}$(J) | $T_{\varphi_1}$(J) | $V_{\varphi_2}$(J) | $T_{\varphi_2}$(J) |
| 0.001 | 0.0371 | 0.0371 | 0.1549 | 0.1549 |
| 0.1 | 390.8243 | 391.2195 | 1369.0733 | 1371.4869 |
| 0.2 | 1561.1209 | 1567.5094 | 5495.7299 | 5534.5863 |
| 0.4 | 6214.0597 | 6317.2804 | 22256.1178 | 22897.3662 |
| 0.6 | 13854.9499 | 14383.9816 | 51227.9150 | 54659.1255 |

**Table 3.** Energies of each mode at the third-order vibration mode

| Amplitude | 1st strain energy | 1st kinetic energy | 2nd strain energy | 2nd kinetic energy | 3rd strain energy | 3rd kinetic energy |
|---|---|---|---|---|---|---|
| $A$(m) | $V_{\varphi_1}$(J) | $T_{\varphi_1}$(J) | $V_{\varphi_2}$(J) | $T_{\varphi_2}$(J) | $V_{\varphi_3}$(J) | $T_{\varphi_3}$(J) |
| 0.001 | 0.0485 | 0.0485 | 0.0172 | 0.0172 | 1.0747 | 1.0748 |
| 0.1 | 493.7189 | 494.2181 | 91.7433 | 91.9050 | 8449.2710 | 8489.8943 |
| 0.2 | 1918.9916 | 1926.8447 | 342.2683 | 344.6883 | 36122.7950 | 36802.3855 |
| 0.4 | 6964.7350 | 7080.4250 | 1041.8344 | 1071.8520 | 176282.2250 | 188862.6647 |
| 0.6 | 14610.3885 | 15168.2654 | 1818.4242 | 1940.2210 | 447113.6270 | 519532.0793 |

Finally, with the known rotation of the cross-section $\theta(\xi, t)$, the beam deflection is

$$w(x,t) = L \int_0^x \sin\theta \, d\xi \; = L \int_0^x \sin\left[\sum_{i=1}^{N} A_i \varphi_i(\xi) \cos\omega_i t\right] d\xi \tag{7}$$

The vibration modes are successfully identified with the largest energy proportions of coupled vibrations, thus providing an important technique for the refined analysis of nonlinear vibrations of structures.

**References**


[1] Gere, J.M. ;Timoshenko, S.P.: *Mechanics of Materials (Fourth Edition)*, PWS Publishing Company, Boston, pp. 601-603, 1997.

[2] Timoshenko, S. P.: *Vibration Problems in Engineering*. D. Van Nostrand Company, New York, 1937.

[3] Wang, J.; Wu, R.: The extended Galerkin method for approximate solutions of nonlinear vibration equations. *Applied Sciences*, vol. 12, no. 6, pp. 2979, 2022.

[4] Lian, C. et al: The Analysis of Higher-order Nonlinear Vibrations of an Elastic Beam with the Extended Galerkin Method, *Journal of Vibration in Engineering & Technologies*, accepted, 2023. *ResearchGate*, 10.13140/RG.2.2.32080.17924, 2022.

[5] Pavić, G.: Vibration damping, energy and energy flow in rods and beams: Governing formulae and semi-infinite systems. *Journal of Sound and Vibration*, vol. 291, no. 3-5, pp. 932-962, 2006.

# Timoshenko frequencies and the Wittrick-Williams algorithm: Some simple exact solutions to complex problems

**W.P. Howson*** **and** **A. Watson#**

* Independent Consultant
Gwanwyn, Craig Penlline, CF71 7RT, UK
w.p.howson@gmail.com

# Dept. of Aero and Auto Engineering
Loughborough University
Loughborough, LE11 3TU, UK
a.watson@lboro.ac.uk

## Introduction

An exact fourth order differential equation governing the motion of a Timoshenko beam-column on a uniformly distributed, bi-parametric foundation is presented in non-dimensional form. Two related problems are then solved simply and efficiently. In the first of these, the governing differential equation is transformed into a standard quadratic equation that provides the core of a simple procedure that yields the exact natural frequencies of the member for the simply supported case. In the second problem, the same quadratic equation is used to solve the complementary problem of predicting the number of simply supported natural frequencies of the member passed by any given trial frequency.

## Theory

An exact, fourth order differential equation governing the motion of an axially loaded Timoshenko beam of length, $L$, that is supported on a bi-parametric, distributed foundation, whose lateral and rotational restraining stiffnesses per unit length are $k_y$ and $k_\theta$, respectively, has been presented in rigorous detail by Capron and Williams [1]. Since this paper adopts an identical sign convention and almost identical notation, the required equation can be written in terms of the amplitude of the sinusoidally varying lateral displacement $V$ as

$$[D^4 + 2\Upsilon_A D^2 - \Upsilon_B]V = 0 \tag{1}$$

where $D = d/d\xi, \xi = x/L$ is the non-dimensional length parameter and $V$ is the amplitude of the lateral displacement.

The equivalent equation for the simply supported case is easily achieved by assuming a general solution of the form $V = C \sin i\pi\xi$, where $C$ is an arbitrary constant, $V$ satisfies the boundary conditions and $i$ defines the modal rank. It can then be written as

$$[\delta_i^2 - 2\Upsilon_A \delta_i - \Upsilon_B] = 0 \tag{2}$$

where

$$\Upsilon_A = (\Delta - k_1^*) \quad \Upsilon_B = (qb^2 - k_2^*)/t \quad \delta_i = (i\pi)^2 \quad i = 1, 2, \ldots \infty \tag{3a,b,c}$$

$$\Delta = [qp^2 + b^2(r^2 + s^2)]/2t \quad q = 1 - b^2r^2s^2 \quad t = 1 - s^2p^2 \tag{4}$$

$$b^2 = \rho AL^4\omega^2/EI \quad p^2 = PL^2/EI \quad r^2 = I/AL^2 \quad s^2 = EI/\kappa AGL^2 \tag{5}$$

$$k_1^* = (s^2k_y^* + tk_\theta^*)/2t \quad k_2^* = qk_y^* - s^2k_\theta^*(b^2 - k_y^*) \quad k_y^* = k_yL^4/EI \quad k_\theta^* = k_\theta L^2/EI \tag{6}$$

and $A$ is the cross-sectional area, $I$ is the second moment of area, $E$, $G$ and $\rho$ are Young's modulus, the modulus of rigidity and the density of the member material, respectively, $\kappa$ is the section shape factor, $\omega$ is the radian frequency of vibration and $P$ is the static axial load in the member, which is positive for compression, zero, or negative for tension.

The non-dimensional parameters $b^2$, $p^2$, $r^2$ and $s^2$ uniquely define the effects of frequency, axial load, rotary inertia and shear deformation, respectively, and together with the two non-dimensional foundation parameters, can be ignored in any combination by setting the relevant parameter to zero.

Substituting Eqs.(3)-(6) into Eq.(2) gives a quadratic frequency equation in the non-dimensional frequency parameter, $b_i^2$, that can be written as

$$\begin{aligned} &b_i^4 r^2 s^2 - \{[r^2(1-s^2p^2)+s^2]\delta_i + [1+s^2(r^2k_y^* + k_\theta^*)]\}b_i^2 \\ &\quad + (1-s^2p^2)\delta_i^2 - [p^2 - s^2k_y^* - (1-s^2p^2)k_\theta^*]\delta_i + (1+s^2k_\theta^*)k_y^* = 0 \quad i = 1,2,\ldots\infty \end{aligned} \tag{7}$$

where $(1-s^2p^2)$ is always positive [1] and the subscript, $i$, has been added to $b$ in order to denote modal rank. Eq.(7) clearly offers a simple way of determining the required Timoshenko frequencies explicitly and it is proven in the Appendix that the roots of this equation are always real and distinct. Furthermore, the lower of the two roots in each pair, corresponds to what is often referred to as the first spectrum of Timoshenko frequencies, while the upper root corresponds to the 'so called' second spectrum. However, the complete spectrum of frequencies, with or without a foundation, comprise all the $b_i$'s from Eq.(7), plus the cut-off frequency [2], which corresponds to the point discontinuity in the Timoshenko beam equation and additionally reduces $\Upsilon_B$ to zero [2]. It therefore occurs when

$$1 - b^2r^2s^2 + s^2k_\theta^* = 0 \quad \text{so that} \quad b_{co}^2 = (1+s^2k_\theta^*)/r^2s^2 \tag{8a,b}$$

The value of $b_{co}^2$ is clearly positive and, as in the case of no foundation [2], it retains its status as a pure shear mode.

Consider now the complementary problem of establishing an efficient root counting procedure. Once more the required solution stems from Eq.(2), but in a contrasting way. In the original problem the unknown frequency parameters, $b^2$, were calculated from a knowledge of $\delta$, while in the present case the unknown $\delta$ are calculated from a knowledge of the given trial frequency parameters, $b^2$. The traditional quadratic solution procedure can then be applied to Eq.(2) in the usual way, to yield

$$\delta = \Upsilon_A \pm \sqrt{\Upsilon_A^2 + \Upsilon_B} \tag{9}$$

or

$$\Phi^2 = \Upsilon_A + \sqrt{\Upsilon_A^2 + \Upsilon_B} \quad \text{and} \quad \Lambda^2 = \Upsilon_A - \sqrt{\Upsilon_A^2 + \Upsilon_B} \tag{10a,b}$$

where the modal subscripts have been dropped since the equations are no longer dealing primarily with modal quantities. However, it is known that at modal values of the sought parameters, both $\Phi_i$ and $\Lambda_i = i\pi$, the former corresponding to the first spectrum frequencies and the latter to the 'so called' second spectrum frequencies. As before, the cut-off frequency must be accounted for where appropriate. Thus, the number of simply supported frequencies passed by a given trial value of the frequency parameter is given by

$$J_{ss} = J_\Phi + J_\Lambda + J_{co} \tag{11}$$

where

$$J_\Phi = \text{largest integer} < \Phi/\pi \quad J_\Lambda = \text{largest integer} < \Lambda/\pi \tag{12}$$

and

$$J_{co} = 1 \quad \text{if} \quad b^2 > (1+s^2k_\theta^*)/r^2s^2 \quad \text{and zero otherwise} \tag{13}$$

Eq.(11) enables exact evaluation of $J_{ss}$ and hence provides the core component of a process that could converge methodically upon any desired natural frequency. Its development is straightforward, easy to explain and simple to implement. It therefore provides a compelling alternative to the corresponding process presented by Capron and Williams [1].

Finally, it is interesting to note that Eq.(10a) also offers the possibility of establishing the modal rank of the cut-off frequency in the Timoshenko spectrum prior to any analysis being undertaken. This can be achieved as follows, due to the fact that the cut-off frequency corresponds to $\Upsilon_B = 0$. In such a case, Eq.(10a) can be written as

$$(i\pi)^2 = 2\Upsilon_A \tag{14}$$

Substituting Eqs.(3a) and (8b) into Eq.(14) and noting that the cut-off frequency corresponds to the first value of $\Phi$ that is not an integer multiple of $\pi$, the required modal rank is given by

$$\text{the smallest integer} > \{[r^2+s^2+s^4(k_\theta^*-r^2k_y^*)]/(1-s^2p^2)r^2s^2\pi^2\}^{1/2} \tag{15}$$

The term $(k_\theta^* - r^2k_y^*)$ influences the modal rank in an important way for the following reason. From Eq.(8b) it can be seen that the cut-off frequency is dependent upon the rotational foundation stiffness, but not the lateral foundation stiffness. However, if the lateral foundation stiffness is increased, all frequencies will increase, except the cut-off frequency, whose modal rank might or might not be required to decrease.

## References


[1] Capron, M.D., Williams F.W.: Exact dynamic stiffnesses for an axially loaded uniform Timoshenko member embedded in an elastic medium. Journal of Sound and Vib, Vol. 124, pp. 453–466, 1988

[2] Howson, W.P., Watson, A.: On the provenance of hinged-hinged frequencies in Timoshenko beam theory. Computers and Structures, Vol. 197, pp. 71–81, 2018


## Appendix

It can be shown straightforwardly that the discriminant of Eq.(7), $\Omega$, can be written as

$$\begin{aligned}\Omega = {} & \delta_i^2[r^4(1-s^2p^2)^2 - 2r^2s^2(1-s^2p^2)+s^4] \\ & + 2\delta_i[r^2(1-s^2p^2)+s^2+r^2s^2(1-s^2p^2)(r^2k_y^*-k_\theta^*)+s^4(k_\theta^*-r^2k_y^*)] \\ & + [1+2s^2(k_\theta^*-r^2k_y^*)+s^4(r^4k_y^{*2}-2r^2k_y^*k_\theta^*+k_\theta^{*2})]\end{aligned} \tag{A.1}$$

However, it can also be shown that

$$\Omega = \{[r^2(1-s^2p^2)-s^2]\delta_i - [1-s^2(r^2k_y^*-k_\theta^*)]\}^2 + 4r^2\delta_i \tag{A.2}$$

where

$$4r^2\delta_i = 4r^2\delta_i(1-s^2p^2)+4p^2r^2s^2\delta_i \tag{A.3}$$

Eq.(A.2) clearly demonstrates that $\Omega$ is always positive, while its expansion shows exact correspondence to the terms of Eq.(A.1), with the self-evident result that Eq.(A.1) is always positive.

# Accurate Free Transverse Vibration Analysis of Homogeneous Mindlin Plates by the Substructure Method

**Shudong Yu**

Department of Mechanical and Industrial Engineering
Toronto Metropolitan University
Toronto, Ontario, Canada M5B 2K3
syu@torontomu.ca

## Summary

An accurate and efficient substructure method (SM) is developed and presented in this paper for free transverse vibration of Mindlin plates of any shape, made of isotropic, orthotropic and anisotropic materials, and subjected to any type of constraint on any edge and at any corner.

**Background.** Exact or accurate analytical methods are known to be superior to the finite element method in accuracy and efficiency for simple structural dynamics problems. However, analytical methods usually lack generality and are limited to some specific problems. The finite element method, on the other hand, is general, but lacks efficiency. The substructure method, proposed by the author, is as general as the FEM and also as efficient and accurate as the analytical methods.

**Governing Equations**. According to Mindlin's improved plate theory or IPT for flexural vibration [1], a straight line normal to the plate midplane in the undeformed state remains straight after deformations. However, this displaced line is not normal to the deformed midplane due to the transverse shear effect. Motion of this line can be regarded as the superposition of the translational motion in the thickness or $z$ direction and the rotation about its intercepting point with the midplane. At time $t$, the displacements of material point at $(x,y,z)$ are determined by three field variables $u_z(x,y,t)$, $\phi_x(x,y,t)$, and $\phi_y(x,y,t)$, which are the transverse displacement of the midplane and the two angles of rotation about the $x$ and $y$- axes, respectively. With the IPT, the transverse displacement is invariant with coordinate $z$; the inplane displacments $u_x$ and $u_y$ vary linearly with coordinate $z$. There are five non-zero strains. The two transverse shear strains $\gamma_{zx}$ and $\gamma_{zy}$ are invariant in the thickness diretion. The three inplane strains $\varepsilon_{xx}$ ,$\varepsilon_{yy}$ and $\gamma_{xy}$ vary lineary with coordinate $z$. As a result, the volume integrals associated with the kinetic and strain energies are reduced to area integrals over the plate midplane.

**Geometric Mapping.** A plate whose mid-plane occupies a closed 2D domain and has no more than four singularity points or corners can be modelled as a Q-substructure or a T-substructure. Plates of geometries excluding triangular plates of straight edges can be modelled as Q-substructures. In this paper, only the Q-substructures are dealt with. For a Q-substructure, every point in the midplane can be mapped uniquely into a corresponding point in a square using the boundary control points and matching orders of bivariate polynomials. The following equations map a point in a Q-substructure domain in the Cartesian coordinates $(x,y)$ into a corresponding point in the parent square in the non-dimensional coordinates $(\xi,\eta)$

$$x=\left[S(\xi,\eta)\right]_{GQ}\left[D\right]_{GQ}\{\bar{x}\},\ y=\left[S(\xi,\eta)\right]_{GQ}\left[D\right]_{GQ}\{\bar{y}\};\ -1\le\xi\le 1, -1\le\eta\le 1 \qquad (1)$$

where $[S(\xi,\eta)]_{GQ}$ is a bivariate polynomial shape function array; $[D]_{GQ}$ is the relationhsip matrix required to transform the coefficients associated with bivariate polynomial terms into the coordinates of control points; $\{\bar{x}\}$ and $\{\bar{y}\}$ are the coordinates of the boundary control points. For a quadrilateral plate, the geometric mapping is done through the use of four corner control points and order-1 bivariate polynomials. The shape array, the relationship matrix and the coordinate arrays are given below for reference

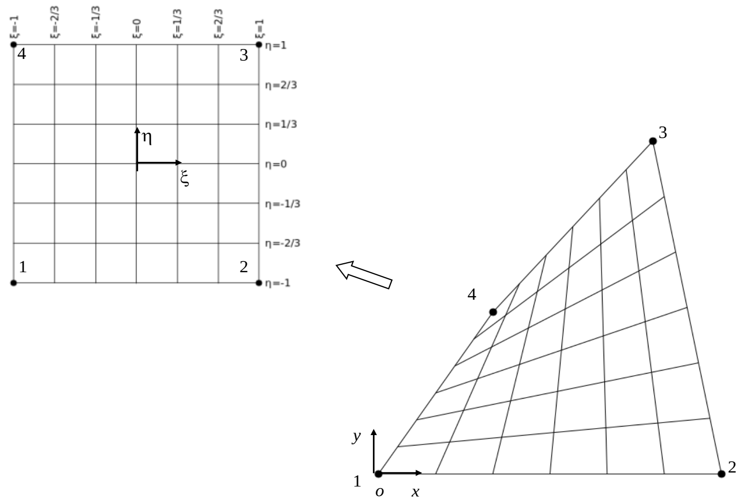


**Figure 1.** Geometric mapping of a quadrilateral plate into a square.

$$[S(\xi,\eta)]_{GQ} = [1 \quad \xi \quad \eta \quad \xi\eta]$$

$$[D]_{GQ} = \begin{bmatrix} [S(\xi_1,\eta_1)]_{GQ} \\ [S(\xi_2,\eta_2)]_{GQ} \\ [S(\xi_3,\eta_3)]_{GQ} \\ [S(\xi_4,\eta_4)]_{GQ} \end{bmatrix}^{-1} = \frac{1}{4}\begin{bmatrix} 1 & 1 & 1 & 1 \\ -1 & 1 & 1 & -1 \\ -1 & -1 & 1 & 1 \\ 1 & -1 & 1 & -1 \end{bmatrix}, \ \{\bar{x}\} = \begin{Bmatrix} 0 \\ 1.5 \\ 1.2 \\ 0.5 \end{Bmatrix}, \{\bar{y}\} = \begin{Bmatrix} 0 \\ 0 \\ 1.75 \\ 0.85 \end{Bmatrix} \tag{2}$$

Figure 1 shows the mapping of 14 lines defined by $\xi,\eta = 0,\pm 1/3,\pm 2/3,\pm 1,$ in the parent square into the corresponding lines in the quadrilateral plate domain.

**Spatial variations of field variables.** For a Q-substructure, at time $t$, the three 2D field variables may be defined in terms of a hybrid bivariate shape function array $[S(\xi,\eta)]_{VQ}$, the relationship matrix $[D]_{VQ}$ and the nodal variable arrays $\{\bar{u}_z(t)\}$, $\{\bar{\phi}_x(t)\}$ and $\{\bar{\phi}_y(t)\}$ as

$$u_z = [S(\xi,\eta)]_{VQ}[D]_{VQ}\{\bar{u}_z(t)\}, \phi_x = [S(\xi,\eta)]_{VQ}[D]_{VQ}\{\bar{\phi}_x(t)\}, \phi_y = [S(\xi,\eta)]_{VQ}[D]_{VQ}\{\bar{\phi}_y(t)\} \tag{3}$$

In this paper, the following generic hybrid shape function array is proposed to capture the spatial variations of all 2D field variables for an $m \times n$ grid

$$[S(\xi,\eta)]_{VQ} = \mathrm{ROW}\left[\hat{H}_n(\eta)\right]^T \left[\overline{H}_m(\xi)\right] \tag{4}$$

$$\left[\overline{H}_m(\xi)\right] = \left[1 \quad \xi \quad \xi^2 \quad \xi^3 \quad \bar{c}_1(\xi) \quad \bar{c}_2(\xi) \quad \cdots \quad \bar{c}_m(\xi)\right] \tag{5}$$

$$\left[\hat{H}_n(\eta)\right] = \left[1 \quad \eta \quad \eta^2 \quad \eta^3 \quad \hat{c}_1(\eta) \quad \hat{c}_2(\eta) \quad \cdots \quad \hat{c}_n(\eta)\right] \tag{6}$$

$$\bar{c}_k(s) = \cos\left\{\frac{k(1+\xi)\pi}{2} + \frac{\pi}{4}\right\}, \hat{c}_k(s) = \cos\left\{\frac{k(1+\eta)\pi}{2} + \frac{\pi}{4}\right\} \tag{7}$$

**Formulation of eigenvalue problem.** For plates made of linearly elastic material, isotropic, orthotropic or generally anisotropic, a set of standard linear eigenvalue problem may be formulated using Hamilton's principle and solved using an eigen-solver.

**Numerical Results.** Numerical results are obtained using the proposed approach, the finite element method and the exact Navier method for a simply supported rectangular isotropic plate of aspect ratio 1.25. For an objective comparison, the substructure and FE models contain 121 nodes. In transverse vibration analysis, the lateral displacement is the dominating field variable. Both SM and FEM models can only yield a maximum of 81 bending modes because the transverse displacements at the 40 boundary nodes are eliminated in the eigenanalysis. Percentage errors in natural frequencies are plotted for the first 26 modes in Figure 2. It can be seen that the natural frequencies predicted by the SM have negligibly small errors while the FEM results are noticeably inaccurate even for the low vibration modes. In the second case, a completely free isotropic circular plate of thickness ratio of $h/r = 0.1$ and a Poisson ratio of 0.3 are obtained using the SM method and compared with those of Irie et al. [2] in Table 1. The corresponding modal contours are plotted in Figure 3.

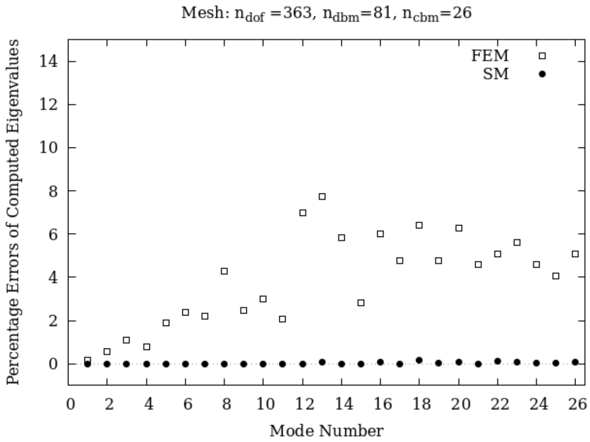


**Figure 2.** Comparison of computed eigenvalues.

**Table 1.** Eigenvalues of a Completely Free Isotropic Circular Plate

| Elastic Modes | SM (5,5)-(9,9)* | Irie et al. (1980) |
|---|---|---|
| 1, 2 | 5.278, 5.279 | 5.278 (2,0)** |
| 3 | 8.868 | 8.868 (0,1) |
| 4,5 | 12.067, 12.067 | 12.064 (3,0) |
| 6,7 | 19.712,19.712 | 19.711 (1,1) |
| 8,9 | 20.807,20.812 | 20.801 (4,0) |
| 10,11 | 31.285,31.285 | 31.270 (5,0) |
| 12,13 | 33.035,33.043 | 33.033 (2,1) |
| *(5,5) refer to the material mapping scheme; (9,9) refer to the variable meshing scheme. **The numbers in parenthesis are the number of waves in the circumferential and radial directions. | | |

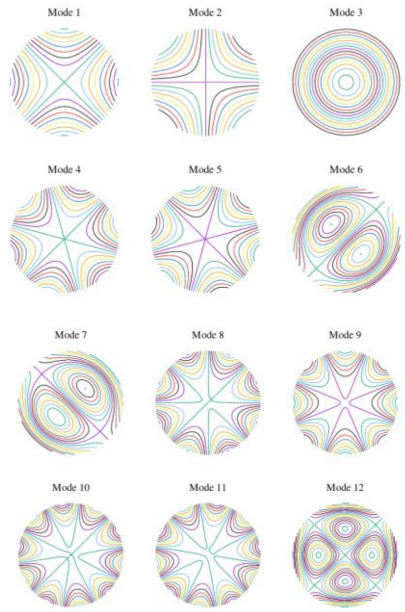


**Figure 3.** Modal contours of a circular plate.

## References

[1] R.D. Mindlin, “Influence of Rotary Inertia and Shear on Flexural Motions of Isotropic Plates,’ Journal of Applied Mechanics, Vol. 18, pp 31-38, 1951.

[2] T. Irie, G. Yamada and S. Aomura, 1980. “Natural Frequencies of Mindlin Circular Plates”, ASME Journal of Applied Mechanics 47, pp 652-655, 1980.

# Investigation on porous FGM plates on elastic foundation by the R-functions and Finite Element Method

**A. Zippo[*], T. Shmatko [†], F. Pellicano [*], L. Kurpa [#]**

[*] Dep. of Engineering "Enzo Ferrari"
University of Modena and Reggio Emilia
Via P.Vivarelli 10, 41125 Modena , IT
antonio.zippo@unimore.it
francesco.pellicano @unimore.it

[#] Dept. of Applied Mathematics, National Technical
University, ''Kharkiv Polytechnic Institute"
21 Frunze St., Kharkiv 310002, Ukraine
l.kurpa@mail.ru

[†] Dept. of Higher Mathematics
National Technical University, ''Kharkiv Polytechnic Institute"
21 Frunze St., Kharkiv 310002, Ukraine
ktv_ua@yahoo.com

## Introduction

Functionally Graded Materials (FGMs) are modern materials that are widely used in many industries: aircraft and rocket building, shipbuilding, for the manufacture of nuclear reactors, automotive engineering, etc. The intensive use of functionally graded materials has led to the need for a thorough study of their behavior during operation, considering such characteristics as porosity, elastic foundation, varying thickness of plate or shell. In this regard, many scientists have devoted their research both to theoretical developments related to the construction of mathematical models [1-4] and to the implementation of experimental work [5, 6].
It can be noted, that in the manufacturing process porosities may arise in functionally graded structures. So, many researchers considered the influence of porosity while they were investigating mechanical, thermal, and other characteristics of FGM structures. Kim et al. [7] used the classical and first-order shear deformation theory to investigate buckling, bending and free vibration characteristics of porous FG plates, moreover the literature on vibration analysis of FGM plates resting on elastic foundation was reported by researchers in the last years and models based on Winkler and Pasternak interaction were considered. Yang and Shen [8] conducted vibration analysis of an initially stressed FGM plate resting on an elastic foundation. They used a simple power law for material gradation with clamped boundary conditions.
Investigations in the field of porous FGM plates and shells with variable thickness resting on elastic foundation are in demand now and they are still limited. Especially concerning the investigation of FGM plates and shells with a complex planform and different boundary conditions.

In this work, the R-functions method (RFM) and the variational Ritz method has been used to investigate the free vibration of porous FGMs plates and results are compared with finite element analysis using COMSOL Multiphysics. The study focuses on plates with various shapes and boundary conditions, considering elastic foundation effects.

For the case of plates and shallow shells of complex shape the difficulties are usually connected with the construction of an admissible functions system. These functions should be linearly independent, differentiable, form a complete system and satisfy the geometrical boundary conditions. Applying the R-functions theory we can construct a sequence of the basic functions. At first the corresponding solution structure is built as

$$\{U\} = \{B(P_1, P_2, ..., P_k, \omega, \omega_i)\}. \tag{1}$$

Here $\{U\}$ is a vector of displacements; $B$ is an operator depending on the system and its boundary conditions; $\omega(x, y) = 0$ is an equation of domain boundary; $\omega_i(x, y) = 0$ are equations of some parts of domain boundary; $P_k$, $k = \overline{1, N}$ are indefinite components. The equation of the domain boundary is constructed by the R-functions theory and the function $\omega(x, y)$ satisfies the following conditions:

$$\omega(x,y)>0,\quad \forall(x,y)\in\Omega,\qquad \omega(x,y)<0,\quad \forall(x,y)\notin\Omega,\qquad \omega(x,y)=0,\quad \forall(x,y)\in\partial\Omega, \quad (2)$$

According to the RFM indefinite components of solution structure are expanded into a truncated series with respect to a system of functions $\{\varphi_i(x,y)\}$:

$$P_k(x,y) = \sum_{i=1}^{N} a_i^{(k)} \varphi_i^{(k)}(x,y) \quad (3)$$

where $a_i^{(k)}$ are indefinite coefficients, taken by such a way that vector-function $\{U\}$ satisfies a given system of differential equations. These coefficients are determined by means of the Ritz method. For a complete system of functions $\varphi_i(x,y)$ power polynomials, Chebyshev's polynomials, trigonometric polynomials, splines and others can be used.

**Numerical results and discussions**

Consider a porous plate on elastic foundation with a variable thickness (Fig. 1) made of FGM (ceramics, top of the plate, and metal, bottom) with exponential variation of material property along thickness. To demonstrate the effectiveness of the proposed method and the correctness of the results obtained a validation study was carried out for square FGM plates for various cases with different parameters of porosity, volume exponent, elastic foundation, different types of FGM and boundary conditions.

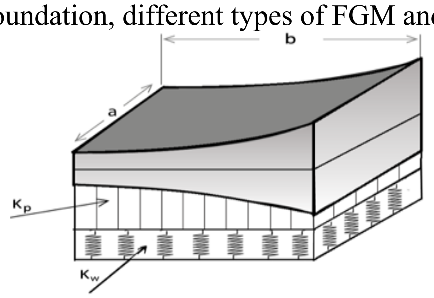


**Figure 1.** FGM plate on elastic foundation with variable thickness

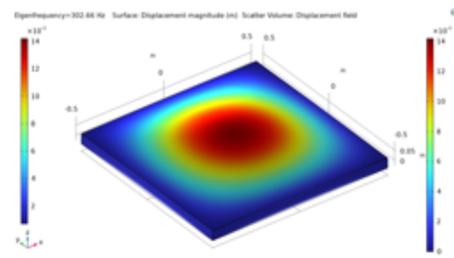

**Figure 2.** FEM results of simply supported $Al/Al_2O_3$plate (Table1)

Investigation of free vibration of a square FGM plate on elastic foundation made of Aluminum and Alumina ($Al/Al_2O_3$) without porosity ($\alpha = 0$) is conducted, see figure 2; mechanical properties are:

| | | | |
|---|---|---|---|
| $Al$ | E=70 GPa | $\nu = 0.3$ | $\rho = 2707\ kg/m^3$ |
| $Al_2O_3$ | E=380 GPa | $\nu = 0.3$ | $\rho = 3800\ kg/m^3$ |

Four different values of the volume exponent index p=0, 1, 2, 5 were considered in Table 1, where the comparison analysis with the results from work [9] and [10] are reported. In Table 2 are shown the results for an isotropic simply supported square tapered plate, and in Table 3 are shown the results for a square FGM $(Al/Al_2O_3)$ plate with different boundary conditions, gradient index, and uniform porosity parameters.

**Table 1.** Comparison of non-dimensional fundamental frequency $\hat{\lambda} = \omega \cdot a^2 \cdot h \cdot \sqrt{\rho_m/E_m}$ for simply supported (without porous) FG ($Al/Al_2O_3$) plates, $\frac{a}{b} = 1, \frac{h}{a} = 0.05$; $\rho_m, E_m$ are density and Young's modulus of metal (Aluminium)

| Kp | Method | p=0 | p=1 | p=2 | p=5 |
|---|---|---|---|---|---|
| 0 | **RFM** | **0.02909** | **0.02221** | **0.02019** | **0.01912** |
| | [9] | 0.0291 | 0.0222 | 0.0202 | 0.0191 |
| | [10] | 0.0291 | 0.0222 | 0.0202 | 0.0191 |
| | **FEM** | **0.02863** | **0.0219** | **0.0199** | **0.0187** |
| 100 | **RFM** | **0.04059** | **0.03780** | **0.03739** | **0.03766** |
| | [9] | 0.0406 | 0.0378 | 0.0374 | 0.0377 |
| | [10] | 0.0406 | 0.0378 | 0.0374 | 0.0377 |
| | **FEM** | **0.0383914** | **0.03523182** | **0.03466274** | **0.03472385** |

**Table 2.** Comparison of the fundamental frequencies $\Lambda = \Omega\,(2a)^2 \sqrt{\rho_m / E_m} / h_0$ for isotropic simply supported square tapered plate with different thickness and taper ratio

| Taper ratio $\beta$ | Method | $a / h_0$ =100 |
|---|---|---|
| **0.5** | **RFM** | **24.554** |
| | [9] | 25.0594 |
| | **FEM** | **21.57** |
| **1** | **RFM** | **29.193** |
| | [9] | 30.8965 |
| | **FEM** | **25.43** |

**Table 3.** Comparison of non-dimensional frequency parameter $\Lambda = \Omega\,(2a)^2 \sqrt{\rho_m / E_m} / h_0$ for square FGM $(Al / Al_2O_3)$ plate with different boundary conditions, gradient index and uniform porosity parameters $\frac{a}{h} = 20, \beta = 0.4$.

| | $p$ | Method | $\alpha = 0$ | $\alpha = 0.1$ | $\alpha = 0.2$ |
|---|---|---|---|---|---|
| SSSS | **3** | **RFM** | **9.406** | **8.7741** | **7.7039** |
| | | [9] | 9.4611 | 8.8289 | 7.7603 |
| | | **FEM** | **9.28** | **8.64** | **7.55** |
| | **5** | **RFM** | **9.1969** | **8.5106** | **7.2713** |
| | | [9] | 9.2501 | 8.5637 | 7.3255 |
| | | **FEM** | **9.23** | **8.53** | **7.25** |

## References


[1] Thai, H.T., Choi, D.H., 2013. A simple first-order shear deformation theory for the bending and free vibration analysis of functionally graded plates. Compos. Struct. 101, 332–340.

[2] Zenkour, A.M., 2018. A quasi-3D refined theory for functionally graded single-layered and sandwich plates with porosities. Compos. Struct. 201, 38–48.

[3] Swaminathan K, Naveenkumar DT, Zenkour AM, Carrera E. Stress, vibration and buckling analyses of FGM plates – a state-of-the-art-review. Compos Struct 2015; 120: 10-31.

[4] H.S. Shen, Functionally Graded Materials, Taylor & Francis CRC Press, Florida, 2009.

[5] Antonio Zippo, Giovanni Iarriccio, Francesco Pellicano, and Tetyana Shmatko Vibrations of Plates with Complex Shape: Experimental Modal Analysis, Finite Element Method, and R-Functions Method. Hindawi Shock and Vibration Volume 2020, Article ID 8882867, https://doi.org/10.1155/2020/8882867

[6] Emad Kadum Njim, Muhannad Al-Waily, Sadeq H. Bakhy A Review of the Recent Research on the Experimental Tests of Functionally Graded Sandwich Panels. Journal of Mechanical Engineering Research and Developments ISSN: 1024-1752 CODEN: JERDFO Vol. 44, No. 3, (2021) 420-441.

[7] Kim J., Zur K.K., Reddy J.N. Bending, free vibration, and buckling of modified couples stress-based functionally graded porous micro-plates. Compos. Struct. 209 (2019) 879-888.

[8] Yang, J., Shen, H.S., 2001. Dynamic response of initially stressed functionally graded rectangular thin plates. Compos. Struct. 54 (4), 497–508

[9] Kumar V., Singh S.J., Saran V.H., Harsha S.P. Vibration characteristics of porous FGM plate with variable thickness resting on Pasternak's foundation, European Journal of Mechanics/A Solids 85 (2021) 104124.

[10] Thai, H.T., Choi, D.H., 2012. A refined shear deformation theory for free vibration of functionally graded plates on elastic foundation. Compos. B Eng. 43, 2335–2347.

Professor **Ranjan Banerjee** received his Bachelor's and Master's degrees in mechanical engineering from the University of Calcutta (1969) and the Indian Institute of Technology, Kharagpur (1971) respectively. He joined the Structural Engineering Division of the Indian Space Research Organisation, Trivandrum and worked there for four years (1971-75) first as a Structural Engineer and then as a Senior Structural Engineer. He was involved in the research and development of multistage solid propellant rocket structures with particular emphasis on dynamic response. Later in the year 1975 he was awarded a Commonwealth Scholarship by the Association of Commonwealth Universities to study for a PhD degree at Cranfield University where he researched within the areas of structural dynamics and aeroelasticity. He completed his PhD in 1978. An important spin-off from his PhD work is the development of an aeroelastic package called CALFUN (CALculation of Flutter speed Using Normal modes) which has been extensively used as a teaching and research tool in aeroelastic studies.

Professor Banerjee joined the University of Cardiff as a Research Associate in 1979 and worked there for six years on vibration and buckling characteristics of space structures using the dynamic stiffness method. He worked in close collaboration with NASA, Langley Research Center, and was principally involved in the development of the well-established computer program BUNVIS (BUckling or Natural VIbration of Space Frames) which was later used by NASA and other organizations to analyse spacecraft structures. He was promoted to the position of Senior Research Associate in 1982.

Professor Banerjee joined City, University of London in 1985 as a Lecturer in Aircraft Structures. He was promoted to Senior Lectureship and Readership in 1994 and 1998 respectively. In March 2003 he was promoted to Professorship. He was elected to the EPSRC Peer Review College in 1996 and served until 1999, and was re-elected in 2002, and is currently serving in the College. He has been conducting research within the technical areas of structural dynamics, aeroelasticity and composite materials for well over40 years. To date he has published around two hundred and fifty papers in international journals and established conferences. In recognition of his research, he was awarded the degree of Doctor of Science (DSc) by City, University of London in 2017. Professor Banerjee is a Chartered Engineer and a Fellow of the Royal Aeronautical Society and the Institution of Structural Engineers and an Associate Fellow of the American Institute of Aeronautics and Astronautics.

Dipartimento Ingegneria Civile e Architettura

Università degli Studi di Catania, Italy

# Salvatore Caddemi, Ph.D.

Prof. Salvatore Caddemi is native of Noto (Siracusa), Italy, on 29th of November 1960. He received his master degree in Civil Engineering in 1984, served as Officer in the Italian Navy until 1986 and obtained his Ph.D. in Structural Engineering in 1990, from the University of Palermo.

His research activity in the period 1988-1991 has been developed at the "FRD/UCT Centre for Research in Computational and Applied Mechanics" of the University of Cape Town, South Africa, as "Visiting Researcher" and "Postdoctoral Research Fellow" contributing to theoretical advances in the integration of nonliner plastic constitutive laws and formulating iterative procedures for the relevant incremental analysis.

Prof. Caddemi was appointed Researcher of Mechanics of Materials in July 1991 at the Department of Structural and Geotechnical Engineering of the University of Palermo and was "Visiting Researcher" within the program HCM network of the European Community at the Department of Structural Engineering and Materials of the Technical University of Denmark in 1996.

In November 1998 he became associate professor of "Strenght of Materials" at the Institute of Structural Engineering of the Engineering Faculty of the University of Catania and since 1 october 2001 he is full professor at the Department of Civil and Architectural Engineering of the University of Catania where he is currently conducting his teaching and research activity.

His research interest has been oriented to deterministic analysis of elastic-plastic and no-tension material structures, stochastic dynamic structural analysis, structural and damage identification, static and dynamic analysis of structures with singularities, seismic vulnerability assessment of masonry structures.

Prof.Caddemi is currently involved in the use of generalised functions for the solution of direct and inverse problems of beam-like and frame structure in presence of strong discontinuites and singularities.

Dipartimento Ingegneria Civile e Architettura,

*Università degli Studi di Catania, Viale Andrea Doria 6, 95128, Catania, Italy*

DIPARTIMENTO INGEGNERIA CIVILE E ARCHITETTURA

UNIVERSITÀ DEGLI STUDI DI CATANIA

**Francesco Cannizzaro is native of Caltagirone (Catania), Italy, on 1st of September 1981. He received his master degree in Civil Engineering in 2007, and obtained his Ph.D. in Structural Engineering in 2011, from the University of Catania. His research activity was at first devoted to computational models of historical masonry constructions contributing with the introduction of a new element for modelling masonry vaults aiming at the enrichment of a modelling strategy based on a discrete macro-element approach. He spent part of his postdoc at the University of Minho at the Institute for Sustainability and Innovation in Structural Engineering (ISISE) as "Visiting Researcher", developing a strategy to numerically simulate the nonlinear behaviour of fiber-reinforced masonry structures. Among the other interests, he has been providing several contributions in the field of statics, stability and dynamics of discontinuous straight and curved beams as well as frames; in particular, exact closed form solutions have been proposed by making use of generalised functions to treat the discontinuities. Since March 2023 he is Associate Professor at the University of Catania in "Mechanics of Structures".**

**Dipartimento Ingegneria Civile e Architettura, Università degli Studi di Catania, Viale Andrea Doria 6, 95128, Catania, Italy**


**CV of Erasmo CARRERA, MUL2 Lab, Politecnico di Torino**

Dr Erasmo Carrera is Professor of Aeronautics and Astronautics at Politecnico di Torino. He acts as President of the Italian Association of Aeronautics and Astronautics, A.I.D.A.A and member of Accademia delle Scienze di Torino and Academie de l'Air et l'Espace.

He has been visiting professor at the University of Stuttgart, Virginia Tech, Royal Melbourne Institute of Technology, Tambov University, Supmeca and Ensam, PMU University.

Dr Carrera has been responsible for various research contracts granted by public and private national and international institutions, including the European Community, European Space Agency, Thales Alenia Space and Embraer. He is founder and Editor-in-Chief of Advances in Aircraft and Spacecraft Science, Editor-in-Chief of Mechanics of Advanced Materials Structures and Section Editor of Journal and Sound and Vibration

He has introduced the Unified Formulation, or CUF (Carrera Unifed Formulation), as a tool to establish a new framework in which to develop theories of beams, plates and shells for metallic and composite multilayered structures. He has been author and co-author of about 800 papers on the above topics. Carrera has been recipient of various 'best paper award' and of the 'JN Reddy Medal'.

In 2013 Professor Carrera has been Highly Cited Researchers (Top 100 Scientist) by Thompson Reuters in the two Sections: Engineering and Materials. He has been confirmed HiCI in 2015 in the Section Engineering. The only aerospace Engineering worldwide.

Due to his scientific outcoming professor Carrera has been recently awarded by the President of Italian Republic, as 'Honoray Commendator'.

He acts as Local Chair of IAC 2024 Milan and ICAS 2024 Florence. Chair of ISVCS 13 and Co-Chair of SSDM by ASME. Seebelow a picture with some of you at ISVCS 12.

**Weiqiu Chen** is the Qiushi Distinguished Professor at the Department of Engineering Mechanics as well as the dean of School of Aeronautics and Astronautics, Zhejiang University. He has engaged himself in mechanics of smart materials/structures, mechanics of soft materials and structures, and vibration/waves in structures for nearly thirty years. He has co-authored over 450 peer-reviewed journal articles and three English monographs. He now serves as the editorial member (or associate editor or associate editor-in-chief) of more than a dozen of academic journals including Mechanics of Advanced Materials and Structures, Journal of Zhejiang University – SCIENCE A, International Journal of Mechanical Sciences, Journal of Thermal Stresses, Composite Structures, Engineering Structures, Acta Mechanica Solida Sinica, and Applied Mathematics and Mechanics (English Edition).

## Piotr Cupiał

I graduated in 1987 in the field of applied and computational mechanics. I obtained my PhD from the Cracow University of Technology, in the field of the application of damping polymers in the vibration suppression of composite structures. Since March 2011 I have been a professor at the Faculty of Mechanical Engineering and Robotics of the AGH University of Science and Technology in Krakow.

During different periods of my scientific career my interests have included: the optimal design of structures subjected to non-conservative loading, vibration suppression of the vibration of composite plates through the use of polymer damping treatments, the dynamics of structures made of composite materials, the modelling of continua subjected to electromagnetic and thermal loading, and the analysis of piezoelectric structures and their use as smart materials. Recently, my main areas of interest have been the active control of rotors and the study of thermal shock in structural components.

During the years 2018-2022 I played an active role in the H2020 project “Feasibility study for employing the uniquely powerful ESS linear accelerator to generate an intense neutrino beam for leptonic CP violation discovery and measurement” (https://essnusb.eu/site/). I coordinated the activities of a work package, the aim of which was to propose a conceptual design of the target station to be used in the future ESSnuSB experiment.

For many years now I have served on the editorial board of the Journal of Sound and Vibration, I am a member of the editorial board of the Journal of Theoretical and Applied Mechanics. I am married to Gabriela and we have one son.

# Bio-sketch

**Hu Ding**, Ph.D.
Shanghai Institute of Applied Mathematics and Mechanics,
School of Mechanics and Engineering Science, Shanghai University
99 Shangda Road, Shanghai 200444, China
Email: dinghu3@shu.edu.cn
https://www.researchgate.net/profile/Hu-Ding-4

**Education:**

09, 1998 - 09, 2002 HeFei University of Technology, Bachelor Degree;
09, 2002 - 09, 2005 HeFei University of Technology, Master Degree;
09, 2005 - 03, 2008 Shanghai University, Doctor Degree: Mechanics;
04, 2012 - 04, 2013 University of Toronto, Visiting Professor;
09, 2016 - 03, 2017 Duke University, Visiting Scholar;
10, 2018 – 10, 2018 University of Technology Sydney, Visiting Scholar.

**Conducted research activities and research interests:**

The nonlinear vibration characteristics of elastic structures, especially the fluid-conveying pipes, and the research of vibration energy regulation and vibration control based on nonlinear dynamic design, especially the dynamic design and application of nonlinear energy sinks.

**Message:**

I'm 45 years old. I have been engaged in scientific research for 18 years since pursuing a doctoral degree. I guess I like this job. Although I paid a lot of price, including a lot of gray hair, a lot of hair loss, frequent shoulder and neck pain... Although I still don't understand what academic achievements are the most valuable... I guess I like this job. I'll keep scratching my head and thinking, hoping for an Epiphany one day.

A photo from ISVCS10 in Colorado in 2015:

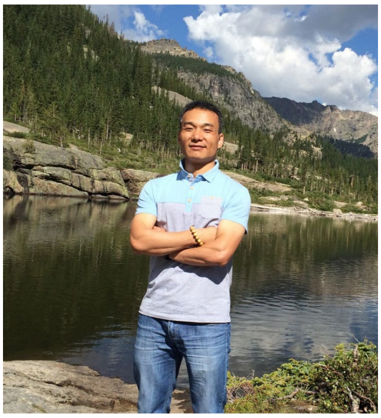

**Technion - Israel Inst. of Technology - Faculty of Civil Engineering**

# Moshe Eisenberger

July 2023

**Degrees**

| | | |
|---|---|---|
| B.Sc. | Civil Engineering, Technion, Haifa | 1977 |
| M.Sc. | Civil Engineering, Stanford University, USA | 1978 |
| Engineer | Civil Engineering, Stanford University, USA | 1979 |
| Ph.D. | Civil Engineering, Stanford University, USA | 1980 |

**Academic Appointments**

| | | |
|---|---|---|
| Lecturer | Civil Engineering, Technion, Haifa | 1980 |
| Senior Lecturer | Civil Engineering, Technion, Haifa | 1985 |
| Tenure Senior Lecturer | Civil Engineering, Technion, Haifa | 1987 |
| Associate Professor | Civil Engineering, Technion, Haifa | 1993 |
| Professor | Civil Engineering, Technion, Haifa | 2003 |
| Professor Emeritus | Civil Engineering, Technion, Haifa | 2020 |

**Publications and Supervision of Graduate Students**

Published over 100 Journal papers and 100 Conference papers

Supervised 32 Ph.D. and MSc. Students

**Research Interests**

Main area is applied and computational mechanics including static, dynamic, and stability analysis of structures. In the last 20 years I have been working on Dynamic Stiffness Analysis of various elements. Recent years were devoted to the exact solution for plate and shell vibrations.

**Personal Interests**

I am an active cyclist both road and mountain, and hiker. In the last years before retirement I was on sabbatical leave in Argentina and Brazil.

***Mark S. Ewing***
***University of Kansas***

***I grew up interested in science and mathematics, largely due to my fascination with the spacecraft I used to watch as they were launched from nearby Cape Canaveral. I was "energized" for science when I attended a National Science Foundation summer school at Rollins College in the summer of 1966. The next year, I was energized for engineering when I attended the JETS summer program at the University of Illinois. In 1972, I received my BS in Engineering Mechanics from the U.S. Air Force Academy, then began a 20-year career in the Air Force. I served for four years in turbine engine stress and durability analysis where I was an "early" user of finite element analysis for hot, rotating turbomachinery. I then served a two-year assignment in turbine engine maintenance and support, which was less technical, but eye-opening. During these early years—and in my spare time—I earned an MS in Mechanical Engineering from Ohio State University.***

***With an MS in hand, I returned to the Air Force Academy to serve on the faculty as an Assistant Professor. After two years, I returned to Ohio State to complete a PhD. As a student of Art Leissa's, I focused on the combined bending, torsion and axial vibrations of beams, thereby establishing my interest in the vibrations of continuous systems.***

***After returning to and teaching at the Air Force Academy for six years, I was assigned to the Air Force Flight Dynamics Lab, where I worked on two interesting projects. The first was the development of a structural design algorithm capable of, among other things, "maximizing" the separation of two natural frequencies in a built-up structure. The utility of this endeavor was to allow the design of aircraft wings for which the bending and torsional natural frequencies are sufficiently separated (in frequency) to avoid flutter. The other interesting project was the analysis of the effect of convected aerodynamic loads on a missile.***

***I am now on the Aerospace Engineering faculty at the University of Kansas. My current research interests are in structural dynamics and structural acoustics, the latter of which is a topic of increasing interest to aircraft manufacturers. In recent years, I have focused on the ability to analyze, design and measure structural damping for built-up fuselage structures. All of the test articles I've used to validate my work through experimentation are simple structural elements, namely beams and plates.***

***I have a great love of the outdoors, and of the mountains in particular. When Art Leissa asked me to help organize the first International Symposium on Vibrations of Continuous Systems, and he told me he wanted to meet in the mountains, I was really excited. I look forward to attending the Symposium this year after a six year absence.***

# Biographical Information

**MUL2, Department of Mechanical and Aerospace Engineering**
**Politecnico di Torino,**
**Corso Duca degli Abruzzi 24, 10129 Torino, Italy**
**matteo.filippi@polito.it**

**Matteo Filippi** is an Assistant Professor at Politecnico di Torino, where he received a Bachelor's degree in Aerospace Engineering in 2009, followed by a Master's degree in 2011. He subsequently obtained his Ph.D. from the same university in 2015.
His research primarily focuses on the development of high-fidelity finite elements for stress and dynamic analyses of structures made of advanced materials, axial rotors, and rotary-wing configurations, as well as coupled thermoelastic formulations and geometric and dynamic stability analyses. Matteo has co-authored more than 70 scientific papers on these topics, which have been published in peer-reviewed international journals.

## Peter Hagedorn

Peter Hagedorn was born in Berlin, Germany. He grew up in Brazil, where he graduated (Engineer's degree) in mechanical engineering in 1964 at EPUSP and in 1966 earned his doctoral degree at the same University. He then worked as a research assistant and later as 'dozent' (similar to lecturer) at the University of Karlsruhe, Germany. In 1971 he got his 'habilitation' (similar to Dr. Sc.) at Karlsruhe. From 1973 to 1974 he was a visiting Research Fellow at the Department of Aeronautics and Astronautics, Stanford University. Since October 1974 he is full professor of mechanics at the Technische Universität Darmstadt and head of the Dynamics and Vibrations group. He also has served as visiting professor at Rio de Janeiro (Brazil), Berkeley, Paris, Irbid (Jordan) and Christchurch (New Zealand), where he also holds an Adjunct Professorship at UCC. He has served as Head of Department and Vice-President to his home University in Darmstadt and he is serving in a number of professional and editorial committees. He is author of over 200 papers and several books on a variety of topics in the general field of dynamics and vibrations and analytical mechanics. He is officially retired since 2009 but still quite active and heads the Dynamics and Vibrations Group, presently affiliated to the chair of professor Michael Schäfer, at the graduate school of computational engineering of TU Darmstadt.

.

**Name:** Marwan Hassan, PhD
**Current Position:** Professor
University of Guelph
Guelph, Ontario, Canada
**Contact Information**
Email: mahassan@uoguelph.ca

**Biography:** Marwan Hassan is a professor of Mechanical Engineering, University of Guelph, Canada. Professor Hassan's main area of expertise is the flow-induced vibrations. His work has contributed significantly to the design and enhance reliability of nuclear power plants components. Professor Hassan is a member of the Canadian Society for Mechanical Engineers, the Canadian Nuclear Society, and a fellow of the American Society for Mechanical Engineers. He has over 25 years of experience in the area of Dynamics, finite element analysis, Fluid-Structure Interaction, and active Vibrations Controls. He was involved in investigating several nuclear power plants in Canada and around the world and worked with nuclear industrial partners such as The Canadian Nuclear Safety Commission, the Atomic Energy Canada Ltd, and Ontario Power Generation.

**Bin Huang** is currently an Associate Professor of Faculty of Mechanical Engineering & Mechanics at Ningbo University. He received a B.S. in Mechanical Engineering and Automation at Tianjin Polytechnic University (2006), and a Ph.D. degree in Vibration Control and Automation at Dongguk University-Seoul (2015). His current research interests include piezoelectric theories and devices, mechanics of composite materials, vibration and control of smart materials and structures. His research work has been supported by several research projects including the National Natural Science Foundation of China and high-tech enterprises. He has won the Best Paper Award twice in the international conferences and has published more than 50 peer-reviewed academic papers.

## Sinniah Ilanko, The University of Waikato/Te Whare Wananga o Waikato

Ilanko was born in the north of Sri Lanka (Jaffna), and according to the common Tamil practice, he does not have/use a family name. Ilanko is his given name and Sinniah is his late father's given name, and conveniently remains informal as 'Ilanko'.

He graduated from the University of Manchester (U.K) with a BSc in civil engineering and also obtained an MSc from the same university under the supervision of late Dr S.C. Tillman, investigating the effect of initial imperfections on in-plane loaded rectangular plates. He commenced doctoral studies at the University of Western Ontario under the supervision of Professor S.M. Dickinson, continuing on the same topic. Soon after completing his PhD, he worked as a postdoctoral fellow at the UWO briefly before joining the University of Canterbury (NZ) in 1986. He continued his academic career at Canterbury for nearly 20 years, in various positions, as lecturer, senior lecturer and associate professor until he joined the University of Waikato in 2006. In 2012 he became a full professor. He has served as the Chairperson and later the Head of School of Engineering from January 2013 to December 2015. He has also previously served as the Head of Mechanical Engineering Department at Canterbury (2001-2202).

His research areas include vibration and stability of continuous systems, numerical modelling and adaptive mechanisms. His most recent research projects include active control for adaptive stiffness foundations for earthquake isolation and crack detection using frequency measurements in structures with roving test bodies possessing rotary inertia. He has published 46 journal papers and in 2014 authored a book "The Rayleigh-Ritz Method for Structural Analysis" jointly with Dr Luis Monterrubio and Dr Yusuke Mochida. He has served as the Subject Editor for Journal of Sound and Vibration (2009-2020), for analytical methods for linear vibration and since 2021 he has been serving as Receiving Editor and a Deputy Editor-in-Chief. He has secured two major grants, a Marsden grant for research into vibration analysis of complex structures and a grant by the New Zealand government's Ministry of Business Innovation and Employment (Category Smart Ideas) to conduct research on the development of an omnidirectional base isolator.

His current research topics include adaptive vibration isolation from vertical seismic excitation and crack detection. He is also interested in computer-aided learning and has developed and used several interactive lectures and tutorials for teaching Mechanics of Materials and Vibration, as well as computer-based interactive tutorials and games for learning/teaching Tamil language. He us married to Krshnanandi, and they have two children and a grandson. In his past time, he enjoys spending time with his family, gardening, and cooking.

Dr. **Jiaqing Jiang** received his Bachelor's degree in civil engineering from Zhejiang University (2014) and Master's degree in earthquake engineering from Imperial College London (2015). He worked on pedestrian-induced force measurement using smart phone and sympathetic vibration attenuation algorithms between crowds and the bridge at that time. He then completed his Ph.D. in 2022. His work is about developing a new mixed finite element method for composite structures, which provides very accurate stress distributions results for multilayered beams, plates and shells. He was rewarded as a three-good student in Zhejiang University and got certificate of distinction from ICL.

He is now a post-doctoral fellow in Zhejiang University under the guidance of Prof. Weiqiu Chen. His research field contains active control methods for piezoelectric metamaterials and deep-learning based optimization algorithms for acoustic cloaking designs. He has published 4 articles in international journals and 1 article for international conference.

## Bio-sketch of Professor Jin-Wei Liang

Jin-Wei Liang accepted his Ph.D. degree in the field of Mechanical Engineering from Michigan State University on 1996. He is currently serving as a professor for the Department of Mechanical Engineering at Ming Chi University of Technology (MCUT), New Taipei City, TAIWAN. He served as the Dean of the College of Engineering, MCUT from 2008-2022. He was also a Distinguish Professor from 2020-2022. His primary research interests include linear/nonlinear vibrations and intelligent control problems.

Professor Jin-Wei Liang is the co-founder of Perseverance Technology Co. Ltd., a start-up company initiated in TAIWAN. He has published about 40 technical papers. Recently, he leads a research team in studying prognosis problem of rotary machines in chemical industry. He was interviewed by “Impact” magazine (www.impact.pub) for the outstanding effort put in handling the industry-based problems.

Title: Ph.D., Professor
Affiliation: Central South University
Address: High-speed train research center,
Central South University, Changsha, Hunan
Phone: +86 138 7314 4366
*E-mail: xiangliu@csu.edu.cn*
URL: https://faculty.csu.edu.cn/liuxiang/en/index.htm

Dr. **Xiang Liu**'s research interests include noise and vibration control in transportation, structural dynamics and instabilities, aeroelasticity, etc. He studied for his Bachelor (civil engineering), Master and PhD (road and railway engineering) in Central South University, another PhD in applied mathematics from University of Glasgow (UK) and then worked as Research Fellow in structural dynamics in City, University London and then Professor in School of Traffic & Transportation Engineering of Central South University in 2017. Dr. Liu serves as the editor board member of 5 scientific journals, regular reviewer of over 40 journals, has published over 90 papers in international journals and conferences and 16 authorized patents. Recently, he has been granted 16 grants, summing up to 15+ million RMB.

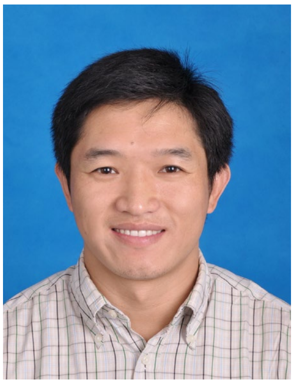

Dr. **Chaofeng Lü** is currently the Vice President and Pao Yue-Kong Distinguished Professor of Ningbo University. He received his Bachelor’s degree and Ph.D. degree in civil engineering from Zhejiang University in 2001 and 2006. Dr. Lü joined College of Civil Engineering and Architecture, Zhejiang University as an Assistant Professor in 2006, and promoted to Associate Professor in 2008 and full Professor in 2013. During this period, he jointly worked as a Research Fellow in City University of Hong Kong from 2007 to 2009, Visiting Scholar in Northwestern University from 2010 to 2012 and Pao Yue-Kong Visiting Professor in 2015. Since January 2022, Dr. Lü has been appointed as the Vice President of Ningbo University, and the Director of Center for Mechanics Plus under Extreme Environments.

Dr. Lü's research interests include mechanics of smart materials and structures, flexible and stretchable intelligent devices, self-assembly of materials, and mechanics of materials under hypergravity conditions. He has co-authored over 120 refereed international journal articles and 50 international conference papers, which have received more than 6200 self-excluded independent SCI citations with an H-index 35. His recent awards include the Elsevier Highly Cited Chinese Researchers (2020, 2021), NSFC Distinguished Young Scientist (2019), Changjiang Scholar Young Scientist (2017), National Natural Science Award (2015), NSFC Outstanding Young Scientist (2013), and MOE Natural Science Award (2012). He is now the Director of the Electronic and Electromagnetic Devices Mechanics Division of CSTAM, the Editorial Board member of Mechanics of Advanced Materials and Structures, Forces in Mechanics, Sensors, Materials, and Journal of Zhejiang University A – Science.

**Bio-sketch of Dr. Yunhua Luo**

Dr. Luo obtained his doctoral degree in Solid Mechanics (specialized on finite element method) from the Royal Institute of Technology, Sweden. Since then, Dr. Luo worked in Karlsruhe University (Germany) and Rensselaer Polytechnic Institute (USA). He joined the University of Manitoba in 2006 and became a full professor in 2019.

With a passion for teaching and research, Dr. Luo has dedicated his efforts to the finite element method and its applications in solving a wide range of engineering problems. For more than 15 years, he has instructed undergraduate and graduate courses on finite element analysis. His research interests encompass various areas, including the advancement of finite element approaches and algorithms, the study of bone strength and hip fracture prediction, brain injury and prevention, micromechanics of composite materials, design and analysis of functionally graded materials, and the nonlinear and dynamic behavior of materials and structures.

Dr. Luo's research endeavors have been supported by esteemed organizations, including the Natural Sciences and Engineering Research Council (NSERC), the Canadian Institutes of Health Research (CIHR), Mitacs, Research Manitoba, and the Manitoba Medical Service Foundation (MMSF). His significant contributions have been disseminated through the publication of two monographs and approximately 120 peer-reviewed papers.

Recognized as a mentor and supervisor, Dr. Luo has successfully guided over 50 high-quality personnel (HQP), including postdoctoral fellows, PhD, MSc/MEng, and undergraduate students, fostering their development and scholarly growth.

In addition to his research and teaching commitments, Dr. Luo has served on various committees at the faculty and department levels. His involvement includes contributions to tenure and promotion committees, graduate and undergraduate scholarships and awards committees, and his current position as Chair of Graduate Studies within the department.

# Brian Mace

I am currently Emeritus Professor in the Department of Mechanical and Mechatronics Engineering at the University of Auckland, having been Professor there since 2011. Prior to that I was Professor of Structural Dynamics at the Institute of Sound and Vibration Research (ISVR), University of Southampton.

I graduated MA (Hons) in Engineering Science and subsequently DPhil (1977) from the University of Oxford. Following that I was Research Fellow at the ISVR (1977-1980), Lecturer in the Department of Civil and Structural Engineering, University College, Cardiff, Wales (1980-1983) and then moved to the University of Auckland, returning in 2000 to the ISVR.

My general research interests concern structural dynamics, waves in structures, vibrations, acoustics and smart structures. More specifically they include uncertainty modelling and wave-based approaches, particularly regarding noise and vibration behaviour at higher frequencies. A strong interest concerns wave motion in structures, including periodic structures and acoustic metamaterials. A significant amount of current work concerns a hybrid wave and finite element (WFE) method for structural dynamic and acoustic analysis and a hybrid FE/WFE method for prediction of transmission through joints. Applications include noise and vibration in buildings, tyre noise and vibration, composites, rail vehicles etc. Recent activity also includes vibrations of complex, built-up structures such as cars, aircraft etc., when data uncertainty and product variability become important. Modelling the uncertainty is an important part of the virtual design process, but computational cost and model size are real problems. Here my research concerns energy approaches and methods based on component mode synthesis. Other interests include smart structures for noise and vibration control, air- and structure-borne noise in buildings and active noise and vibration control.

Interests outside work include fishing, bridge, golf, walking and doing what my wife Gwyneth tells me to do in the garden.

# YUSUKE MOCHIDA

**University of Waikato**
**Te Whare Wananga o Waikato**
**Hamilton, New Zealand**
yusuke@waikato.ac.nz

I am currently working at the University of Waikato in New Zealand. The overall aim of my current research is to develop a vibration isolator for earthquake protection and non-destructive testing method using frequency measurements. The methods under consideration includes the use of the concept of pseudo-zero/negative stiffness mechanism, and natural frequency shifts by roving mass with rotary inertia.

I was born and grew up in Japan. After I graduated with a B.E. in Mechanical Engineering from the Tokyo Metropolitan University (Japan) I worked for a while in Japan and went to New Zealand as a working holiday maker to travel around and work. Actually I was away from the engineering field for several years. This made me miss engineering and so after learning English, I enrolled in a Postgraduate Diploma programme at the University of Canterbury (New Zealand). During my postgraduate study I became interested in vibration and decided to continue towards an M.E. under the supervision of Professor Ilanko, who had at this time relocated to the University of Waikato. I completed my M.E. and then continued working towards a Ph.D at the same university. Since commencing my M.E. studies I have developed several codes based on the Superposition Method, the Rayleigh-Ritz Method and the Finite Difference Method to solve free vibration problems of plates and shells using MATLAB. I was also involved in research on the development of analytical procedure for vibration analysis of complex structures using the concept of negative structures, and structural health monitoring using frequency measurement. In addition to my research experience, I have been lecturing in Dynamics and Mechanisms, Vibration, Mechanics and Finite Element Analysis classes.

Through my career, I hope I can contribute to the development of research relationships between New Zealand and other countries, especially Japan, and the advancement of research in New Zealand.

Personally, I am also interested in snowboarding, golf, playing drums, Shorinji Kempo (Japanese martial arts), foreign exchange, personal development and cooking.

# Yoshi (Yoshihiro Narita)

Hokkaido University (Prof. Emeritus), Sapporo, Japan

I am a retired professor of Mechanical Engineering at Hokkaido University (HU) and other institutions. I started my research on vibration of continuous systems when I was a PhD student under adviser Prof. Irie of HU in 1976, and had a chance to study one year in 1978-1979 under Prof.Leissa at the Ohio State University. I have attended all the ISVCS's except for only once. I am very delighted to see old and new friends in Canada.

Let's enjoy!

<career>

| | |
|---|---|
| 1951 | Born in Sapporo, Japan (now, age 72) |
| 1980 | PhD Hokkaido University |
| 1980-2004 | Hokkaido Institute of Technology (Sapporo) |
| 2004-2017 | Hokkaido University (Sapporo) |
| 2017-2020 | JICA (Japan Intl. Corp. Agency) advisor for universities in east Indonesia |
| 2020-2023 | Yamato University (Osaka) |
| 2023-present | Board chairman of Hokkaido Lutheran Institution (four kindergartens) |

**Alfonso Pagani** serves as associate professor of spacecraft structures at the Department of Mechanical and Aerospace Engineering, Politecnico di Torino. He obtained a Ph.D. in Aerospace Engineering from City University of London in 2016 and, prior to that, a Ph.D. in Fluid-dynamics (Aeroelasticity) from Politecnico di Torino.

As an active fellow of the Italian Association of Aeronautics and Astronautics (AIDAA, www.aidaa.it), which is a distinguished founding member of the International Astronautical Federation (IAF) and the hosting organization of IAC 2024, dr. Pagani holds several significant responsibilities. These include being AIDAA's IAF delegate, chair of the European research actions initiative, and invited member of the AIDAA Governing Board.

Alfonso Pagani is associate editor for Advances in Aircraft and Spacecraft Structures and the International Journal of Dynamics and Control. He conducts his research on structures, space mechanisms and advanced materials mechanics at the MUL2 Lab (www.mul2.com). His scholarly pursuits encompass a broad spectrum of fundamental and applied studies, having forged numerous fruitful collaborations with international organizations and industry. Recognizing his contributions to the field, he has indeed garnered several prestigious awards, including a Wiley Best Paper Award in 2023 and the Ian Marshall's Award in 2013.

Dr. Pagani is the PI of the EU-H2020 ERC-StG project PRE-ECO, which aims to explore a novel approach to addressing the challenges associated with the design of variable stiffness structures for aerospace applications (www.pre-eco.eu). Additionally, he is the deputy for Spoke 8 in the Extended Partnership "Space It Up!", a program funded by the Italian Space Agency that focuses on advancing human and robotic space exploration.

Previously, in 2018, Alfonso joined the California Institute of Technology as a visiting associate to study deployable space booms. He also spent research periods at various institutions, including Purdue University in 2016, where he explored the micro-mechanics of fibre-reinforced composites. In addition, he conducted research at RMIT Melbourne in 2014 and at Universidade do Porto in 2013.

# Biography

# of Francesco Pellicano

Francesco Pellicano is Aeronautical Engineer and Ph.D. in Theoretical and Applied Mechanics, he is currently Full Professor, Head of the Centre Intermech MoRe and was committee president of 2 BsC and 2 MsC programmes. He was coordinator (PI or local) of several projects: COMETA, NATO (composite metamaterials), METaGEAR POR-FESR (Gears, Materials, Robotics), INDGEAR, EU-Fp7 (condition monitoring) and HPGA Fortissimo, EU-Fp7 (applications of high performance computing). He published 2 Books, more than 80 Journal papers and more than 100 conference papers. Bibliometry: 176 papers on Scopus, h-index 36, more than 3000 citations.
His research activities are:
Fluid-structure interaction: cooperating with Prof. Amabili and Païdoussis developed models for vibration and stability analyses of shells interacting with incompressible heavy fluids, compressible and supersonic fluids; recently interactions with non-Newtonian fluids were investigated.
Gear stress and vibration modelling and testing, the research was focused on vibration aspects of gears including non-smooth dynamics and chaotic vibration, optimization using Genetic Algorithms, Diagnostics and Prognostics.
Vibration control using active passive techniques: active control through piezo-electric actuators, active control of suspension through variable stiffness for earthquake applications; linear and nonlinear dynamic absorbers and applications to railways bridges; quasi-zero stiffness suspension for earthquake applications; origami isolators and applications to automotive.
Shell dynamics and stability: modal interactions, nonlinear random responses and synchronization phenomena, thermal effects and their impact on the dynamic scenario.
Vibration of carbon nanotubes: development of new continuous shell models for investigating the vibration characteristics of single and multiwalled nanotubes considering size effects and van der Waals interactions.

**Silvio Sorrentino**

**Associate Professor in Mechanics of Machines**

**University of Modena and Reggio Emilia**

Master Degree in Mechanical Engineering at the *Politecnico di Torino* (I). PhD in Mechanics of Machines at the *Politecnico di Torino*, Department of Mechanics. Certificate in Advanced English at the *University of Cambridge* (UK).

Research Associate at the *University of Sheffield*, Sheffield (UK), Department of Mechanical Engineering (2003-2004). Research Associate at the *Georgia Institute of Technology*, Atlanta (USA), Institute of Aerospace, Aeronautical and Astronautical Engineering (2004).

Research Associate at the *University of Bologna*, Department of Mechanical Engineering (2005-2010), lecturing on Mechanics of Machines (2006-2010).

Assistant Professor in Mechanics of Machines at the *University of Modena and Reggio Emilia* (I), Department of Engineering *Enzo Ferrari* (2010-2016). Since 2016 Associate Professor in Mechanics of Machines at the *University of Modena and Reggio Emilia*, Department of Engineering *Enzo Ferrari*, lecturing on Vehicle Mechanics (2016-present) and Vehicle Dynamics (2011-present).

Research topics: (1) identification methods from vibration data (output-only methods, subspace stochastic methods); (2) vibration analysis of viscoelastic models (general damping distributions, fractional derivative models with analytical developments and experimental validation); (3) dynamics of oleohydraulic systems coupled with mechanical systems (non-newtonian fluids); (4) dynamic behaviour of structures with travelling loads (deterministic, stochastic); (5) wave propagation in solid structures (catenary-pantograph problem); (6) dynamic analysis of plates (coordinate mapping, homogenization of periodic lattices); (7) rotor-dynamics (distributed parameter and finite element modelling, stability analysis of parametrically excited rotors); (8) vehicle dynamics (motorcycle stability, self-excited oscillation analysis).

Coordinator of the Corsi di studio in Ingegneria Meccanica (Laurea L-9 and Laurea Magistrale LM-33) at the Department of Engineering *Enzo Ferrari* of the University of Modena and Reggio Emilia (November 2019 – present).

Awarded the *Premio Scientifico 'Francesco Masi'* by the University of Bologna in 2009.

Prof. Yury Vetyukov

Biosketch

Yury Vetyukov studied applied mechanics at St. Petersburg State Polytechnical University, Russia and graduated in 2000 with distinction. His master thesis was devoted to large spatial deformations of thin curved rods. As a doctoral student of the same university he studied self-excited axial-torsional vibrations of rotating drillstrings at deep oilwell drilling and obtained his PhD in 2004. Between 2002 and 2004 he worked as a research assistant at the Johannes Kepler University Linz, Austria. From 2004 until 2008 he was an assistant professor in St. Petersburg. Here he started his career as a university teacher and independent researcher, focusing on nonlinear mechanics of thin-walled structures (elastic shells, rods and thin-walled rods). In 2008 he returned to Linz as a post-doctoral researcher and stayed there until 2015, working in various basic and industrial research projects. A monograph entitled "Nonlinear mechanics of thin-walled structures: asymptotics, direct approach and numerical analysis" was published by him in 2014 at Springer. Since 2015 Yury Vetyukov is working at the Institute of Mechanics and Mechatronics at Technische Universitaet Wien (formerly known as Vienna University of Technology), Austria. Here he received his venia docendi in 2017. Having started as a post-doctoral researcher, in 2021 he was appointed as a full university professor and is currently the head of division of mechanics of solids.

Research interests of Yury Vetyukov comprise various aspects of structural mechanics and thin-walled structures. He actively puts into practice analytical methods based on direct tensor calculus, asymptotic techniques and analytical mechanics. Problem specific novel numerical approaches also stay in the focus of his basic and applied research. In the recent years, he mainly deals with axially moving structures such as flexible belts, elevator cables or moving metal sheets during forming processes. Nonlinear effects of material inelasticity, various contact phenomena and dynamics along with the motion of the structure across various qualitatively different domains make respective problem formulations often inaccessible for conventional methods of analysis or by means of commercial software. Along with several novel analytical solutions, Yury Vetyukov and his colleagues are developing problem-specific numerical approaches featuring non-material kinematic description in the framework of mixed Eulerian-Lagrangian formulation.

## Professor Ji Wang, Ningbo University, China

**Professor Ji Wang** has been a Qianjiang Chair Professor of Zhejiang Province at Ningbo University since 2002. He also served as Associate Dean for Research and Graduate Study, School of Mechanical Engineering and Mechanics, Ningbo University, from 2013 to 2019. Professor Ji Wang is the founding director of the Piezoelectric Device Laboratory, which is a designated Key Laboratory of City of Ningbo. Professor Ji Wang was employed at SaRonix, Menlo Park, CA, as a senior engineer from 2001 to 2002; NetFront Communications, Sunnyvale, CA, as senior engineer and manager from 1999 to 2001; Epson Palo Alto Laboratory, Palo Alto, CA, as Senior Member of Technical Staff from 1995 to 1999. Professor Ji Wang also held visiting positions at Chiba University, University of Nebraska-Lincoln, and Argonne National Laboratory. He received his PhD and Master degrees from Princeton University in 1996 and 1993 and a bachelor's degree from Gansu University of Technology in 1983. Professor Wang has been working on acoustic waves, high-frequency vibrations of elastic and piezoelectric solids for resonator design and analysis, and nonlinear analysis of vibrations with several US and Chinese patents, about 240 journal papers, and frequent invited, keynote, and plenary presentations in major conferences around the world. He has been board member, advisor, and consultant to many leading companies in the acoustic wave device industry. Professor Wang has been a member of many international conference committees and currently serving the IEEE UFFC Technical Program Committees of the Frequency Control and Ultrasonics Symposia, the IEEE MTT-S, and the IEC TC-49. He is also the funding chair of Committee on Mechanics of Electronic and Magnetic Devices, CSTAM, and the SPAWDA. From 2015, Profess Wang was the editor-in-chief of *Structural Longevity* and members of the editorial boards of several international journals.

**Andrew Watson**

**Lecturer of Aerospace Structures**

**Department of Aeronautical and Automotive Engineering**

**Loughborough University, United Kingdom**

Andrew obtained his undergraduate and higher degrees from Cardiff University. His PhD looked at the stability analysis and optimisation of light weight structures. After two post-doctoral appointments at Cardiff Andrew joined Loughborough University as a member of academic staff in 2004.

His research includes buckling and postbuckling of aerospace panels and vibration of Timoshenko beams. Buckling and vibration problems can be approached by using the Dynamic Stiffness Method along with the Wittrick-Williams algorithm. Vibrating structures can be modelled as quantum graphs and Andrew is currently researching higher order graphs to obtain the spectral results of tree shaped graphs all using the DSM.

Outside of this research Andrew has been looking at fossil fuels and other finite resources. To facilitate this he is developing analytical methods to optimise structures where the objective function can be mass, energy costs or environmental degradation. Jaguar Land Rover are funding a research studentship looking at thermal management of electric vehicles.

In his spare time he likes to keep up with current affairs and enjoys walking and swimming.

**Brief CV Shudong Yu**

Shudong Yu received his bachelor's degree 1982 from Jiangxi University of Technology (Mechanical Engineering), master's degree in 1984 from Northeastern University (Applied Mechanics), and PhD degree in 1995 from University of Toronto (Mechanical Engineering).

He studied the method of superposition and its applications to vibrations of plates and shells as a research associate at University of Ottawa under Professor D.J. Gorman during 1988-1989. He worked as a nuclear fuel design engineer for Atomic Energy of Canada Limited (AECL) during 1994-1997. He joined Ryerson University (Mechanical Engineering) in 1997, and held assistant professorship (1997-2004), associate professorship (2004-2009), and full professorship (2009-present).

Dr. Yu's research areas are structural dynamics, chaos and bifurcations, and fluid dynamics. He has published over 62 papers in recognized scientific and technical journals, and presented 87 papers at various technical conferences. He authored and co-authored 47 technical reports, resulted from the industrial projects.

Dr. Yu is a fellow of Canadian Society for Mechanical Engineering (CSME). He served as Vice President for CSME Ontario during 2002-2009.

Professor **Antonio Zippo** is a mechanical engineer with PhD in "Advanced Mechanics and Vehicle Techniques", he is currently an Associate Professor of Mechanism and Machine Theory, Applied Mechanics and Mechanical Vibration since 1 June 2023 at "Enzo Ferrari" Department of Engineering, University of Modena and Reggio Emilia - UNIMORE.

He has received the following funding for research activities:

- FAR2022 - Identification, modelling and analysis of nonlinear EMG signals of pathological tremor - University Research Fund 2022 for financing departmental development plans in the field of research. 27/07/2022 €10,000
- Funding from CONSORZIO FUTURO IN RESEARCH for research on "MODELLING AND EXPERIMENTAL MEASUREMENTS OF NON-LINEAR COMPLEX SYSTEMS AIMED AT THE ACTIVE CONTROL OF ESSENTIAL AND PARKINSONIAN TREMOR" 01/05/2022 €30870
- Project "International Higher Education School in NVH for Industry 4.0 Higher Education school in NVH for Industry 4.0" from 22/11/2021 to 31/12/2023 13750 €
- Individual funding of 3000€ for basic research activities REFERRED to ARTICLE 1, PARAGRAPHS 295 AND FOLLOWING OF LAW NO. 232 OF 11 DECEMBER 2016

He has participated in various international, European and national research projects:

- 2019 “DiaPro4.0 Diagnostic-Prognostic multi-sensor cost-effective system integrated in mechanical drives of Industry 4.0”, POR-FESR 2014-2020ER
- 2018 “Omnidirectional earthquake isolation system”, Ministry of Business, Innovation & Employment (New Zealand);
- 2016 "Integrated platform for the design and advanced production of industrial gearboxes - MetAGEAR" (PG/2015/732270) POR-FESR 2014-2020ER
- 2014 “FORTISSIMO, Experiment: HPGA”, FP7 (applications for high performance computing);
- 2013 INDGEAR, FP7-SME (condition monitoring);

He teaches the courses of multibody dynamics in the master's degree course in mechanical engineering (industry 4.0 curriculum), Mechanical Vibration in the master's degree course Advanced Automotive Engineering and Mechanics of the Vehicle in the bachelor’s degree course in vehicle engineering.

He have published 16 articles in international journals, 54 articles for international conferences and 1 book chapter and received the national scientific qualification Settore Concorsuale 09 / A2-II fascia on 31/05/2021

Bibliometric: h-index 9, 277 citations. He reaches the threshold for full professor.

His research activities are in experimental tests, modelling and numerical simulations in complex nonlinear dynamics, linear and nonlinear vibration analysis of mechanical systems and nonlinear vibrations of structures and control. His research focused on chaos and nonlinear time series analysis, non-smooth dynamics, diagnostic, prognostic, predictive maintenance and condition monitoring of complex systems, fluid-structure interaction, the effect of thermal gradients and bioengineering. He is part of the Vibration, NVH and Powertrain Laboratory of the Department of Engineering "Enzo Ferrari".